The Dissertation Committee for Talea Lashea Mayo
certifies that this is the approved version of the following dissertation:

Data assimilation for parameter estimation in coastal ocean hydrodynamics modeling

Committee:

Clint Dawson, Supervisor

Omar Ghattas

Oscar Gonzalez

Ibrahim Hoteit

Richard Tsai

Data assimilation for parameter estimation in coastal ocean hydrodynamics modeling

by

Talea Lashea Mayo, B.S., M.S. C.A.M.

Dissertation

Presented to the Faculty of the Graduate School of

The University of Texas at Austin

in Partial Fulfillment

of the Requirements

for the Degree of

Doctor of Philosophy

The University of Texas at Austin

December 2013

Dedicated to science students from historically underrepresented groups.

You become what you believe.

Acknowledgments

There are no words to express my gratitude to my village. A little under five years ago I broke down wondering what on earth I had gotten myself into and how I would ever manage to get out. The answer has always been you.

I am so grateful to God, who for 27 years has guided my steps and led me to this moment. There are many other places I could and should and probably deserve to be. But by His grace I am here. I am forever indebted to my parents, Pamela and Frank Isom, and Tony Mayo. Because of your hard work and sacrifice, I was given a chance, and I will never take all that you have given for granted. Thank you so much for the encouragement and support you have always shown me. You are incredible parents. I will continue to make you proud. And of course, thank you to my partner, Mario Scroggins, for believing in me when I didn't believe in myself. Thank you for loving me, and thank you for your unwavering faith in us.

Thank you to my advisor, Prof. Clint Dawson, for your guidance and leadership throughout this process. Thank you for seeing something in me when my application came across your desk, and for continuing to believe in me throughout my years of graduate school. I am so blessed to have had you as an advisor. Thank you to the rest of the CHG. It has been such a privilege to work with such great people. Special thanks to my academic siblings, Jessica

Meixner, Steven Mattis, Nishant Panda, and Timothy Povich.

I have so much love for ICES, the CAM (CSEM) program, our faculty, and our staff. Thank you to my committee, Prof. Omar Ghattas, Prof. Oscar Gonzalez, and Prof. Richard Tsai, as well as all of the professors who devote your time and energy to making us strong scholars. I owe special thanks to Prof. Ibrahim Hoteit of KAUST for your role in my academic development and care for me as your own student. Thank you to an amazing staff for going above and beyond to make our lives so easy. I should mention Stephanie Rodriguez in particular, as without you I would have surely been kicked out of school by now for failing to confirm my attendance. I am also very grateful to Troy Butler and Tan Bui for the roles you have both played and continue to play in my academic success, in addition to being the very best of role models. And of course, thank you to my many peers, especially Mike Harmon, Omar Al Hinai, Andrea Hawkins, Kent Van Vels, and Ju Liu, and those outside of ICES, especially Sofia Garcia, Shanna Forbes, Madlene Hamilton, Juanita Chinn, Elysia Aseltine, Jeanine McLean, and the list goes on. Whether you realize it or not, when I felt so alone my first years at UT, you always reminded me that I wasn't. I am so grateful to call you all friends.

Thank you to the many other mentors who have played a role in my success. To my first advisor, Dr. Parashu Sharma, thank you for your love and support, and the time and energy you gave to make sure I did not become a lawyer. Thank you to Raj Pandya and Rebecca Haacker-Santos for all of the work that you do to aid in the success of kids like me, and more importantly,

those kids who have not been given as many opportunities. I can only hope to make such a difference. Thank you to Dr. Ricardo Cortez and your cohort for your vision, and to Dr. Juan Meza for helping to make it a reality. And thank you for the ongoing support you have given long after my six weeks were done. Of course I am so thankful for the love and friendship of you all as well.

Thank you to those faculty and staff at my alma mater, Grambling State University, who have continued to lift me up and show me that I am somebody. In particular, thank you to the band staff and the professors in the mathematics department. Choosing GSU remains one of the best decisions of my life. I am especially grateful for the friendships that blossomed there including that of my very close friend, Lessie Wilkins. Thank you for being there for me throughout the last nine years, including the particularly difficult past one.

To the Austin Alumnae Chapter of Delta Sigma Theta Sorority, Inc. I am forever grateful for the love and kindness you have shown me over the last five years. To be a part of a group of such phenomenal women is a privilege. To Gwendolyn Greene, thank you for four years of passionate leadership. You personify everything a woman should be and I am honored to have worked so closely with you. To Catherine Lee, thank you for your support, love, prayers, and encouragement. Everyone should be blessed with such a friend.

And finally, to all of those who came before me, thank you for your blood, sweat, and tears. Your efforts are not forgotten or unappreciated. Because of you, I can.

Data assimilation for parameter estimation in coastal ocean hydrodynamics modeling

Publication No. _____

Talea Lashea Mayo, Ph.D.
The University of Texas at Austin, 2013

Supervisor: Clint Dawson

Coastal ocean models are used for a vast array of applications. These applications include modeling tidal and coastal flows, waves, and extreme events, such as tsunamis and hurricane storm surges. Tidal and coastal flows are the primary application of this work as they play a critical role in many practical research areas such as contaminant transport, navigation through intracoastal waterways, development of coastal structures (e.g. bridges, docks, and breakwaters), commercial fishing, and planning and execution of military operations in marine environments, in addition to recreational aquatic activities. Coastal ocean models are used to determine tidal amplitudes, time intervals between low and high tide, and the extent of the ebb and flow of tidal waters, often at specific locations of interest. However, modeling tidal flows can be quite complex, as factors such as the configuration of the coastline, water depth, ocean floor topography, and hydrographic and meteorological impacts can have significant effects and must all be considered.

Water levels and currents in the coastal ocean can be modeled by solving the shallow water equations. The shallow water equations contain many parameters, and the accurate estimation of both tides and storm surge is dependent on the accuracy of their specification. Of particular importance are the parameters used to define the bottom stress in the domain of interest [50]. These parameters are often heterogeneous across the seabed of the domain. Their values cannot be measured directly and relevant data can be expensive and difficult to obtain. The parameter values must often be inferred and the estimates are often inaccurate, or contain a high degree of uncertainty [28].

In addition, as is the case with many numerical models, coastal ocean models have various other sources of uncertainty, including the approximate physics, numerical discretization, and uncertain boundary and initial conditions. Quantifying and reducing these uncertainties is critical to providing more reliable and robust storm surge predictions. It is also important to reduce the resulting error in the forecast of the model state as much as possible.

The accuracy of coastal ocean models can be improved using data assimilation methods. In general, statistical data assimilation methods are used to estimate the state of a model given both the original model output and observed data. A major advantage of statistical data assimilation methods is that they can often be implemented non-intrusively, making them relatively straightforward to implement. They also provide estimates of the uncertainty in the predicted model state. Unfortunately, with the exception of the estimation of initial conditions, they do not contribute to the information contained

in the model. The model error that results from uncertain parameters is reduced, but information about the parameters in particular remains unknown.

Thus, the other commonly used approach to reducing model error is parameter estimation. Historically, model parameters such as the bottom stress terms have been estimated using variational methods. Variational methods formulate a cost functional that penalizes the difference between the modeled and observed state, and then minimize this functional over the unknown parameters. Though variational methods are an effective approach to solving inverse problems, they can be computationally intensive and difficult to implement as they generally require the development of an adjoint model. They also are not formulated to estimate parameters in real time, e.g. as a hurricane approaches landfall. The goal of this research is to estimate parameters defining the bottom stress terms using statistical data assimilation methods.

In this work, we use a novel approach to estimate the bottom stress terms in the shallow water equations, which we solve numerically using the Advanced Circulation (ADCIRC) model. In this model, a modified form of the 2-D shallow water equations is discretized in space by a continuous Galerkin finite element method, and in time by finite differencing. We use the Manning's n formulation to represent the bottom stress terms in the model, and estimate various fields of Manning's n coefficients by assimilating synthetic water elevation data using a square root Kalman filter. We estimate three types of fields defined on both an idealized inlet and a more realistic spatial domain. For the first field, a Manning's n coefficient is given a constant value over the entire

domain. For the second, we let the Manning's n coefficient take two distinct values, letting one define the bottom stress in the deeper water of the domain and the other define the bottom stress in the shallower region. And finally, because bottom stress terms are generally spatially varying parameters, we consider the third field as a realization of a stochastic process. We represent a realization of the process using a Karhunen-Loève expansion, and then seek to estimate the coefficients of the expansion.

We perform several observation system simulation experiments, and find that we are able to accurately estimate the bottom stress terms in most of our test cases. Additionally, we are able to improve forecasts of the model state in every instance. The results of this study show that statistical data assimilation is a promising approach to parameter estimation.

Table of Contents

List of Tables

List of Figures

Chapter 1

Introduction

1.1 Background and Motivation

In recent years, coastal ocean modeling has been recognized as an increasingly important research area. The coastal ocean is an especially important region as it is home to more than 50% of the human population, many biological species, as well as many of the ports and harbors that are vital to the U.S. economy [102]. Through coastal ocean modeling, important information about these regions, such as water elevation levels, currents, temperature, and salinity can be obtained. Such information has many applications, one of the most important being the prediction of hurricane storm surge. Hurricane storm surge is the abnormal rise of coastal water generated by the wind and the effects of low atmospheric pressure that come from a tropical storm. The storm surge often inundates coastal areas, and sometimes has the additional consequence of acting as a pathway for short surface or wind waves to move and break farther inland [51]. This poses a significant threat to life and property in coastal regions, and can also cause structural damage and erosion of beaches and dunes. For those surges that travel inland, saltwater intrusion threatens public health and the environment.

The prediction of hurricane storm surge through coastal ocean modeling plays a major role in mitigating the aforementioned devastation. It allows for the real-time prediction of coastal inundation as a tropical storm approaches, which can improve warning systems and emergency response. In addition, the ability to accurately model storm surge allows the future risk of flooding to be assessed, guiding decision-makers in coastal development and coastal hazard mitigation.

Hurricane storm surge is significantly impacted by tides. However, the impact is nonlinear [95], so accurately modeling tides is critical to accurate storm surge forecasting. Furthermore, modeling tides is important in its own right. The accurate estimation of both tides and storm surge is dependent on many of the parameters in the coastal ocean model, especially those parameters used to define the bottom stress in the domain of interest [50]. Unfortunately, these parameters cannot be measured directly and relevant data is both expensive and difficult to obtain. The parameter values must often be inferred and the estimates are often inaccurate and will always contain a high degree of uncertainty [28]. There are many approaches for parameter estimation, however these approaches are often computationally intensive, requiring the development of adjoint models, and they typically cannot be performed in real time. Another method of compensating for the uncertainty in the bottom stress parameters is by modifying the model output itself to match observed data through what are known as statistical data assimilation methods (Chapter 3). These methods are advantageous over typical parameter estimation

methods as they are generally nonintrusive (i.e. they do not require adjoint models) and can be applied online, as data becomes available. They also allow information about the uncertainty in the estimate of the model output to be computed. However, they generally do not provide information about the true model parameters; they only provide updates to the model state. Recently, statistical data assimilation methods have been reformulated to update model parameters along with model state variables, but these approaches are mostly found in atmospheric modeling and neural network applications. Furthermore, for an application such as coastal ocean modeling, the updates to the model state (e.g. water elevation) are generally not based on physical principles, often violating conservation of mass and/or momentum.

An additional challenge arises in estimating bottom stress parameters as a result of the typically heterogeneous nature of these parameters across common domains of interest; the parameters are often highly variable in space. With statistical data assimilation methods, it is not unreasonable to estimate the value of a parameter at each point of the domain, however, we know that there is generally some correlation between neighboring parameter values and such a point-wise approach to parameter estimation is computationally wasteful. Thus, for many applications of coastal ocean modeling it is necessary to first parameterize a highly variable field of bottom stress parameters in order to reduce the number of values to be estimated while still allowing the bottom stress parameters to vary in space.

1.2 Research Contributions

In this thesis we develop a novel approach to parameter estimation using statistical data assimilation methods. The methods generally used for the estimation of a model state are reformulated to estimate the bottom stress terms in a 2-D coastal ocean model. For our test cases, we implement a square root Kalman filter to minimize the amount of noise introduced to the system as a result of the data assimilation. The background error covariance of the parameters that is used in the initialization and the forecast steps of statistical data assimilation methods has been shown to significantly affect the accuracy of the estimation. We have developed a systematic method of estimating this covariance. We have extended our method of parameter estimation to determine a field of spatially varying bottom stress terms by representing the field as a stochastic process, and then parameterizing the process using the Karhunen-Loève expansion. In order to define the stochastic process, we have analyzed the properties of a number of well known covariance functions. To determine the deterministic function used in its Karhunen-Loève expansion, we have computed the eigendecomposition of the covariance function numerically, using a Galerkin scheme. And finally, we have determined a method of ensuring that the parameters that are estimated in this case correspond to a field that is physical. We perform observation system simulation experiments (OSSEs) in order to test our parameter estimation method for both an idealized and a more complex domain. Through these experiments, we find that our method is a promising approach for estimating the bottom stress terms in a coastal

ocean model. Thus, there is potential for significant contributions to the field of computational hydraulics particularly for the prediction of hurricane storm surges.

1.3 Outline

The remainder of this thesis is organized as follows. A review of the literature for coastal ocean modeling as well as applications of parameter and state estimation is provided in Chapter 2. In Chapter 3 we discuss statistical data assimilation methods for state estimation and then describe how we reformulate the methods to estimate model parameters. In Chapter 4 we discuss the representation of a spatially varying field as a stochastic process and review the theory of representation for such a process. We show numerical results for our approach to parameter estimation in Chapter 5, and conclude the thesis in Chapter 6.

Chapter 2

Literature Review

Coastal ocean models determine the state of a fluid (e.g. the fluid depth, velocity, temperature, and salinity) through the numerical solution of the shallow water equations (SWEs). The primary assumption of the SWEs is that the horizontal length scale of the domain of interest is large relative to the vertical length scale. The SWEs are obtained by the depth integration of the incompressible Navier-Stokes equations, assuming hydrostatic pressure. The result is a first-order hyperbolic continuity equation for the depth of the fluid coupled to the momentum equations for horizontal depth-averaged velocities. Here, we use the SWEs to model the flow of water, though the equations are often used to model various other fluids.

2.1 The Shallow Water Equations

The Navier-Stokes equations describe the flow (i.e. velocity) of a fluid. They are comprised of equations for the conservation of the fluid's mass and momentum. The SWEs can be derived from the incompressible Navier-Stokes equations under several assumptions. The first assumption is that the effects of the variations in the density of the fluid on the momentum equations are

negligible with the exception of the gravity term in the equation for the z-component of the velocity. The fluid density can thus be modeled as a constant everywhere else it appears in the momentum equations. This is known as the Boussinesq approximation. In formulating the kinematic boundary conditions it is assumed that the fluid does not cross the boundary of the solid bottom or that of the free surface, i.e. the normal velocity components are zero at the bottom of the domain, and the relative normal velocity components are zero at the top. For the dynamic boundary conditions, a no-slip condition is assumed at the bottom surface (i.e. the velocity here is zero), and at the free surface it is assumed that the stresses are continuous across the fluid boundary. Finally, the central assumption in shallow water theory is that the fluid has a hydrostatic pressure distribution. This means that the gradient of the pressure in the vertical direction is simply assumed to be the (negative) product of density and gravitational acceleration [95].

With these assumptions, we can derive the 3-D SWEs. To obtain the 2-D SWEs, we integrate the 3-D SWEs over the depth of the fluid. The result is a first-order hyperbolic continuity equation for water elevation and the momentum equations for horizontal depth-averaged velocities. The equations are coupled through the fluid velocities and can be expressed:

$$\frac{\partial H}{\partial t} + \frac{\partial}{\partial x}(Q_x) + \frac{\partial}{\partial y}(Q_y) = 0 \tag{2.1}$$

$$
\begin{aligned}
\frac{\partial Q_x}{\partial t} + \frac{\partial UQ_x}{\partial x} + \frac{\partial VQ_x}{\partial y} - fQ_y &= -gH\frac{\partial[\zeta + P_s/g\rho_0 - \alpha\eta]}{\partial x} \\
&+ \frac{\tau_{sx}}{\rho_0} - \frac{\tau_{bx}}{\rho_0} + M_x - D_x - B_x \\
\frac{\partial Q_y}{\partial t} + \frac{\partial UQ_y}{\partial x} + \frac{\partial VQ_y}{\partial y} - fQ_x &= -gH\frac{\partial[\zeta + P_s/g\rho_0 - \alpha\eta]}{\partial y} \\
&+ \frac{\tau_{sy}}{\rho_0} - \frac{\tau_{by}}{\rho_0} + M_y - D_y - B_y.
\end{aligned} \tag{2.2}
$$

Here, ζ is the free surface departure from the geoid, h is the bottom surface departure from the geoid (bathymetric depth), $H = \zeta + h$ is the total water column height, U_i is the depth-averaged velocity in the x_i direction (where x_1 = x and x_2 = y), $Q_{x_i} = U_{x_i}H$ is the flux per unit width in the x_i direction, f is the Coriolis parameter, P_s is the atmospheric pressure at the free surface, ρ_0 is the reference density of water, α is the effective earth elasticity factor, η is the Newtonian equilibrium tide potential, τ_{sx_i} are the imposed surface stresses, τ_{bx_i} are the bottom stress components, M_{x_i} is the vertically-integrated lateral stress gradient, D_{x_i} is the momentum dispersion, and B_{x_i} is the vertically-integrated baroclinic pressure gradient. Here, the momentum equations have been written in conservative form.

What can be considered as the earliest form of the SWEs was developed in 1755 by Euler, however the equations developed were primitive and only contained terms for Coriolis forcing, gravity, and tidal potential. Model development continued over the next century, with the addition of (linear) bottom stress and the no-slip boundary condition [67]. The SWEs are also sometimes referred to as the Saint-Venant equations because Saint-Venant derived the modern form of the 1-D SWEs in 1843 [95].

2.1.1 Bottom Stress

The bottom stress components, τ_{bx_i}, in the momentum equations are unknown parameters, however, in many cases they significantly impact the model solution. In order to close the system of equations given by the SWEs, they must be expressed in terms of other model variables. They are often calculated from the fluid velocities at the bottom of the domain, which depend on external variables such as surface stresses, fluid depth, and gradients of the free surface elevation. There have been many formulations of such expressions.

The bottom stress is often defined using a linear or quadratic drag law,

$$\frac{\tau_{bx}}{\rho_0} = \frac{(c_{f_1} + c_{f_2}|\mathbf{U}|)Q_x}{H},$$

where c_{f_i} is a standard friction coefficient and one of the coefficients is equated to 0 (i.e. $c_{f_2} = 0$ or $c_{f_1} = 0$ to specify a linear or quadratic drag law, respectively). Groen and Groves [40] used a quadratic drag law and modeled the bottom stress as:

$$\begin{aligned} \frac{\tau_{bx}}{\rho_0} &= \frac{c_f|\mathbf{U}|Q_x}{H} - \gamma\frac{\tau_{w_x}}{\rho_0} \\ \frac{\tau_{by}}{\rho_0} &= \frac{c_f|\mathbf{U}|Q_y}{H} - \gamma\frac{\tau_{w_y}}{\rho_0}, \end{aligned} \tag{2.3}$$

where τ_{wx_i} is the wind stress. They recommended that the coefficient γ be set to 0.05. It turns out that the wind stress only significantly impacts the bottom stress when the wind speed is more than 100 times greater than the flow velocity [95]. This only occurs in rare instances and the effect of wind

can often be ignored as a result. In these cases, the rightmost terms in (2.3) can be set to zero and the expression for the bottom stress reduces to

$$\begin{aligned} \frac{\tau_{bx}}{\rho_0} &= \frac{c_f|\mathbf{U}|Q_x}{H} \\ \frac{\tau_{by}}{\rho_0} &= \frac{c_f|\mathbf{U}|Q_y}{H}. \end{aligned} \tag{2.4}$$

The bottom stress is thus given the same direction as the depth averaged velocity with a quadratic dependence on its magnitude. This is the expression most commonly used in coastal ocean models and such approximations turn out to be sufficiently accurate in a number of problems. Unfortunately, determining the standard friction coefficient presents its own difficulties. Experimental evidence of its value is scarce, and many calculations use the order of magnitude estimate $c_f = 2 \times 10^{-3}$ [19]. The friction coefficient is also often used as a tuning parameter [20].

2.1.2 The Manning's n Formulation

One way of defining the standard friction coefficient, c_f, in (2.4) is through the Manning's n formulation. This formulation comes from the model developed by Robert Manning to describe flow in an open channel [64]. Manning derived his model in 1885 by considering the mean results of seven formulae for open channel flow commonly used at that time [33]. His approximation can be reformulated and substituted into the bottom stress terms in the momentum equations. The constant c_f can then be defined in terms of the

empirical value n, the Manning's n coefficient of roughness:

$$c_f = \frac{gn^2}{H^{1/3}}. \tag{2.5}$$

The reformulation is shown in Appendix 1. This formulation describes a depth-dependent friction relation. When the roughness of the bottom surface is constant, the bottom stress increases with decreasing depth.

The Manning's n coefficient characterizes the loss of energy near the bottom surface of the domain. It is a highly variable spatial parameter dependent on the surface characteristics of the land and the seabed (e.g. Figure 2.1). It also includes the effects of surface stresses, form drag, wave resistance, and resistance due to flow instabilities [28]. Specifically, it is dependent on silting and erosion of the bottom surface, bed forms, and vegetation, as well as many other factors. It cannot be measured directly, and there is no exact method for its selection; it is often assigned a constant value, obtained from tables defining well established empirical estimates of common land classifications (e.g. Table 2.1). In coastal ocean models such as ADCIRC, the Manning's n coefficient is specified at the vertices (nodes) of a given discretization of a physical domain. From these nodal values, a continuous, piecewise linear representation of bottom friction can be constructed. The nodal values are determined from data (e.g., satellite images used to define land classifications) that may be incomplete, erroneous, or contain data from different, inapplicable time periods. Furthermore, data is often collected on a sub-grid scale and an upscaling procedure (e.g., local spatial averaging) must be used. As a

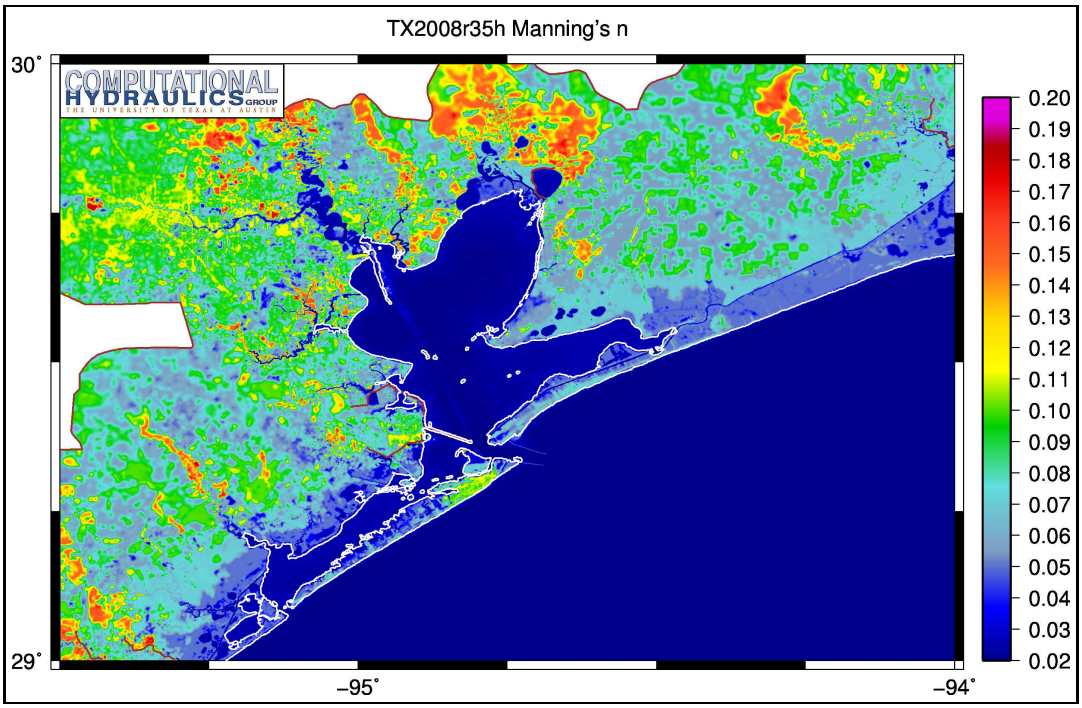

Figure 2.1: Empirically defined values of the Manning's n coefficient along the upper Texas coast

result, the Manning's n coefficients used in coastal ocean models often contain a significant amount of uncertainty.

2.2 Uncertainty in Coastal Ocean Models

The SWEs must be solved numerically for all but the simplest cases [36, 65, 2]; accurately solving the SWEs is a difficult problem in itself, even without the added complexity that the uncertain bottom stress parameters introduce. However, the problem can be significantly simplified by neglecting bottom stress altogether [19]. Citing bottom friction as "one of least under-

Open water	0.020	Mixed forest	0.170
Ice/snow	0.022	Shrub land	0.070
Pasture	0.033	Grassland	0.035
Commercial	0.050	Low residential	0.120
Bare rock/sand	0.040	High residential	0.121
Gravel pit	0.060	Row crops	0.040
Fallow	0.032	Small grains	0.035
Transitional	0.100	Recreational grass	0.030
Deciduous forest	0.160	Woody wetland	0.140
Evergreen forest	0.180	Herbaceous wetland	0.035
Mixed forest	0.170		

Table 2.1: Values of the Manning's n coefficient for various surfaces [14]. The left columns in the tables describe the land characteristics and the right columns are the associated empirically defined Manning's n coefficients.

stood phenomena," Jelesnianski modeled storm surge without it [50]. He found that its effects on storm surge were negligible for certain storms, namely those traveling at a moderate or high speed, as well as for those storms that spent a limited time on the continental shelf. For slower moving storms, he also found the storm surge to the right of the location of landfall (for the observer on the sea, facing land) to be insensitive to the bottom stress terms. However, for the storm surge to the left of landfall, inclusion of and variations in the bottom stress terms resulted in significant variations in the storm surge profile. The bottom stress terms were also found to have a significant impact on the storm surge model for storms located near the coast, traveling nearly parallel to the shore. In these instances, particularly in the case of a basin with a sloped bathymetry, his storm surge model generated resurgences and edge waves, the periods and amplitudes of which were dependent on the formula-

tion of the bottom stress. In [51], Jelesnianski modeled those storms unable to be modeled when the bottom stress terms were omitted by implementing Platzman's scheme [81] for the linear representation of bottom stress. Due to the uncertainty of the bottom stress, it was necessary to include a dissipating mechanism to control both large amplitude resurgences and initialization phenomena of storms of all speeds moving parallel to the coast as well as for slowly moving storms that made landfall. Additionally, Platzman's scheme had to be modified to include a bottom slip current in order for the model output to match observed data.

The importance of including the bottom stress parameters in coastal ocean models was also discussed in [21] and [43]. The terms are generally included in the present-day numerical models of shallow water flow, though the coefficients used in the formulation generally contain large amounts of uncertainty. The uncertainty in the Manning's n coefficient on any given grid leads to uncertainties in common quantities of interest corresponding to experimentally observable data (e.g., maximum water elevations and currents) computed from the solution of a coastal ocean model. Moreover, the solution of the model and the quantities of interest are often highly sensitive to changes in these parameters. In this paper, we consider a specific numerical model for solving the SWEs and implement a statistical data assimilation methodology for estimating the value of and quantifying the uncertainty in the Manning's n coefficient.

In general, there are two main approaches to reducing the model error

that results from the uncertainties in the bottom stress parameters. The goal of both approaches is to achieve model solutions that match observed data, however, the first approach, parameter estimation, attempts to reduce the uncertainty in the bottom stress itself. The second approach attempts to compensate for the errors in the parameters by correcting the model output. This approach is called state estimation, and is the approach we have taken previously [16, 3].

2.2.1 Parameter Estimation for Coastal Ocean Models

Parameter estimation problems are traditionally solved using numerical methods based on optimal control theory. In these methods, a cost functional penalizing model-data discrepancies is minimized over the unknown model parameters. The minimization can be constrained so that the parameter estimates remain within specified bounds. The minimization of the cost functional requires the computation of its gradient, which can be achieved through sensitivity analyses. Ding et al. grouped methods of sensitivity analysis into three categories: influence-coefficient methods, sensitivity-equation methods, and adjoint-equation methods [28]. Influence-coefficient methods perturb model parameters individually in order to determine their effects on the model output. In a similar fashion, sensitivity-equation methods evaluate partial derivatives of the model state variables with respect to the unknown model parameters. Finally, adjoint-equation methods are based on variational principles and are the methods most commonly used in parameter estimation. In these

methods, the construction of the gradient of the cost functional leads to an adjoint problem that must be solved backwards in time. In all three methods of sensitivity analysis, an efficient procedure is needed in order to minimize the cost functional for complex models. Commonly used procedures include conjugate gradient methods and truncated Newton methods.

Many parameter estimation methods have been used to estimate the bottom stress terms used in coastal ocean models. In 1990, [88] was able to accurately estimate the bottom friction and wind stress terms in a model of both 1-D and 2-D shallow water flows. The friction parameters in their test cases were spatially distributed in space and they were estimated with an accuracy of approximately 2%, though they accounted for the uncertainty in the uncertain boundary conditions in the model. The authors described this as the first instance of automatic calibration (i.e. the sensitivity analyses were not done by hand). They again estimated a spatially varying bottom friction coefficient in [89]. In this case, they applied parameter estimation to a simplified 2-D shallow water model, neglecting the advection and wind stress terms, and used a linearized form of the bottom stress. They used a gradient-based algorithm, with a quasi-Newton scheme to minimize the cost functional, and they used a combination of the model and adjoint solutions to determine the best estimate of the model state. They were able to reduce the root mean square error of the parameters substantially, but again found that the parameter estimates compensated for other model errors. Das et al. estimated both linear and quadratic friction coefficients in a channel of uni-

form width [20]. One end of the channel was closed and the other was open, given a specified water elevation which was varied harmonically with a known amplitude to simulate a tide. Using data of the tidal amplitudes and phases recorded at two locations, they were able to estimate a single bottom stress coefficient. They were also able to estimate two bottom stress terms, however they found that there was not sufficient data to resolve three terms. They were able to accurately estimate distributed parameters as long as the number of parameters did not exceed twice the number of observation stations. In [98], Manning's n coefficients were estimated for a model of unsteady flow in a river. The spatially varying field of coefficients was first parameterized using the singular value decomposition. Manning's n coefficients in a river were also estimated in [55]. They simulated flooding events in the river as well as tidal waves. They found that the parameter estimation suffered from noise in the data and that the data of one historic event did not produce reliable results. They also observed that the error in their parameter estimates inherited the uncertainty in the observation data used for the estimation. A more complex model domain, an open channel with a trapezoidal cross section, was used to estimate bottom stress parameters in [6]. In estimating the bottom stress parameters in an open channel, [75] found that the type of data used for the parameter estimation had a significant impact on the accuracy. They inverted data of the flow depth as well as the flow velocity and found that the velocity data did not provide sufficient information to recover the Manning's n coefficients for a a single channel or a domain with multiple reaches with rectangular

cross sections. Additionally, they found that accurate parameter estimation required a number of observation stations greater than or at least equal to the number of parameters being estimated. Ishii and Kawahara estimated the Manning's n coefficient in a 2-D shallow water model coupled to a model of sediment transport [48]. They were unable to recover the true parameter when the initial guess of the Manning's n coefficient was too small.

Though we see that many authors have been able to successfully estimate bottom stress parameters using variational parameter estimation methods, the estimation has mostly been implemented for a single or very small number of values on very simple model domains. The estimation of such parameters on larger, 2-D domains as well as the estimation of more complex configurations is an active area of research. For these problems implementing a variational method is quite computationally expensive.

A problem with parameter estimation problems in general is that the inverse problems are often ill-posed. The parameter estimation often suffers from instabilities as well as non-uniqueness; parameter estimates can vary significantly depending on the initial guesses and can fail to converge to their optimal values. Regularization algorithms are often implemented to obtain stable and unique solutions [6], but there are no methods that can guarantee stability and uniqueness for a wide range of applications [68]. Additionally, though adjoint methods are commonly used and are efficient when estimating a large number of parameters that generate only a few model responses (i.e. states), the backward computations required for their implementation make

their storage requirements prohibitive [28].

2.2.2 State Estimation for Coastal Ocean Models

In recent years, state estimation has been another approach to reducing the error in costal ocean models resulting from uncertainty in the bottom stress parameters (as well as various other parameters). Originally, the main application of state estimation (i.e. statistical data assimilation methods) was atmospheric modeling. Currently, there are many examples of state estimation in oceanography, though few of the applications are for coastal ocean modeling specifically.

One of the earliest examples of state estimation in storm surge modeling was the work of Budgell [13]. He applied the Kalman filter to a linearized version of the 1-D SWEs with the goal of reducing the uncertainty in the boundary conditions and the momentum balances. The model state was estimated for two domains, a wedge shaped estuary forced with an inaccurate river discharge and an unknown open boundary surface elevations, and a channel closed at both ends forced with an unknown momentum source. For both cases, the true state was recovered with the accuracy of the numerical approximation of the governing equations. In his subsequent work, he estimated the true state for the nonlinear SWEs using the extended Kalman filter. He still used the 1-D form of the equations, but included branched channels in his domain. He found that the filter performance did not degrade when the model and observation errors were non-Gaussian, and furthermore, that assimilating

water elevation data improved not only estimates of water elevations, but also estimates of velocities. Heemink and Kloosterhuis [44] applied the extended Kalman filter to a 2-D shallow water model used to model tides that contained error in the momentum equations (the continuity equation was assumed to be error free), and in [94] an extended Kalman filter was again applied to a 2-D shallow water model to predict water levels during storm surges. In this work, the state estimation problem could be solved on a large, realistic domain because a reduced rank approximation of the model error covariance was used in the Kalman filter. A simplified, linear version of the non-linear model with linear bottom stress was also used. Sørensen and Madsen estimated the state variables of a 3-D model of surface flow in the North Sea and Baltic Sea [84]. They assimilated tidal gauge data using several versions of the ensemble Kalman filter in order to determine the water levels throughout the domain. The state estimation was tested using a four-week hindcast, which included a storm surge event, and they determined that the methods were appropriate for online applications. Sørensen et al. [85] applied several variations of the ensemble Kalman filter to a 3-D hydrodynamic model. They assimilated tidal gauge data obtained from coastal areas with the goal of testing the sensitivity of the filters to the often uncertain error statistics in the data assimilation system. They found that the performance of each of the filters was robust with respect to the error statistics (e.g. Gaussian noise, the rank of the model error covariance, and the standard deviation of the measurement error). The accuracy of the state estimates was independent of the error statistics, though

the estimates of the corresponding error covariance was more dependent. In [29], a simplified version of the ensemble Kalman filter is also applied to a 3-D hydrodynamic model in order to improve the predictions of the salinity and velocity in a Japanese bay by assimilating the same type of data. Both forecast and hindcast error was significantly reduced when the state estimation was implemented, though the effect of the assimilation was reduced for long forecast times. Tossavainen et al. [91] used the ensemble Kalman filter to estimate the velocity field in a 2-D shallow water model of a river containing erroneous boundary conditions (their model used Manning's formulation of the bottom stress). Observations of elevation and current data, taken at various spatial locations and times, were assimilated and improvement was consequently seen in the velocity field. Estimates of the water depths, however, were not accurate due to error in the measurements of the surface elevation. A large number of ensemble members (i.e. model simulations) were required for the estimation in this case, making the method computationally expensive.

Though not specifically with the goal of improving the error resulting from uncertain bottom stress parameters, state estimation has been successfully implemented for a number of hydrodynamic models, including both simplified and full versions of the 2-D SWEs. Several statistical data assimilation methods have been used to estimate any of the model state variables under various conditions, including tidal forcing and storm surge. We have recently implemented several variants of the ensemble Kalman filter in order to estimate water elevations in the Gulf of Mexico for hindcasts of the hurricanes Ike

and Katrina [16, 3]. State estimation is a promising approach to reducing error in shallow water models, and the moderate computational cost of the statistical data assimilation methods commonly used makes it advantageous over typical parameter estimation methods. Statistical data assimilation methods are described in detail in Chapter 3.

Chapter 3

Statistical Data Assimilation

Numerical forecast models have many sources of uncertainty. These include but are not limited to the approximation of physics, the numerical discretization of continuous differential equations, uncertainty in the boundary and initial conditions of the model, and the source of error that is the focus of this work, the approximation of uncertain model parameters. These sources of uncertainty in numerical models negatively affect the quality of model forecasts. Similarly, there is uncertainty in observed data, generally due to factors such as instrumental noise, environmental noise, and sampling techniques.

Combining the model forecast and observed data to determine the best estimate of the modeled state defines the data assimilation problem. Statistical data assimilation methods have been derived to minimize the error of this estimate in terms of the statistics of the model and data error [77]. The methods are advantageous in that they produce not only the best estimate of the modeled state, but also an estimate of the corresponding error covariance.

3.1 Kalman Filtering

For linear models, the data assimilation problem has been solved by the Kalman filter. The Kalman filter was proposed in 1960 by Rudolf Kalman [31]. In this method, a model forecast, generally represtented as an n-dimensional state vector, $\mathbf{x}_k^f$, is updated (i.e. analyzed) by data observed prior to and at the time, t_k, of the forecast. The data available at this time is represented by a p-dimensional vector, $\mathbf{y}_k^o$, and the model forecast is updated by a weighted residual between $\mathbf{x}_k^f$ and $\mathbf{y}_k^o$ to form the analyzed state, $\mathbf{x}_k^a$. The weight used in the update has been derived to minimize the error covariance of the analyzed state under certain assumptions and is called the Kalman gain. The derivation of the Kalman gain is shown below.

For all statistical data assimilation methods, we assume we begin with an initial estimate of the true model state, and a numerical forecast model, $\mathcal{M}_k$, used to predict the state at some later time, t_k:

$$\mathbf{x}_k^t = \mathcal{M}_k(\mathbf{x}_{k-1}^t) + \eta_k.$$

The model error, η_k, is unknown, however, it is assumed to be Gaussian, with zero mean and an error covariance, $\mathbf{Q}_k$, which is given.

The current model state, $\mathbf{x}_k^t$, can be projected into the observation space through an observation operator, $\mathcal{H}_k$:

$$\mathbf{y}_k^t = \mathcal{H}_k(\mathbf{x}_k^t) + \epsilon_k.$$

Here, $\mathbf{y}_k^t$ denotes the true, noise-free data of the physical system. Again, it is assumed that the error in the observation operator, ϵ_k, is unknown, Gaussian,

and zero-mean, with error covariance, $\mathbf{R}_k$, which is given. Often $\mathbf{R}_k$ is set to the diagonal matrix $\sigma_k^2\mathbf{I}$, where $\mathbf{I}$ is the identity matrix (with dimensions defined by those of the observation space). The coefficient, σ_k^2, is thus used to represent the error variance. This models the case of statistical errors for each datum that are independent and identically distributed, which is a common assumption.

The Kalman filter utilizes both operators for its two primary steps, the forecast step and the analysis step. In the forecast step, the forecast model, $\mathbf{M}_k$, which is linear in this case, is used to estimate the evolution of the initial state, $\mathbf{x}_{k-1}^a$, at some later time, t_k:

$$\mathbf{x}_k^f = \mathbf{M}_k\mathbf{x}_{k-1}^a.$$

Here, we have denoted the forecasted model state by $\mathbf{x}_k^f$ to differentiate it from the true, error-free state, $\mathbf{x}_k^t$. The linearity of the forecast model allows the error covariance of the initial state, $\mathbf{P}_{k-1}^a$, to be computed directly:

$$\begin{aligned}
\mathbf{P}_k^f &= \overline{(\mathbf{x}_k^t - \mathbf{x}_k^f)(\mathbf{x}_k^t - \mathbf{x}_k^f)^T} \\
&= \mathbf{M}\overline{(\mathbf{x}_{k-1}^t - \mathbf{x}_{k-1}^a)(\mathbf{x}_{k-1}^t - \mathbf{x}_{k-1}^a)^T}\mathbf{M}^T + \overline{\eta_k^2} \\
&\quad + \ 2\mathbf{M}\overline{(\mathbf{x}_{k-1}^t - \mathbf{x}_{k-1}^a)\eta_k} \\
&= \mathbf{M}\mathbf{P}_{k-1}^a\mathbf{M}^T + \mathbf{Q}_k. \qquad (3.1)
\end{aligned}$$

In the analysis step, the observation operator is used to update both the forecasted model state and its error covariance. First, the forecasted model

state, $\mathbf{x}_k^f$, is projected (linearly, in this case) into the observation space, allowing a direct comparison to the current (and possibly noisy) data, $\mathbf{y}_k^o$. The residual is then weighted by the Kalman gain matrix, $\mathbf{K}_k$, and this weighted residual is used to update $\mathbf{x}_k^f$. We define the updated state as the analysis, $\mathbf{x}_k^a$:

$$\mathbf{x}_k^a = \mathbf{x}_k^f + \mathbf{K}_k(\mathbf{y}_k^o - \mathbf{H}_k\mathbf{x}_k^f). \tag{3.2}$$

The error covariance of $\mathbf{x}_k^a$, $\mathbf{P}_k^a$, can be computed in several steps. Expressing each of the vectors, $\mathbf{x}_k^f, \mathbf{x}_k^a$, and $\mathbf{y}_k^o$, in terms of their unknown errors, we have

$$\begin{aligned}
\mathbf{x}_k^f &= \mathbf{x}_k^t + \epsilon_k^f \\
\mathbf{y}_k^o &= \mathbf{H}_k\mathbf{x}_k^t + \epsilon_k^y \\
\mathbf{x}_k^a &= \mathbf{x}_k^t + \epsilon_k^a.
\end{aligned}$$

Using these equations, we can define an expression for the error in the analyzed state, $\mathbf{x}_k^a$ (3.2):

$$\epsilon_k^a = \epsilon_k^f + \mathbf{K}_k(\epsilon_k^y - \mathbf{H}_k\epsilon_k^f).$$

The analysis error covariance is then

$$\begin{aligned}
\mathbf{P}_k^a &= \overline{\epsilon_k^a \epsilon_k^{aT}} \\
&= \overline{[\epsilon_k^f + \mathbf{K}_k(\epsilon_k^y - \mathbf{H}_k\epsilon_k^f)][\epsilon_k^f + \mathbf{K}_k(\epsilon_k^y - \mathbf{H}_k\epsilon_k^f)]^T} \\
&= \overline{\epsilon_k^f \epsilon_k^{fT}} + \overline{\mathbf{K}_k\epsilon_k^y\epsilon_k^{yT}\mathbf{K}_k^T + \mathbf{K}_k\mathbf{H}_k\epsilon_k^f\epsilon_k^{fT}\mathbf{H}_k^T\mathbf{K}_k^T} - \overline{\mathbf{K}_k\mathbf{H}_k\epsilon_k^f\epsilon_k^{fT} + \epsilon_k^f\epsilon_k^{fT}\mathbf{H}_k^T\mathbf{K}_k^T} \\
&= \mathbf{P}_k^f + \mathbf{K}_k\mathbf{R}_k\mathbf{K}_k^T + \mathbf{K}_k\mathbf{H}_k\mathbf{P}_k^f\mathbf{H}_k^T\mathbf{K}_k^T - \mathbf{K}_k\mathbf{H}_k\mathbf{P}_k^f - \mathbf{P}_k^f\mathbf{H}_k^T\mathbf{K}_k^T \\
&= (\mathbf{I} - \mathbf{K}_k\mathbf{H}_k)\mathbf{P}_k^f,
\end{aligned} \tag{3.3}$$

where the last equality holds when

$$\mathbf{K}_k = \mathbf{P}_k^f \mathbf{H}_k^T [\mathbf{H}_k \mathbf{P}_k^f \mathbf{H}_k^T + \mathbf{R}_k]^{-1}.$$

Alternatively, $\mathbf{K}_k$ can be written $\mathbf{P}_k^a \mathbf{H}_k^T \mathbf{R}_k^{-1}$:

$$\begin{aligned}
\mathbf{K}_k &= \mathbf{P}_k^f \mathbf{H}_k^T [\mathbf{H}_k \mathbf{P}_k^f \mathbf{H}_k^T + \mathbf{R}_k]^{-1} \\
&= \mathbf{P}_k^f \mathbf{H}_k^T [\mathbf{H}_k \mathbf{P}_k^f \mathbf{H}_k^T + \mathbf{R}_k]^{-1} \mathbf{R}_k \mathbf{R}_k^{-1} \\
&= \mathbf{P}_k^f \mathbf{H}_k^T [\mathbf{I} + \mathbf{R}_k^{-1} \mathbf{H}_k \mathbf{P}_k^f \mathbf{H}_k^T]^{-1} \mathbf{R}_k^{-1} \\
&= \mathbf{P}_k^f (\mathbf{I} + \mathbf{H}_k^T \mathbf{R}_k^{-1} \mathbf{H}_k \mathbf{P}_k^f)^{-1} \mathbf{H}_k^T \mathbf{R}_k^{-1} \\
&= [(\mathbf{P}_k^f)^{-1} + \mathbf{H}_k^T \mathbf{R}_k^{-1} \mathbf{H}_k]^{-1} \mathbf{H}_k^T \mathbf{R}_k^{-1} \\
&= [(\mathbf{P}_k^f)^{-1} + \mathbf{H}_k^T \mathbf{R}_k^{-1} \mathbf{H}_k]^{-1} (\mathbf{P}_k^f)^{-1} \mathbf{P}_k^f \mathbf{H}_k^T \mathbf{R}_k^{-1} \\
&= (\mathbf{I} + \mathbf{P}_k^f \mathbf{H}_k^T \mathbf{R}_k^{-1} \mathbf{H}_k)^{-1} \mathbf{P}_k^f \mathbf{H}_k^T \mathbf{R}_k^{-1} \\
&= [\mathbf{I} - (\mathbf{I} + \mathbf{P}_k^f \mathbf{H}_k^T \mathbf{R}_k^{-1} \mathbf{H}_k)^{-1} \mathbf{P}_k^f \mathbf{H}_k^T \mathbf{R}_k^{-1} \mathbf{H}_k] \mathbf{P}_k^f \mathbf{H}_k^T \mathbf{R}_k^{-1} \\
&= [\mathbf{I} - (\mathbf{I} + \mathbf{P}_k^f \mathbf{H}_k^T \mathbf{R}_k^{-1} \mathbf{H}_k)^{-1} \mathbf{P}_k^f \mathbf{H}_k^T \mathbf{R}_k^{-1} (\mathbf{H}_k \mathbf{P}_k^f \mathbf{H}_k^T + \mathbf{R}_k) \\
&\qquad *(\mathbf{H}_k \mathbf{P}_k^f \mathbf{H}_k^T + \mathbf{R}_k)^{-1} \mathbf{H}_k] \mathbf{P}_k^f \mathbf{H}_k^T \mathbf{R}_k^{-1} \\
&= [\mathbf{I} - (\mathbf{I} + \mathbf{P}_k^f \mathbf{H}_k^T \mathbf{R}_k^{-1} \mathbf{H}_k)^{-1} (\mathbf{P}_k^f \mathbf{H}_k^T \mathbf{R}_k^{-1} \mathbf{H}_k \mathbf{P}_k^f \mathbf{H}_k^T + \mathbf{P}_k^f \mathbf{H}_k^T) \\
&\qquad *(\mathbf{H}_k \mathbf{P}_k^f \mathbf{H}_k^T + \mathbf{R}_k)^{-1} \mathbf{H}_k] \mathbf{P}_k^f \mathbf{H}_k^T \mathbf{R}_k^{-1} \\
&= [\mathbf{I} - (\mathbf{I} + \mathbf{P}_k^f \mathbf{H}_k^T \mathbf{R}_k^{-1} \mathbf{H}_k)^{-1} [(\mathbf{I} + \mathbf{P}_k^f \mathbf{H}_k^T \mathbf{R}_k^{-1} \mathbf{H}_k) \mathbf{P}_k^f \mathbf{H}_k^T] \\
&\qquad *(\mathbf{H}_k \mathbf{P}_k^f \mathbf{H}_k^T + \mathbf{R}_k)^{-1} \mathbf{H}_k] \mathbf{P}_k^f \mathbf{H}_k^T \mathbf{R}_k^{-1} \\
&= [\mathbf{I} - \mathbf{P}_k^f \mathbf{H}_k^T (\mathbf{H}_k \mathbf{P}_k^f \mathbf{H}_k^T + \mathbf{R}_k)^{-1} \mathbf{H}_k] \mathbf{P}_k^f \mathbf{H}_k^T \mathbf{R}_k^{-1} \\
&= (\mathbf{I} - \mathbf{K}_k \mathbf{H}_k) \mathbf{P}_k^f \mathbf{H}_k^T \mathbf{R}_k^{-1} \\
&= \mathbf{P}_k^a \mathbf{H}_k^T \mathbf{R}_k^{-1}, \qquad (3.4)
\end{aligned}$$

where we have used the identity $(\mathbf{I}+\mathbf{X})^{-1} = \mathbf{I} - (\mathbf{I}+\mathbf{X})^{-1}\mathbf{X}$. The matrix $\mathbf{K}_k$ is the weight that minimizes the error covariance, $\mathbf{P}_k^a$, of $\mathbf{x}_k^a$, and is called the Kalman gain matrix. In the case of linear models, the equation for the analyzed state (3.2) is equivalent to the one obtained by minimizing the cost functional developed in the variational formulation of the data assimilation problem.

3.2 Kalman Filtering for Nonlinear Forecast Models

The Kalman filter solves the data assimilation problem with several assumptions, including the assumtion that the numerical forecast model is linear. However, for most practical applications, this assumption is not realistic. While the initial model state can be forecasted with a nonlinear model, the forecast of the initial error covariance is not as straightforward. Several methods have been developed to address this issue.

3.2.1 Extended Kalman Filtering

The extended Kalman filter [34] is one method that accounts for a nonlinear forecast model. It differs from the original Kalman filter only in the forecast step. The forecast model, $\mathcal{M}_k$, is used to forecast the initial state, however, the nonlinearities of $\mathcal{M}_k$ prevent the direct computation of the updated error covariance used in the linear case (3.1). As a solution, the forecast model is linearized through a Taylor series expansion of $\mathcal{M}_k$ about

$\mathbf{x}^t_{k-1}$:

$$\mathcal{M}_k(\mathbf{x}^t_{k-1}) = \mathcal{M}_k(\mathbf{x}^a_{k-1}) + \mathbf{M}_k(\mathbf{x}^a_{k-1})(\mathbf{x}^t_{k-1} - \mathbf{x}^a_{k-1}) + \text{ h.o.t.}, \tag{3.5}$$

where $\mathbf{M}_k$ is the Jacobian of $\mathcal{M}_k$. Then,

$$\begin{aligned} \mathbf{P}^f_k &= \overline{(\mathbf{x}^t_k - \mathbf{x}^f_k)(\mathbf{x}^t_k - \mathbf{x}^f_k)^T} \\ &= \overline{[\mathcal{M}_k(\mathbf{x}^t_{k-1}) - \mathcal{M}_k(\mathbf{x}^a_{k-1}) + \eta_k][\mathcal{M}_k(\mathbf{x}^t_{k-1}) - \mathcal{M}_k(\mathbf{x}^a_{k-1}) + \eta_k]^T} \\ &\approx \mathbf{M}_k\mathbf{P}^a_{k-1}\mathbf{M}^T_k + \mathbf{Q}_k. \end{aligned} \tag{3.6}$$

Here we have approximated the forecast error covariance with just the Jacobian of $\mathcal{M}_k$ by assuming the contribution from higher order terms (i.e. statistical moments of $\mathbf{x}^a_{k-1}$ and derivatives of $\mathcal{M}_k$) is negligible. With this approximation of the forecast error covariance, the analysis step for the extended Kalman filter remains the same as that of the original Kalman filter.

In practice, the extended Kalman filter has prohibitive storage requirements and computational costs. The dimension of the error covariance matrix $\mathbf{P}^a_{k-1}$ is n^2, the square of the dimension of the state vector, $\mathbf{x}^a_{k-1}$, so storing this matrix is not reasonable for large forecast models. The method also requires the computation of the Jacobian, $\mathbf{M}_k$, of the forecast model as well as its adjoint, $\mathbf{M}^T_k$, at each time step (3.6). Not only can this computation become costly, the subsequent approximation of $\mathbf{P}^f_k$ becomes inaccurate for highly nonlinear forecast models, when the neglected higher order derivatives of $\mathcal{M}_k$ are significant. In this case higher order terms can be included in the Taylor series expansion (3.5) but this is also computationally expensive and has even larger storage requirements (e.g. the dimension of the Hessian is n^4).

Furthermore, the higher order terms include additional statistical moments of the state vector, which are almost never known. Evolving the error covariance $\mathbf{P}^a_{k-1}$ matrix requires $2n$ model integrations at each time step, thus the availability of computational resources severly limits the ability to use the extended Kalman filter in practical applications.

3.2.2 Reduced Rank Kalman Filtering

Reducing the rank of the initial (and forecasted) error covariance matrices is one method of reducing the computational cost of the extended Kalman filter. Fewer model integrations are required to forecast an error covariance matrix with low rank, $r < n$, as such an error covariance matrix can be represented in factored form by a matrix containing just r columns. For the same reason, an r-rank error covariance matrix has fewer storage requirements than the full n rank matrix.

In the analysis step of the Kalman filter, current observations are used to reduce errors that lie in the space spanned by the columns of the forecast error covariance (3.2). Thus, for a forecast error covariance of low rank, errors that do not lie in the corresponding subspace cannot be reduced and can in fact diverge in the case of unstable dynamics [17]. Consequently, when using a low rank approximation of the forecast error covariance matrix, the space spanned by its r columns must capture those directions of the state space where the errors are increasing, otherwise the computational savings gained come at the cost of an accurate state estimation.

There is a natural way to ensure this property of the forecast error covariance matrix. It is well known that many dynamical systems, such as ocean models, possess what is known as an attractor. An attractor is a low-dimensional subspace of the state space to which the model solution eventually converges regardless of the initial state. It is a property of many models such as the 2-D Navier Stokes equations, for example [59]. The directions where model errors increase are those directions tangent to the attractor [73]. These directions of the attractor can be approximated using an empirical orthogonal function (EOF) or principal component analysis (PCA) [74]. Then the low rank approximation of the initial error covariance can be chosen accordingly; the rank r should be chosen to be at least equal to the dimension of the attractor, and the columns of the initial error covariance matrix should span the directions determined by the EOF/PCA. With this approach, the computational and storage savings of a low rank approximation can be achieved while maintianing acceptable filter performance. This is precisely what is done in the SEEK filter.

The SEEK filter was developed in 1998 by Pham et al [92]. In this method the low rank covariance matrix is decomposed into three matrices, $\mathbf{P}^a_{k-1} = \sigma^2 \mathbf{L}_{k-1}\mathbf{U}_{k-1}\mathbf{L}^T_{k-1}$, where $\mathbf{U}_{k-1}$ is $r \times r$. As in the EKF, the nonlinear forecast model is linearized and then used to evolve the initial error covariance, however, because of the decomposition of $\mathbf{P}^a_{k-1}$, it is only necesarry that $\mathbf{L}_{k-1}$ be evolved:

$$\mathbf{L}_k = \mathbf{M}_k \mathbf{L}_{k-1}.$$

The forecast error covariance becomes

$$\mathbf{P}_k^f = \mathbf{L}_k \mathbf{U}_{k-1} \mathbf{L}_k^T + \mathbf{Q}_k.$$

In the analysis step, $\mathbf{U}_{k-1}$ is updated recursively through its inverse:

$$\mathbf{U}_k^{-1} = \mathbf{U}_{k-1}^{-1} + (\mathbf{H}_k \mathbf{L}_k)^T \mathbf{R}_k^{-1} (\mathbf{H}_k \mathbf{L}_k), \tag{3.7}$$

and $\mathbf{U}_k$ is used to compute the Kalman gain matrix:

$$\mathbf{K}_k = \mathbf{L}_k \mathbf{U}_k (\mathbf{H}_k \mathbf{L}_k)^T \mathbf{R}_k^{-1}.$$

The forecasted state is updated by the current data,

$$\mathbf{x}_k^a = \mathbf{x}_k^f + \mathbf{K}_k (\mathbf{y}_k^o - \mathbf{H}_k \mathbf{x}_k^f),$$

and the analysis error covariance can be written as

$$\mathbf{P}_k^a \;=\; \mathbf{L}_k \mathbf{U}_k \mathbf{L}_k^T.$$

If the model noise $\mathbf{Q}_k$ is assumed to be zero, it can be shown that these equations are those of the (extended) Kalman filter, where the initial error covariance matrix $\mathbf{P}_{k-1}^a$ is first approximated by a matrix of low rank and then factored, e.g. using an eigenvalue decomposition.

As previously discussed, the low rank representation of the initial error covariance matrix reduces the computational cost of forecasting and storing the error covariance matrix. Furthermore, as a result of the initial decomposition, $\mathbf{P}_{k-1}^a = \mathbf{L}_{k-1} \mathbf{U}_{k-1} \mathbf{L}_{k-1}^T$, corrections to the forecasted state are made

in directions that might otherwise be amplified by the model. This is shown below.

For a forecast model that is (nearly) linear, possibly over a limited time span, the gradient of $\mathcal{M}_k$, $\mathbf{M}_k$, can be represented as a constant, $\mathbf{M}$, and $\mathbf{L}_k = \mathbf{M}\mathbf{L}_{k-1}$. The space spanned by the r columns of $\mathbf{L}_k$ (commonly referred to as the correction basis) will consequently converge to the space spanned by the eigenvectors corresponding to the r largest eigenvalues of $\mathbf{M}$. Here, we will choose r to be equal to the number of eigenvalues of $\mathbf{M}$ with modulus greater than one (i.e. the dimension of the attractor of the dynamical system). We define a matrix $\mathbf{V}$ so that its columns span the space of these r eigenvectors, and $\mathbf{V}_\theta$ as a matrix whose columns span the remaining eigenspace. Then, if an initial estimate of the state has some error, $\mathbf{e}_0$, which can be expressed in the basis of the eigenvectors, $\mathbf{e}_0 = \alpha_{e_0}\mathbf{v} + \beta_{e_0}\mathbf{v}_\theta$, after k forecasts this state and its error will be projected into the range of $\mathbf{M}^k$, and the portion of the initial error that lies in $\mathbf{V}_\theta$, $\beta_{e_0}\mathbf{v}_\theta$, dies out since the eigenvalues corresponding to this space have modulus less than one; this error is attenuated by the model dynamics. However, the initial error that lies in $\mathbf{V}$, $\alpha_{e_0}\mathbf{v}$, diverges. This is the error we wish to correct, and the SEEK filter has been formulated to do so.

Assuming linearity of the observation operator, the gradient of $\mathcal{H}_k$, $\mathbf{H}_k$, can also be represented as a constant and the update of $\mathbf{U}_k$ (3.7) can be expressed as

$$\mathbf{U}_k^{-1} = \mathbf{U}_0^{-1} + \sum_{j=1}^{k} \mathbf{L}_j^T \mathbf{H}^T \mathbf{R}^{-1} \mathbf{H} \mathbf{L}_j,$$

and thus

$$\begin{aligned}\mathbf{\Lambda}^{-k}\mathbf{U}_k^{-1}\mathbf{\Lambda}^{-k} &= \mathbf{\Lambda}^{-k}\mathbf{U}_0^{-1}\mathbf{\Lambda}^{-k} + \sum_{j=1}^{k}\mathbf{\Lambda}^{-k}\mathbf{L}_j^T\mathbf{H}^T\mathbf{R}^{-1}\mathbf{H}\mathbf{L}_j\mathbf{\Lambda}^{-k} \\ &= \mathbf{\Lambda}^{-k}\mathbf{U}_0^{-1}\mathbf{\Lambda}^{-k} + \sum_{l=0}^{k-1}\mathbf{\Lambda}^{-l}(\mathbf{L}_{k-l}\mathbf{\Lambda}^{l-k})^T\mathbf{H}^T\mathbf{R}^{-1}\mathbf{H}(\mathbf{L}_{k-l}\mathbf{\Lambda}^{l-k})\mathbf{\Lambda}^{-l},\end{aligned}$$

where $\mathbf{\Lambda}$ is the diagonal matrix of eigenvalues corresponding to the eigenspace $\mathbf{V}$. $\mathbf{L}_{k-l}\mathbf{\Lambda}^{l-k}$ converges to $\mathbf{V}$ as $k \to \infty$ for all l, so each term in the above summation converges and is bounded in matrix norm by $c\rho(\mathbf{\Lambda}^{-1})^{2l}$, where c is a constant and $\rho(\mathbf{\Lambda}^{-1})$ is the maximum modulus of the eigenvalues of $\mathbf{\Lambda}^{-1}$. We have constructed $\mathbf{V}$ so that $\rho(\mathbf{\Lambda}^{-1}) < 1$, thus by the Lebesgue dominated convergence theorem,

$$\begin{aligned}\mathbf{\Lambda}^{-k}\mathbf{U}_k^{-1}\mathbf{\Lambda}^{-k} &\to \sum_{l=0}^{\infty}\mathbf{\Lambda}^{-l}\mathbf{V}^T\mathbf{H}^T\mathbf{R}^{-1}\mathbf{H}\mathbf{V}\mathbf{\Lambda}^{-l} \\ &:= \mathbf{\Pi}^{-1},\end{aligned}$$

and $\mathbf{P}_k^a \to \mathbf{V}\mathbf{\Pi}\mathbf{V}^T$ as $k \to \infty$. Then by (3.1), $\mathbf{K}_k \to \mathbf{V}\mathbf{\Pi}\mathbf{V}^T\mathbf{H}^T\mathbf{R}^{-1}$.

To see that this formulation of the Kalman gain matrix, $\mathbf{K}_k$, corrects the error that lies in the portion of the eigenspace, $\mathbf{V}$, we observe the propagation of the initial error $\mathbf{e}_0$. We first express the analysis of the state vector, $\mathbf{x}_k^a$, in terms of the previous analysis, $\mathbf{x}_{k-1}^a$:

$$\begin{aligned}\mathbf{x}_k^a &= \mathbf{x}_k^f + \mathbf{K}_k(\mathbf{y}_k^o - \mathbf{H}\mathbf{x}_k^f) \\ &= \mathbf{M}\mathbf{x}_{k-1}^a + \mathbf{K}_k(\mathbf{H}\mathbf{x}_k^t + \epsilon_k - \mathbf{H}\mathbf{M}\mathbf{x}_{k-1}^a) \\ &= \mathbf{M}\mathbf{x}_{k-1}^a + \mathbf{K}_k[\mathbf{H}(\mathbf{M}\mathbf{x}_{k-1}^t + \eta_k) + \epsilon_k - \mathbf{H}\mathbf{M}\mathbf{x}_{k-1}^a] \\ &= \mathbf{M}\mathbf{x}_{k-1}^a + \mathbf{K}_k\mathbf{H}\mathbf{M}\mathbf{x}_{k-1}^t + \mathbf{K}_k\mathbf{H}\eta_k \ + \mathbf{K}_k\epsilon_k - \mathbf{K}_k\mathbf{H}\mathbf{M}\mathbf{x}_{k-1}^a.\end{aligned}$$

Then we have

$$\begin{aligned}\mathbf{e}_k &= \mathbf{x}_k^a - \mathbf{x}_k^t \\ &= (\mathbf{I} - \mathbf{K}_k\mathbf{H})\mathbf{M}[\mathbf{x}_{k-1}^a - \mathbf{x}_{k-1}^t] + \mathbf{K}_k\epsilon_k,\end{aligned}$$

and the initial error is thus propogated by the matrix $(\mathbf{I} - \mathbf{K}_k\mathbf{H})\mathbf{M}$.

$$\begin{aligned}(\mathbf{M} - \mathbf{K}_k\mathbf{H}\mathbf{M})\mathbf{V} &\rightarrow \mathbf{V}\boldsymbol{\Lambda} - \mathbf{V}\boldsymbol{\Pi}\mathbf{V}^T\mathbf{H}^T\mathbf{R}^{-1}\mathbf{H}\mathbf{V}\boldsymbol{\Lambda} \\ &= \mathbf{V}\boldsymbol{\Pi}(\boldsymbol{\Pi}^{-1} - \mathbf{V}^T\mathbf{H}^T\mathbf{R}^{-1}\mathbf{H}\mathbf{V})\boldsymbol{\Lambda} \\ &= \mathbf{V}\boldsymbol{\Pi}\boldsymbol{\Lambda}^{-1}\boldsymbol{\Pi}^{-1},\end{aligned}$$

where the last equality is a result of the Lyapounov equation [42]. Thus for an initial error that lies in $\mathbf{V}$, $\mathbf{e}_0 = \alpha_{e_0}\mathbf{v}$, its magnitude is reduced with each application of the SEIK filter since the eigenvalues of $\boldsymbol{\Pi}\boldsymbol{\Lambda}^{-1}\boldsymbol{\Pi}^{-1}$, i.e. the eigenvalues of $\boldsymbol{\Lambda}^{-1}$, have modulii less than one.

Here we have assumed no model error, i.e. $\mathbf{Q}_k = 0$ for all k. While the algorithm remains stable when there is model noise present, for nonzero $\mathbf{Q}_k$ the low rank of the initial error covariance matrix is not retained and a loss of performance can result. To correct this, one approach is to project the forecast model noise onto the range of the error covariance matrix, ignoring the noise component in the orthogonal complement, as it will be attenuated by the model. Another approach is to reduce the weight of the model forecast, which can be achieved by the introduction of a forgetting factor, ρ. $\mathbf{U}_{k-1}^{-1}$ in (3.7) is multiplied by $\rho < 1$, increasing the magnitude of $\mathbf{P}_k^f$ and more heavily weighing observations. Over assimilation cycles, older model forecasts and

observations cease to influence the analysis at all, i.e. they are "forgotten." This allows the algorithm the additional ability to account for changes in the dynamical process. The forgetting factor also enhances the stability of the filter by reducing error propagation.

As was true for the EKF, the SEEK filter can be disadvantageous in the case of highly nonlinear models. In these instances, the gradient $\mathbf{M}_k$ of the model is only accurate over a very small time period if at all. To combat this issue, the gradient of the model can be recalculated at each assimilation step, however this is generally prohibitively computationally expensive and can nevertheless fail to prevent the introduction of large errors.

3.2.3 Ensemble Kalman Filtering

Another alternative to the EKF is the ensemble Kalman filter (EnKF) [32], proposed by Evensen in 1994 as a Monte Carlo approximation to the EKF. This method is also low rank, though implicitly, as an ensemble of r model states is used to represent the error statistics, where generally $r < n$. The EnKF thus reduces the computational requirements of the EKF. Additionally, the inaccuracy in highly nonlinear models is addressed, as the use of an ensemble generally allows the forecast error covariance to be more accurately estimated than it is in the EKF. The EKF relies on the linearization of $\mathcal{M}_k$ to evolve the initial error covariance matrix. In practical implementations, higher order moments of the model are ignored in this linearization (3.5), which degrades the accuracy of both the estimate of the forecast error covari-

ance and the Kalman filter when models are highly nonlinear. Furthermore, once the initial error covariance matrix is forecasted, it must be stored for the computation of $\mathbf{K}_k$ (3.1) and $\mathbf{P}_k^a$ (3.3). This storage cost can be prohibitive. In the EnKF, both of these issues are avoided. Also, the implementation itself of the EnKF is less computationally intensive than that of the EKF, as the cost of determining the Jacobian of $\mathcal{M}_k$ is completely eliminated.

Rather than linearizing the numerical model to forecast the analyzed error covariance matrix, an ensemble of initial model states representing this matrix, $\mathbf{P}_{k-1}^a$, is forecasted and then used to estimate the statistics of the forecast error. The initial ensemble, $\mathbf{x}_{i,k-1}^a, i = 1, \ldots, r$, is created by adding zero-mean, Gaussian noise to the initial estimate of the state, $\mathbf{x}_{k-1}^a$, in such a way that the sample covariance of the ensemble approximates the initial forecast error covariance:

$$\begin{aligned} \mathbf{P}_{k-1,e}^a &= \overline{(\mathbf{x}_{i,k-1}^a - \overline{\mathbf{x}_{i,k-1}^a})(\mathbf{x}_{i,k-1}^a - \overline{\mathbf{x}_{i,k-1}^a})^T}, \quad i = 1, \ldots, r \\ &\approx \mathbf{P}_{k-1}^a. \end{aligned}$$

Each ensemble member is then forecasted by the nonlinear forecast model:

$$\mathbf{x}_{i,k}^f = \mathcal{M}_k(\mathbf{x}_{i,k-1}^a).$$

The sample covariance of this ensemble is computed and used to estimate the forecast error covariance matrix:

$$\mathbf{P}_{k,e}^f = \overline{(\mathbf{x}_{i,k}^f - \overline{\mathbf{x}_{i,k}^f})(\mathbf{x}_{i,k}^f - \overline{\mathbf{x}_{i,k}^f})^T}, \quad i = 1, \ldots, r.$$

Computing the forecast error covariance this way provides an accurate estimate even in the case of an initial model state with a non-Gaussian probability density function. The sample error covariance of the $\mathbf{x}^f_{i,k}$ is used to compute the Kalman gain matrix (3.1):

$$\mathbf{K}_{k,e} \;=\; \mathbf{P}^f_{k,e}\mathbf{H}^T_k[\mathbf{H}_k\mathbf{P}^f_{k,e}\mathbf{H}^T_k + \mathbf{R}_k]^{-1}.$$

This Kalman gain can then be used to update each member of the forecast ensemble, creating an ensemble of updated states, $\mathbf{x}^a_{i,k}$:

$$\mathbf{x}^a_{i,k} = \mathbf{x}^f_{i,k} + \mathbf{K}_{k,e}(\mathbf{y}^o_k - \mathbf{H}_k\mathbf{x}^f_{i,k}), \quad i = 1, \ldots, r. \tag{3.8}$$

$\mathbf{P}^f_k$ does not have to be stored in order to compute the analysis error covariance, $\mathbf{P}^a_k$ as in (3.3). Instead, the analysis error covariance can be estimated from the sample error covariance of the $\mathbf{x}^a_{i,k}$.

In [15], it was shown that the result of updating each member of the forecast ensemble with the same observations, $\mathbf{y}^o_k$, is an underestimated analysis error covariance. This is because updating each ensemble member with the same observations causes spurious correlations to arise between analyzed model states. Additionally there is no analog to the $\mathbf{K}_k\mathbf{R}_k\mathbf{K}^T_k$ term in the fourth equality of (3.3). This issue was not observed in earlier applications of the EnKF, most likely because these applications were for ocean models, where the observation error covariance, $\mathbf{R}_k$, is generally small. In atmospheric applications, as well as other applications were observation errors are significant, the analysis error covariance is significantly underestimated, and the accuracy

of EnKF is degraded. To remedy this problem, the observations can be treated as random variables. An ensemble of observations, $\mathbf{y}^o_{i,k}, i = 1, \ldots, r$, can be generated from the $\mathbf{y}^o_k$ again through the addition of zero-mean Gaussian noise, where the sample covariance of the $\mathbf{y}^o_{i,k}$ is equal to $\mathbf{R}_k$. The ensemble of observations is then used along with the Kalman filter equations (3.8) to update each member of the forecast ensemble. Although perturbing the observations improves the accuracy of the analysis error covariance estimate, it also introduces additional error to the system, particularly when the size of the ensemble is small. An approach that eliminates this issue is discussed in section 3.2.4.1.

For linear operators, the ensemble Kalman filter converges to the Kalman filter with increasing ensemble size, i.e. as $r \to \infty$. Contrarily, very small ensembles result in poor approximations of the model state that minimizes the analysis error covariance. The ensemble size should be large enough to accurately encompass the relative error covariance matrices of the system. Monte Carlo sampling converges slowly with $r^{-1/2}$, so large ensembles are required for most applications, e.g. $r \geq 100$ [70]. The sampling error that results from using an ensemble to estimate the forecast and analysis error covariances in the Kalman filter equations is an issue that plagues all ensemble Kalman filters, even when r is large. Additionally, when the observations are perturbed, there is sampling error in $\mathbf{R}_k$. These sampling errors can result in inaccurate estimation (generallly underestimation) of $\mathbf{P}^a_k$. The interpolated version of the SEEK filter is an ensemble Kalman filter that minimizes r while maintaining acceptable performance of the filter. It is discussed in section 3.2.4.2.

3.2.4 Square Root Ensemble Kalman Filtering

While the EnKF has been shown to accurately solve the data assimilation problem in the case of a nonlinear forecast model, the perturbation of measurements used to create the ensemble of observations that updates the ensemble of forecasted states becomes an additional source of error in the system. Square root filters have been developed to eliminate this introduction of error. In these methods, rather than updating each member of the ensemble of forecasted states, the Kalman filter update is instead applied to the mean of the forecast ensemble using the unperturbed measurement. An ensemble of analyzed state vectors is then generated by resampling around this updated state.

3.2.4.1 Square Root Ensemble Kalman Filters

The initial error covariance matrix, $\mathbf{P}^a_{k-1}$, is symmetric and positive definite by definition, and as a result it can be represented in terms of "square root" matrices,

$$\mathbf{P}^a_{k-1} = \mathbf{C}^a_{k-1}\mathbf{C}^{aT}_{k-1}.$$

For full rank $\mathbf{P}^a_{k-1}$, $\mathbf{C}^a_{k-1}$ is generally symmetric, and is also rank n. On the other hand, if $\mathbf{P}^a_{k-1}$ is of low rank $r < n$, $\mathbf{C}^a_{k-1}$ is $n \times r$. The decomposition is nonunique, as $\mathbf{P}^a_{k-1} = \mathbf{C}^a_{k-1}\mathbf{C}^{aT}_{k-1} = \mathbf{C}^a_{k-1}\mathbf{U}_{k-1}\mathbf{U}^T_{k-1}\mathbf{C}^{aT}_{k-1}$ for any $r \times r$, orthonormal matrix $\mathbf{U}_{k-1}$. The space spanned by the r columns of $\mathbf{C}^a_{k-1}$, however, is unique. Statistical data assimilation methods which use ensemble representations readily admit a square root formulation, as the sample covariance of

an ensemble of r vectors, $\mathbf{x}_i$, can be expressed in terms of two perturbation matrices, $\mathbf{X}^{'} = [(\mathbf{x}_1 - \overline{\mathbf{x}_i}) \ldots (\mathbf{x}_r - \overline{\mathbf{x}_i})]$. For example, $\mathbf{P}^a_{k-1}$ can be expressed as

$$\mathbf{P}^a_{k-1,\mathbf{e}} = \frac{\mathbf{X}^{a'}_{k-1}\mathbf{X}^{a'T}_{k-1}}{r+1}. \tag{3.9}$$

To compute $\mathbf{P}^f_k$, (each column of) the square root matrix $\mathbf{C}^a_{k-1}$ is evolved by the numerical forecast model, $\mathcal{M}_k$. In the case of a low rank $\mathbf{P}^a_{k-1}$, this can significantly reduce computational costs, as only the r columns of $\mathbf{C}^a_{k-1}$ are evolved rather than the full n columns. From (**??**), we have

$$\begin{aligned}
\mathbf{P}^a_k &= [\mathbf{I} - \mathbf{P}^f_k\mathbf{H}^T_k(\mathbf{H}_k\mathbf{P}^f_k\mathbf{H}^T_k + \mathbf{R}_k)^{-1}\mathbf{H}_k]\mathbf{P}^f_k \\
&= \mathbf{C}^f_k[\mathbf{I} - \mathbf{C}^{fT}_k\mathbf{H}^T_k(\mathbf{H}_k\mathbf{C}^f_k\mathbf{C}^{fT}_k\mathbf{H}^T_k + \mathbf{R}_k)^{-1}\mathbf{H}_k\mathbf{C}^f_{k-1}]\mathbf{C}^{fT}_{k-1} \\
&= \mathbf{C}^f_k(\mathbf{I} - \mathbf{S}_k\mathbf{D}^{-1}_k\mathbf{S}^T_k)\mathbf{C}^{fT}_k,
\end{aligned}$$

where $\mathbf{S}_k = (\mathbf{H}_k\mathbf{C}^f_k)^T$ and $\mathbf{D}_k = \mathbf{S}^T_k\mathbf{S}_k + \mathbf{R}_k$. An eigenvalue deomposition of $\mathbf{D}_k$ yields

$$\begin{aligned}
\mathbf{P}^a_k &= \mathbf{C}^f_k(\mathbf{I} - \mathbf{S}_k\mathbf{X}_k\mathbf{\Lambda}^{-1}_k\mathbf{X}^T_k\mathbf{S}^T_k)\mathbf{C}^{fT}_k \\
&= \mathbf{C}^f_k[\mathbf{I} - (\mathbf{S}_k\mathbf{X}_k\mathbf{\Lambda}^{-1/2}_k)(\mathbf{S}_k\mathbf{X}_k\mathbf{\Lambda}^{-1/2}_k)^T]\mathbf{C}^{fT}_k \\
&= \mathbf{C}^f_k[\mathbf{I} - (\mathbf{U}_k\mathbf{\Sigma}_k\mathbf{V}^T_k)(\mathbf{U}_k\mathbf{\Sigma}_k\mathbf{V}^T_k)^T]\mathbf{C}^{fT}_k \\
&= \mathbf{C}^f_k(\mathbf{I} - \mathbf{U}_k\mathbf{\Sigma}_k\mathbf{\Sigma}^T_k\mathbf{U}^T_k)\mathbf{C}^{fT}_k \\
&= \mathbf{C}^f_k\mathbf{U}_k(\mathbf{I} - \mathbf{\Sigma}_k\mathbf{\Sigma}^T_k)\mathbf{U}^T_k\mathbf{C}^{fT}_k \\
&= (\mathbf{C}^f_k\mathbf{U}_k\sqrt{\mathbf{I} - \mathbf{\Sigma}_k\mathbf{\Sigma}^T_k})(\mathbf{C}^f_k\mathbf{U}_k\sqrt{\mathbf{I} - \mathbf{\Sigma}_k\mathbf{\Sigma}^T_k})^T \\
&= \mathbf{C}^a_k\mathbf{C}^{aT}_k,
\end{aligned}$$

where $\mathbf{U}_k\mathbf{\Sigma}_k\mathbf{V}_k^T$ is a singluar value decomposition of $\mathbf{S}_k\mathbf{X}_k\mathbf{\Lambda}_k^{-1/2}$, and thus the square root matrix of $\mathbf{P}_k^a$ can be computed as an update of the square root matrix of $\mathbf{P}_k^f$:

$$\mathbf{C}_k^a = \mathbf{C}_k^f\mathbf{U}_k\sqrt{\mathbf{I}-\mathbf{\Sigma}_k\mathbf{\Sigma}_k^T}.$$

The class of square root filters includes the ensemble Kalman filter, however, the term is generally reserved to refer to those filters which do not require the perturbation of measurements for the update of the forecasted model state. By (3.8), the update to the ensemble of forecasted states can be expressed as

$$\begin{aligned}
\mathbf{X}_k^a &= \mathbf{X}_k^f + \mathbf{P}_k^a\mathbf{H}^T\mathbf{R}_k^{-1}(\mathbf{Y}_k^o - \mathbf{H}_k\mathbf{X}_k^f) \\
&= \mathbf{X}_k^f + \mathbf{C}_k^a\mathbf{C}_k^{aT}\mathbf{H}^T\mathbf{R}_k^{-1}(\mathbf{Y}_k^o - \mathbf{H}_k\mathbf{X}_k^f) \\
&= \mathbf{X}_k^f + \left(\mathbf{C}_k^f\mathbf{U}_k\sqrt{\mathbf{I}-\mathbf{\Sigma}_k\mathbf{\Sigma}_k^T}\right)\left(\mathbf{C}_k^f\mathbf{U}_k\sqrt{\mathbf{I}-\mathbf{\Sigma}_k\mathbf{\Sigma}_k^T}\right)^T\mathbf{H}^T\mathbf{R}_k^{-1}(\mathbf{Y}_k^o - \mathbf{H}_k\mathbf{X}_k^f) \\
&= \mathbf{X}_k^f + \mathbf{C}_k^f\mathbf{U}_k(\mathbf{I}-\mathbf{\Sigma}_k\mathbf{\Sigma}_k^T)\mathbf{U}_k^T\mathbf{C}_k^{fT}\mathbf{H}^T\mathbf{R}_k^{-1}(\mathbf{Y}_k^o - \mathbf{H}_k\mathbf{X}_k^f) \\
&= \mathbf{X}_k^f + \frac{\mathbf{X}_k^{f'}}{\sqrt{n-1}}(\mathbf{C}_k^{fT}\mathbf{H}^T\mathbf{R}_k^{-1} - \mathbf{U}_k\mathbf{\Sigma}_k\mathbf{\Sigma}_k^T\mathbf{U}_k^T\mathbf{C}_k^{fT}\mathbf{H}^T\mathbf{R}_k^{-1})(\mathbf{Y}_k^o - \mathbf{H}_k\mathbf{X}_k^f) \\
&= \mathbf{X}_k^f + \frac{\mathbf{X}_k^{f'}}{\sqrt{n-1}}(\mathbf{S}_k\mathbf{R}_k^{-1} - \mathbf{U}_k\mathbf{\Sigma}_k\mathbf{\Sigma}_k^T\mathbf{U}_k^T\mathbf{S}_k\mathbf{R}_k^{-1})(\mathbf{Y}_k^o - \mathbf{H}_k\mathbf{X}_k^f) \\
&= \mathbf{X}_k^f + \frac{\mathbf{X}_k^{f'}}{\sqrt{n-1}}(\mathbf{S}_k\mathbf{R}_k^{-1} - \mathbf{S}_k\mathbf{D}_k^{-1}\mathbf{S}_k^T\mathbf{S}_k\mathbf{R}_k^{-1})(\mathbf{Y}_k^o - \mathbf{H}_k\mathbf{X}_k^f) \\
&= \mathbf{X}_k^f + \frac{\mathbf{X}_k^{f'}}{\sqrt{n-1}}\mathbf{S}_k(\mathbf{R}_k^{-1} - \mathbf{D}_k^{-1}\mathbf{S}_k^T\mathbf{S}_k\mathbf{R}_k^{-1})(\mathbf{Y}_k^o - \mathbf{H}_k\mathbf{X}_k^f) \\
&= \mathbf{X}_k^f + \frac{\mathbf{X}_k^{f'}}{\sqrt{n-1}}\mathbf{S}_k\left[\mathbf{R}_k^{-1} - (\mathbf{S}_k^T\mathbf{S}_k + \mathbf{R}_k)^{-1}\mathbf{S}_k^T\mathbf{S}_k\mathbf{R}_k^{-1}\right](\mathbf{Y}_k^o - \mathbf{H}_k\mathbf{X}_k^f) \\
&= \mathbf{X}_k^f + \mathbf{X}_k^{f'}\mathbf{S}_k\mathbf{D}_k^{-1}(\mathbf{Y}_k^o - \mathbf{H}_k\mathbf{X}_k^f). \qquad (3.10)
\end{aligned}$$

Here, $\mathbf{X}_k^a$, $\mathbf{X}_k^f$, and $\mathbf{Y}_k^o$ are the matrices with columns equal to the members of the analysis, forecast, and observation ensembles, respectively, and the forecast ensemble members with the mean, $\overline{\mathbf{x}_{i,k}^f}$, removed form the columns of $\mathbf{X}_k^{f'}$. The mean of the analysis ensemble can be obtained by right-multiplying (3.10) by $\mathbf{1}_n$, the $n \times n$ matrix whose entries are $1/n$, and gives

$$\overline{\mathbf{x}_{i,k}^a} = \overline{\mathbf{x}_{i,k}^f} + \mathbf{X}_k^{f'} \mathbf{S}_k \mathbf{D}_k^{-1} (\mathbf{y}_k^o - \mathbf{H}_k \overline{\mathbf{x}_{i,k}^f}).$$

Thus, rather than taking the mean of the analysis ensemble to be the updated state, $\mathbf{x}_k^a$ can be obtained directly by applying the Kalman filter equations to the mean of the forecast ensemble. Then from (3.9), an ensemble of analyzed states can be resampled by adding the columns of $\mathbf{X}_k^{a'} = (\sqrt{n+1})\mathbf{C}_k^f \mathbf{U}_k \sqrt{\mathbf{I} - \mathbf{\Sigma}_k \mathbf{\Sigma}_k^T} \mathbf{\Omega}_k$ to $\mathbf{x}_k^a$, where the $n \times n$ orthonormal matrix $\mathbf{\Omega}_k$ is included to redistribute the variance of the ensemble members $\mathbf{x}_{i,k}^a$. By updating the mean of the ensemble of forecasted states rather than updating each forecast ensemble member, the sampling issues associated with the use of perturbed observations are avoided.

Examples of algorithms belonging to the class of square root Kalman filters are the ensemble transform Kalman filter [10], the ensemble adustment Kalman filter [4], and the ensemble square root Kalman filter [101]. These methods are compared in [90]. An additional algorithm has since been developed and is discussed in [30]. In [71], it was shown that the statistical data assimilation method used in this work, the singular evolutive interpolated Kalman (SEIK) filter, is a square root Kalman filter as well.

3.2.4.2 Singular Evolutive Interpolated Kalman Filter

The singular evolutive interpolated Kalman (SEIK) filter is the Monte Carlo approximation to the SEEK filter. Both the SEEK and SEIK filters were developed in 1998, prior to the development of square root ensemble Kalman filters (in the sense described above), however the equivalence of the methods has been shown [71]. Square root filters decompose the initial error covariance matrix, $\mathbf{P}^a_{k-1}$, into two matrices, $\mathbf{C}^a_{k-1}\mathbf{C}^{aT}_{k-1}$, a square root matrix and its transpose. This square root matrix is then forecasted and updated in the analysis step. The SEIK filter, on the other hand, decomposes the initial error covaraiance matrix into three matrices, $\mathbf{L}_{k-1}\mathbf{U}_{k-1}\mathbf{L}^T_{k-1}$, and updates the matrix $\mathbf{U}_{k-1}$. The matrix $\mathbf{L}_{k-1}$ is the square root of the error covariance and is effectively transformed analogously to $\mathbf{C}_{k-1}$ of the square root Kalman filter [71]. One main difference between the square root Kalman filter and the SEIK filter is that after the model state, $\mathbf{x}^f_k$, is updated, the ensemble is resampled stochasticly. This differs from square root Kalman filters, which generally resample the ensemble deterministically.

The SEIK filter was developed to address the issues of the SEEK filter in the same way the ensemble Kalman filter was developed to address the issues of the extended Kalman filter [46]. Again the initial error covariance is represented using an ensemble of states, however, the size of this ensemble can be minimized due to the reduced rank of this matrix. In this case, the ensemble only contains $r+1$ members. Additionally, an ensemble formulation is used to represent the matrix $\mathbf{H}_k\mathbf{L}_k$ used in (3.7) and (3.8), avoiding the

linearization required of the observation operator when $\mathcal{H}_k$ is nonlinear.

In comparison to the EnKF, the SEIK filter minimizes computational cost by using a low rank representation of the initial error covariance in the same way that the SEEK filter minimizes the cost of the EKF. Again, this can be done without degrading the filter performance, provided the numerical forecast model admits an attractor, a common assumption in ocean modeling. The SEIK filter is then constructed to operate on the low-dimensional subspace of the attractor, as described above in section 3.2.2.

The forecast and analysis steps of the SEIK filter differ from those of the SEEK filter only slightly. An ensemble of initial state vectors, $\mathbf{x}^a_{i,k-1}$, is first determined from an initial estimate of the model state, $\mathbf{x}^a_{k-1}$, and the factored form of its corresponding error covariance, $\mathbf{P}^a_{k-1} = \mathbf{L}_{k-1}\mathbf{U}_{k-1}\mathbf{L}^T_{k-1}$. As in the SEEK filter, $\mathbf{L}_{k-1}$ is $n \times r$, and $\mathbf{U}_{k-1}$ is an $r \times r$ positive definite matrix, where $r << n$ is the rank of $\mathbf{P}^a_{k-1}$. A Cholesky factor of $\mathbf{U}^{-1}_{k-1}$, $\mathbf{C}_{k-1}$, is computed and multiplied by an $(r+1) \times r$ random matrix, $\mathbf{\Omega}_{k-1}$ with orthonormal columns and zero column sums. $\mathbf{P}^a_{k-1}$ can thus be written as

$$\mathbf{P}^a_{k-1} = \mathbf{L}_{k-1}(\mathbf{C}^{-1}_{k-1})^T\mathbf{\Omega}^T_{k-1}\mathbf{\Omega}_{k-1}\mathbf{C}^{-1}_{k-1}\mathbf{L}^T_{k-1}.$$

The result of introducing $\mathbf{\Omega}_{k-1}$ is a stochastic sampling of the initial state:

$$\mathbf{x}^a_{i,k-1} = \mathbf{x}^a_{k-1} + \sqrt{r+1}\mathbf{L}_{k-1}(\mathbf{\Omega}_{k-1}\mathbf{C}^{-1}_{k-1})^T, i = 1, \ldots, r+1.$$

As in the EnKF, the nonlinear model is applied to this ensemble of initial state vectors to create an ensemble of forecasted state vectors, $\mathbf{x}^f_{i,k}$. The average of

these, $\overline{\mathbf{x}^f_{i,k}}$, is then considered as the forecasted state, and the sample covariance is considered as the forecast error covariance, which can be represented as

$$\mathbf{P}^f_k = \mathbf{L}_k \mathbf{U}_{k-1} \mathbf{L}^T_k + \mathbf{Q}_k, \tag{3.11}$$

where

$$\begin{aligned} \mathbf{L}_k &= [\mathbf{x}^f_{1,k} - \overline{\mathbf{x}^f_{i,k}} \dots \mathbf{x}^f_{r+1,k} - \overline{\mathbf{x}^f_{i,k}}]\mathbf{T} \\ &= [\mathbf{x}^f_{1,k} \dots \mathbf{x}^f_{r+1,k}]\mathbf{T}, \end{aligned} \tag{3.12}$$

and

$$\mathbf{U}_{k-1} = [(r+1)\mathbf{T}^T\mathbf{T}]^{-1}.$$

Here, $\mathbf{T}$ is an $(r+1) \times r$ full rank matrix with zero column sums. It subtracts the mean of the columns of a matrix it left multiplies from each of those columns, so the second equality in (3.12) holds because of its inclusion, and (3.11) is in fact the sample error covariance of the $\mathbf{x}^f_{i,k}$.

In the analysis step, $\mathbf{U}_{k-1}$ is updated through its inverse, just as in the SEEK filter, however with the new definition of $\mathbf{U}^{-1}_{k-1}$, this equation is no longer recursive:

$$\mathbf{U}^{-1}_k = \mathbf{U}^{-1}_{k-1} + (\mathcal{H}_k \mathbf{L}_k)^T \mathbf{R}^{-1}_k (\mathcal{H}_k \mathbf{L}_k).$$

Here, $\mathcal{H}_k \mathbf{L}_k$ is computed by applying the observation operator $\mathcal{H}_k$ to the columns of $\mathbf{L}_k$ (3.12). $\mathbf{U}_k$ and $\mathcal{H}_k \mathbf{L}_k$ are then used to compute the Kalman gain matrix,

$$\mathbf{K}_k = \mathbf{L}_k \mathbf{U}_k (\mathcal{H}_k \mathbf{L}_k)^T \mathbf{R}^{-1}_k,$$

and the forecasted state is updated by the current data:

$$\mathbf{x}_k^a = \mathbf{x}_k^f + \mathbf{K}_k(\mathbf{y}_k^o - \mathcal{H}_k\mathbf{x}_k^f). \tag{3.13}$$

The analysis error covariance can be written as

$$\mathbf{P}_k^a \;=\; \mathbf{L}_k\mathbf{U}_k\mathbf{L}_k^T. \tag{3.14}$$

We have chosen to utilize the SEIK filter for state estimation in previous work [16, 3] as it provides the benefits specific to both a square root Kalman filter as well as a reduced rank Kalman filter; an ensemble is used to accurately capture the error statistics of the system without introducing additional observation noise to the system, and the size of the ensemble is minimized without sacrificing the filter's effectiveness. In this work, in our efforts to accurately estimate coastal ocean model parameters, we again utilize the SEIK filter.

3.3 Statistical Data Assimilation for Parameter Estimation

While state estimation is beneficial in describing the state of a physical system at one particular instance, larger scientific contributions can be made through the estimation of model parameters; reducing the uncertainty in a model's parameters will result in reduced uncertainty in the model state, however the converse is not true. Parameter estimation is thus a worthwhile endeavor. Historically, model parameters have been estimated using varia-

tional methods, however, in this work we seek to estimate parameters using statistical data assimilation methods.

As previously discussed, statistical data assimilation methods do not require the use of adjoint models. They are nonintrusive and relatively straightforward to implement. In addition, they provide statistical information regarding the uncertainty associated with the estimated parameters, specifically the second order moments. Also, many statistical data assimilation methods are filters as opposed to smoothers, and this allows parameters to be estimated sequentially as new data becomes available, making these methods more appropriate for online applications. Finally, they allow parameters to vary in time, which is useful when representing time-varying models.

While statistical data assimilation methods are used to compensate for various sources of uncertainty, parameters are traditionally assumed to be known and data assimilation methods are implemented to estimate the model state variables. In recent years, statistical data assimilation methods have been used to estimate parameters by two different methods, known as joint estimation and dual estimation. In joint estimation, parameters are treated as state variables and are simply appended to the vector of model state variables to be estimated. Parameters can then be estimated along with the state variables using statistical data assimilation methods. In dual estimation, on the other hand, two separate state spaces are used to represent the model state and the model parameters. Each of the "state" vectors are then forecasted and updated by two distinct filters. We describe both methods in detail here.

3.3.1 Joint Estimation

In 2001, Anderson showed that the EnKF could be used to estimate the parameters of a complex nonlinear model through joint estimation [4]. In this process, uncertain model parameters are considered to be part of the model state, and are appended to the initial state vector. For this reason, joint estimation is also commonly referred to as state augmentation. The appended parameters are then forecasted and analyzed along with the state variables.

An initial guess of the model parameters, $\mathbf{w}_{k-1}^a$, is appended to the initial state vector, $\mathbf{x}_{k-1}^a$, to form the state-parameter vector, $\tilde{\mathbf{x}}_{k-1}^a$:

$$\tilde{\mathbf{x}}_{k-1}^a = \begin{bmatrix} \mathbf{x}_{k-1}^a \\ \mathbf{w}_{k-1}^a \end{bmatrix}.$$

For ensemble methods, an initial ensemble of state-parameter vectors can be created by adding Gaussian noise to $\tilde{\mathbf{x}}_{k-1}^a$. The magnitude of the variance in this noise significantly impacts the ability of Kalman filters to accurately estimate the parameters, so it is important to choose it carefully. Ideally, the noise added to the model parameters should reflect the uncertainty in the values. A procedure for the initialization of parameters is described in [1].

After augmenting the state vector with the initialized parameters, only a few modifications to the Kalman filter equations are necessary to estimate the true parameter values. The evolution of the model parameters is often considered to be a stationary process, and so the (state) numerical forecast model, $\mathcal{M}_k$, can be modified so that the parameters remain constant after the

model is applied:

$$\tilde{\mathbf{x}}_k^f = \begin{bmatrix} \mathbf{x}_k^f \\ \mathbf{w}_k^f \end{bmatrix} = \begin{bmatrix} \mathcal{M}_k \mathbf{x}_{k-1}^a \\ \mathbf{w}_{k-1}^a \end{bmatrix} = \tilde{\mathcal{M}}_k \tilde{\mathbf{x}}_{k-1}^a,$$

and so $\tilde{\mathcal{M}}_k := \begin{bmatrix} \mathcal{M}_k & \mathbf{I}_k \end{bmatrix}$. The model parameters are not observed,

$$\tilde{\mathcal{H}}_k \tilde{\mathbf{x}}_k^f = \begin{bmatrix} \mathcal{H}_k \mathbf{x}_k^f \\ \mathbf{0} \end{bmatrix},$$

and so the observation operator, $\mathcal{H}_k$, can easily be modified by appending zeros: $\tilde{\mathcal{H}}_k := \begin{bmatrix} \mathcal{H}_k & \mathbf{0} \end{bmatrix}$. Finally, the initial error covariance matrix should be reformulated as a cross-covariance matrix, $\tilde{\mathbf{P}}_{k-1}^a$, describing the relationship between the errors in $\mathbf{x}_{k-1}^a$ and $\mathbf{w}_{k-1}^a$. With these modifications, the forecast and analysis steps for estimating $\tilde{\mathbf{x}}_k^a$ using statistical data assimilation methods are the same as in any of the state estimation methods previously discussed, and Kalman filters can be used to estimate both the model state and unknown parameters as well as the respective error statistics.

Several properties of joint estimation make this method a desirable approach to parameter estimation. Most obviously, the implementation of this method is straightforward. Particularly when statistical data assimilation has already been implemented, the parameters only need to be appended to the state vector and only simple modifications need to be made to the dynamical and observation operators. As is the case for state estimation, the computational cost of this method is modest, and information about the error in the parameter estimates is provided.

There are practical considerations that should be made when implementing this approach. First, the initial cross-covariance matrix $\tilde{\mathbf{P}}_{k-1}^a$ is gen-

erally unknown and must be estimated. This issue also arises in state estimation, however the introduction of the second variable adds an additional layer of complexity. Also, the cross-covariance matrix can be extremely ill-conditioned when the state variables and parameter variables have vastly different scales. One way to improve the condition number of this matrix is by scaling the model variables by (an approximation to) the standard deviation of the state and parameter variables, respectively.

Another issue surrounds the assumption that the parameter is stationary. The analysis step of the assimilation reduces the variance in the ensemble of augmented states. The forecast model increases this variance in the state variables, however the parameter evolution is considered a stationary process, causing the parameter variance to become increasingly narrow over assimilation cycles, i.e. the ensemble members eventually collapse. The effect of this is a continuously decreasing impact of the observations in the analysis step, which often results in filter divergence. There are several techniques that can be employed to effectively prevent this collapse of the ensemble. (Additional) noise can be added to the observations as proposed in the EnKF for state estimation, however, this again is problematic as it introduces additional uncertainty to an already uncertain system. Additional ensemble members can be generated by linear combinations of the augmented states or through the back projection of the residuals between the analyzed states and the data [82, 83]. However, this approach increases the computational storage costs as well as the cost of filtering. Most commonly an inflation factor is used.

In this case, the posterior standard deviation is inflated by some factor to maintain the variance in the ensemble members. This approach was applied in [1], where the covariance inflation factor used was conditional. A conditional inflation factor is only applied when the standard deviation falls below some predetermined value, chosen to reflect the acceptable variability of the corresponding parameter. This way the parameter ensemble always has some minimum spread but that spread is prevented from growing uncontrollably. Aksoy et al. [1] found that this approach is effective for some but not all model parameters; the effectiveness of the inflation factor is dependent on the parameter being estimated.

In joint estimation, there are no observations of parameter values; information is only available indirectly through observations of state variables, which are also being estimated. The model state is thus adjusted toward the observations directly, whereas the parameters are not. As a result, model state variables consistently converge to the true state more rapidly than the parameters converge to their true values; more assimilation cycles are required for joint estimation than for state estimation. Also, it has been found that the effectiveness of joint estimation is significantly influenced by the size of the ensembles and the observation locations [1].

Joint estimation has been successfully implemented for a variety of problems. In [4], an ensemble based method is used to estimate the state and forcing parameter of a Lorenz model. The root mean square error (RMSE) of the estimated states is nearly identical to that obtained when the correct

forcing parameter is used. The RMSE of the forcing parameter was also small. These results indicate that joint estimation successfully estimates a parameter of a simplified model using an ensemble statistical data assimilation method. In 2005, Annan et al. [5] apply joint estimation to a simplified global climate model using the EnKF. This is the first application of the method to a realistic, large scale model. In this study, twelve parameters describing the ocean, atmosphere, and ice are estimated for the steady state solution of the model. The global domain is divided into many subregions and the estimation is performed locally across each. Then an average of all of the local parameter estimates is taken to determine a global estimate. The study finds that though it is difficult to accurately recover multiple parameters, all twelve parameters are estimated within distributions consistent with the true values. Additionally, the width of the posterior parameter distribution is comparable to the difference between the truth and the posterior mean. Aksoy et al. [1] apply joint estimation to a two-dimensional sea breeze model using a square root filter. They aim to reduce parametric model error when the initial conditions are also uncertain by focusing on this model which has a shorter time scale. They estimate combinations of six model parameters believed to significantly impact sea-breeze circulation. The estimation of any single model parameter is found to be very successful, with RMSE indistinguishable from the respective cases when the true parameter is used. However, when multiple parameters are estimated simultaneously, the level of improvement declines as the attempt to improve the estimate of one parameter influences the estimation

of the others. Jafarpour and McLaughlin [49] use joint estimation to estimate the permeability field in a reservoir model. The permeability is treated as a spatially variable random field and is discretized by dividing the model domain into grid blocks. The EnKF is then used to estimate the grid block values of the permeability in addition to the pressure and saturation. Their findings indicate that joint estimation is able to accurately retrieve the large scale features of the permeability field, though recovering small scale features is more difficult. Furthermore, the Kalman filter updates continuously improve the predictive power of the reservoir model. Finally, in [45], joint estimation is used to estimate parameters in a groundwater flow model with the EnKF. In this case, the parameters are spatially and temporally variable. The method significantly reduced the RMSE in the parameters when a sufficient ensemble size was used. Though we are not claiming that this summary of implementations is exhaustive, joint estimation is clearly a promising approach for using statistical data assimilation methods to estimate various types of parameters in a large variety of numerical forecast models.

3.3.2 Dual Estimation

Dual estimation is another approach to parameter estimation that utilizes statistical data assimilation methods. While joint estimation makes use of a single Kalman filter applied to one state vector that has been augmented with the uncertain model parameters, dual estimation makes use of two Kalman filters run simultaneously. Dual estimation was proposed in the 1970s by Nelson

and Stear as an alternative to joint estimation [69]. Two separate state space representations are used for the model state variables and the model parameters, respectively. Then, one Kalman filter is formulated to estimate the state while the other is formulated to estimate the parameters.

For the state, the numerical forecast model, $\mathcal{M}_k^{\mathbf{x}}$, and the observation operator $\mathcal{H}_k^{\mathbf{x}}$, are identical to those operators described in Section 3.1. For the parameters, it is necessary that the operators be reformulated. As in joint estimation, the parameter evolution is considered to be a stationary process. The parameter transition operator, $\mathcal{M}_k^{\mathbf{w}}$, is consequently set to the identity, and

$$\mathbf{w}_k^f = \mathbf{w}_{k-1}^a + \epsilon_k. \tag{3.15}$$

To represent (artificial) model error, process noise, ϵ_k, can again be added to the parameters as part of the forecast step. This is an option often implemented to prevent the collapse of the variance in the parameter ensemble, though we will not use this technique in the numerical results shown in this work. For the parameter observation operator, $\mathcal{H}_k^{\mathbf{w}}$, the (observed) output of a numerical forecast model can be considered as a nonlinear observation of the model parameters. $\mathcal{H}_k^{\mathbf{w}}$ can thus be set to the numerical forecast model of the state. Specifically, it is the composition of the state observation operator and the state forecast model, where the forecasted parameters, $\mathbf{w}_k^f$ (from), are used in the state forecast model:

$$\mathcal{H}_k^{\mathbf{w}}\mathbf{w}_k^f = \mathcal{H}_k^{\mathbf{x}}[\mathcal{M}_k^{\mathbf{x}}(\mathbf{x}_{k-1}^a, \mathbf{w}_k^f)].$$

Note that in this case there is a high probability that the parameter observation operator is nonlinear. With the addition of these parameter operators, the Kalman filter equations can be used to estimate the parameter variables of the numerical model. The residual between the "forecasted" parameters and observations can be computed, and the model parameters can be updated using any statistical data assimilation method in the same way that model state variables are updated:

$$\mathbf{w}_k^a = \mathbf{w}_k^f + \mathbf{K}_k^{\mathbf{w}}(\mathbf{y}_k^o - \mathcal{H}_k^{\mathbf{w}}\mathbf{w}_k^f). \tag{3.16}$$

The updated parameters are then used to estimate the model state:

$$\begin{aligned} \mathbf{x}_k^f &= \mathcal{M}_k^{\mathbf{x}}(\mathbf{x}_{k-1}^a, \mathbf{w}_k^a) \\ \mathbf{x}_k^a &= \mathbf{x}_k^f + \mathbf{K}_k^{\mathbf{x}}(\mathbf{y}_k^o - \mathcal{H}_k^{\mathbf{x}}\mathbf{x}_k^f), \end{aligned}$$

and the updated model state can then be used to estimate the model parameter for recursive parameter and state estimation.

Upon its introduction, the primary application of dual estimation was estimating the weights in a neural network [69]. In 1989, Singhal and Wu first applied it to a nonlinear model, using the EKF [80]. Wan et al. estimated the parameters in two simple time series to compare the effectiveness of the unscented Kalman filter (which can be classified as a square root filter [97]) and an ensemble-based Kalman filter [96]. They found that the square root filter had superior performance for parameter estimation. In [58], dual estimation was used to estimate parameters in a snow model using the EnKF, a

square root Kalman filter, and a particle filter. All of the methods improved the snow model forcasts, although they found that in one case the square root filter suffered from ensemble collapse. This is one example of the importance of sufficient variation in model parameters, which we discuss further in Chapter 5. In [23], the EnKF was used to estimate the parameters in two hydrological models, with varying complexity. They found that while dual estimation accurately predicted model parameters, it tended to underestimate the uncertainty of the prediction. They also found that the accuracy of dual estimation was model dependent and that more complex models are better at uncertainty prediction. Though these are just a few examples of the implementation of dual estimation, it is clear that this method has been a successful approach to parameter estimation for a wide array of numerical models.

Both joint and dual estimation are ideal for cases when both the state and parameters of a model contain uncertainty. As is the case for all statistical data assimilation methods, both provide estimates of the state and parameter as well as estimates of their uncertainty; a probabilistic characterization of the parameter replaces the traditionally deterministic view, providing more complete information. Additionally, these approaches do not suffer from the curse of dimensionality in the same way as variational methods; the computational costs of the methods remain low even as the number of parameters to be estimated increases, as the most expensive component in computing the Kalman gain matrix is a matrix inversion (3.1), which is dependent, not on the number of parameters being estimated, but on the number of data ob-

served. In theory, joint estimation should provide better estimates of the state variables and model parameters, as joint estimation takes into account the relationship between the state variables and the model parameters through the cross-covariance matrix, whereas the dual filter does not. In practice, however, this is not observed [96]. This is likely because although the cross-covariance between the state variables and parameters exists, it is not well estimated, and thus the initial cross-covariance matrix used in the filtering equations is only a guess of the true matrix. Furthermore, the estimation of $\tilde{\mathbf{P}}^{a}_{k-1}$ may actually introduce *more* error to the system.

There are also several issues to be considered when using dual estimation. In contrast to joint estimation, dual estimation assumes that the state variables and model parameters are uncorrelated, but due to the very nature of the algorithm, it is obvious this is not true. Additionally, in this method the state variables are used to update the model parameters, which are then used to update the state variables. The error in each filter should thus be accounted for by the other, however, this generally does not occur. And finally, it has been shown that the convergence of dual estimation methods is strongly influenced by the artificial process noise used in the forecast of the model parameters, however this is another value used in the filter equations that is often unknown, and additional uncertainty is introduced to the system when artificial process noise is included. For both joint and dual estimation, it should be considered that the indirect observations of model parameters may not be sufficient to accurately estimate parameters in highly complex numerical mod-

els. It is true that some observations may have stronger influences on various model parameters, however, in statistical data assimilation, all observations are equally weighted. There is no natural way to restrict which observations are used to update the model parameters (e.g. through the Kalman gain matrix), and as a result the data assimilation can be adversely affected by too many observations that have little relation to the model parameters of interest. Even with these considerations, we feel that the benefits of dual estimation makes this parameter estimation method preferable to many others.

One of the major drawbacks of using statistical data assimilation methods for state estimation, joint estimation, and dual estimation is that updates to model state variables are not always physical. For example, coastal ocean models are formulated under the assumption that mass and momentum is conserved, however, this assumption is generally violated when coastal ocean model states (i.e. water elevations and currents) are updated by the Kalman filter equations; in these cases, mass (water) and momentum (through updates of the velocity) are usually either added to or removed from the system. One way to circumvent this issue is to use the statistical data assimilation methods for parameter estimation only. In fact, when the joint estimation and dual estimation methods update only the model parameter, the two methods are equivalent. By restricting the methods to parameter estimation only, all of the benefits of statisitical data assimilation are retained, while preserving the properties that govern the physical system. This is the approach we will use for the estimation of the Manning's n friction coefficient parameter in this

work.

There are several issues inherent to parameter estimation problems, regardless of the solution methodology. Although *updating* a model parameter rather than the model state is physically sound, the value resulting from the update may not be; the estimated parameter may be prescribed a nonphysical value. For example, the Manning's n coefficient is a small, positive number, with values typically ranging from 0 to $\sim$0.2 (Table 2.1). If a parameter estimation method prescribes a negative Manning's n coefficient, the value will be squared in the formulation of the bottom stress term in the momentum equations (2.2), and in this case the sign of the coefficient does not adversely affect the model solution. However, an estimate that is too large simply does not make physical sense and for many model parameters, this type of issue can be especially problematic, resulting in nonphysical forecasts of the model state or even causing the numerical model to become unstable. Another issue that plagues parameter estimation is computational cost. Parameter estimation using statistical data assimilation is significantly less computationally expensive than other methods, however, for real-time forecasting, it can become prohibitively costly when the parameter vector is large. Consider, for example, a spatially variable parameter that is defined at every vertex in the computational domain. For realistic domains, where the number of vertices is sometimes as large as several million, the storage requirements alone may be prohibitive. Additionally, in the case when parameter values are spatially correlated, the storage and estimation itself can be wasteful. Lastly, what is

perhaps the most significant issue in parameter estimation is that these types of problems are often ill-posed; multiple parameters can result in very similar model output, and the parameter estimation problem does not have a unique solution. Though we cannot completely solve all of these issues with statistical data assimilation methods alone, we can mitigate them by choosing an appropriate representation of the parameter we estimate. We discuss this further in Chapter 4.

Chapter 4

Stochastic Processes

The Manning's n coefficient is a parameter that is highly variable in space (e.g. see Figure 2.1). These types of parameters are particularly difficult to estimate as it is necessary to first describe them deterministically, adding another layer of complexity to the estimation problem. An obvious approach to describing such a parameter is to specify its values at every vertex of the discretized domain. The resulting parameter vector of nodal values can then be estimated using established parameter estimation techniques. However, for any nontrivial discretization of a spatial domain, this results in a parameter vector of large dimension, increasing the computational cost of the parameter estimation methods by potentially prohibitive amounts. Additionally, if the parameter values are continuous on the model domain, neighboring values are correlated and this pointwise estimation is inefficient. Also, it is often the case that numerical models, though sensitive to a particular parameter, are not sensitive to its value at every point in the computational domain. Thus, we find that a more effective approach to deterministically describing a spatially varying parameter is to model it as a stochastic process. The stochastic process can then be represented as a series of random variables and the parameter estimation problem is reduced to estimating a finite number of them. This

approch not only provides a method for representing the parameter, but the corresponding uncertainty in the parameter values as well.

4.1 Stochastic Processes

Stochastic processes can be used to define quantities that are not known exactly. A stochastic process, $\omega(\mathbf{x}, \theta)$, is a function defined on the product space $\mathbf{D} \times \Omega$, where $\mathbf{x} \in \mathbf{D}$, the index set of random variables (often the physical problem domain), and $\theta \in \Omega$, the sample space (i.e. the set of possible outcomes) of the probability space, $(\Omega, \mathcal{F}, P)$. (Here, $\mathcal{F}$ is the set of events and P maps each event to its probability). For a fixed $\mathbf{x}$ and variable θ, $\omega(\mathbf{x}, \cdot)$ is a random variable defined at location $\mathbf{x}$. For fixed θ and variable $\mathbf{x}$, $\omega(\cdot, \theta)$ is a sample, or realization, of the stochastic process defined over the entire domain $\mathbf{D}$. Thus fixed $\mathbf{x}$ and fixed θ gives $\omega(\mathbf{x}, \theta)$, a number representing a realization θ of the random variable at location $\mathbf{x}$. By defining model quantities of interest as stochastic processes, information about the uncertainty in the quantities can also be expressed, as the process defines a random variable with a probability density function and statistical moments at every point, $\mathbf{x}$, in the domain.

The probability distribution of a random variable can be described through its statistical moments. The moments are weighted averages of functions of the random variable, defined using Lebesgue integration. A power of the random variable is first weighted by its probability density function, $f(\omega)$,

and then integrated over the sample space:

$$\begin{aligned} \mu_n &= E\{\omega^n\} \\ &= \int_{-\infty}^{\infty} \omega^n f(\omega) \mathrm{d}\omega. \end{aligned}$$

The first moment ($n = 1$, often denoted as simply μ) is the expectation of ω and describes the statistical mean of the random variable. Central moments are found similarly, but the random variable is first "centered" by subtracting its expectation:

$$\begin{aligned} \sigma_n &= E\{(\omega - \mu)^n\} \\ &= \int_{-\infty}^{\infty} (\omega - \mu)^n f(\omega) \mathrm{d}\omega. \end{aligned}$$

The second central moment ($n = 2$) is the variance of ω, and is a measure of the dispersion in the value of the random variable. The correlation between two random variables can be expressed similarly through what is known as the covariance function:

$$C(\omega_1, \omega_2) = \int_{-\infty}^{\infty} \int_{-\infty}^{\infty} (\omega_1 - \mu_{\omega_1})(\omega_2 - \mu_{\omega_2}) f(\omega_1, \omega_2) \mathrm{d}\omega_1 \mathrm{d}\omega_2. \tag{4.1}$$

Here, $f(\omega_1, \omega_2)$ is the joint probability density function of ω_1 and ω_2. For a stochastic process with random variables indexed by their spatial location, the covariance function is often denoted $C(\mathbf{x_1}, \mathbf{x_2})$.

In this work, we consider a field of Manning's n values that is to be estimated for a particular domain of interest, $\mathbf{D}$, as a stochastic process, $\omega(\mathbf{x}, \theta)$. We let the initial estimate of the field define the expectation of the process,

and wish to determine a covariance function $C(\mathbf{x}_1, \mathbf{x}_2)$ of the process that accurately models the relationships between uncertainties in the field. Then, the problem of estimating the field of Manning's n coefficients becomes one of estimating the correct realization of the stochastic process that defines it. This problem can be simplified by first representing the stochastic process as a series of random variables and then estimating those.

4.2 The Representation of a Stochastic Process

The representation of a stochastic process has a well developed mathematical theory [72]. One of the most important results is the spectral representation of stochastic processes [35], which describes the regular oscillations of the process through the oscillations of the covariance function. The covariance function is first decomposed into a stochastic integral of deterministic functions over the sample space of random events. The stochastic process can then be expressed as another stochastic integral, which can be represented by a series expansion using random coefficients to linearly combine the deterministic functions of the covariance matrix.

4.2.1 Spectral Representation

Various types of expansions result from varying the deterministic basis functions of the series. For example, in the spectral representation method described in [79, 39], sine and cosine functions are used. These deterministic functions are simple to determine, however, except for the case when the

stochastic process is weakly stationary (i.e. that its expectation is constant and it second order moments are finite) and its index set is infinite or periodic, this method assumes that the random coefficients are correlated. This is undesirable, as the joint probability functions are difficult to accurately determine. In [103], the basis functions used are Legendre polynomials. In this expansion, the random coefficients are always assumed correlated. The use of other polynomials is discussed in [60]. The Karhunen-Loève expansion is the method used to represent stochastic processes in this work [53, 61, 52]. It can actually be shown to be a generalization of the spectral representation method [39]. This expansion uses the eigenfunctions of the associated covariance function as basis functions. It has the desirable property of uncorrelated random coefficients, allowing it to optimally encapsulate the information of the random process with the fewest amount of terms. We describe this method in detail below.

4.2.2 The Karhunen-Loève Expansion

Consider a second order, stochastic process, $\omega(\mathbf{x}, \theta)$, with a covariance function $C(\mathbf{x}_1, \mathbf{x}_2)$ that is continuous on $\mathbf{D} \times \mathbf{D}$. The eigenvalues, λ_i, and the eigenfunctions, $f_i(\mathbf{x})$, of the covariance function are the solutions of the integral equation

$$\int_{\mathbf{D}} C(\mathbf{x}_1, \mathbf{x}_2) f_i(\mathbf{x}_1)\, \mathrm{d}\mathbf{x}_1 = \lambda_i f_i(\mathbf{x}_2). \tag{4.2}$$

By definition, the covariance kernel, C, of the stochastic process, $\omega(\mathbf{x}, \theta)$, is bounded, symmetric, and positive semi-definite, which ensures that the eigen-

values are real and non-negative, and that the eigenfunctions form a basis of $L^2(\mathbf{D})$, and are orthonormal, i.e.

$$\int_{\mathbf{D}} f_i(\mathbf{x}) f_j(\mathbf{x}) \, \mathrm{d}\mathbf{x} = \delta_{ij}. \tag{4.3}$$

By Mercer's theorem [18], the covariance function has the spectral decomposition

$$C(\mathbf{x}_1, \mathbf{x}_2) = \sum_{i=1}^{\infty} \lambda_i f_i(\mathbf{x}_1) f_i(\mathbf{x}_2). \tag{4.4}$$

Furthermore, the stochastic process $\omega(\mathbf{x}, \theta)$ can be expressed as

$$\omega(\mathbf{x}, \theta) = \overline{\omega}(\mathbf{x}) + \sum_{i=1}^{\infty} \xi_i(\theta) \sqrt{\lambda_i} f_i(\mathbf{x}), \tag{4.5}$$

where $\overline{\omega}(\mathbf{x})$ is the expected value of $\omega(\mathbf{x}, \theta)$ and $\xi_i(\theta)$ are random variables. We can solve the expansion for $\xi_i(\theta)$ using the orthonormal property of the eigenfunctions (4.3):

$$\xi_i(\theta) = \frac{1}{\sqrt{\lambda_i}} \int_{\mathbf{D}} [\omega(\mathbf{x}, \theta) - \overline{\omega}(\mathbf{x})] f_i(\mathbf{x}) \mathrm{d}\mathbf{x}.$$

Examining the first and second order moments, we see

$$\begin{aligned} E[\xi_i(\theta)] &= 0 \\ E[\xi_i(\theta)\xi_j(\theta)] &= \delta_{ij}, \end{aligned}$$

i.e. the random coefficients have zero mean and are also orthogonal (i.e. uncorrelated). The expansion thus preserves the mean and covariance of the stochastic process. The expression, (4.5), known as the Karhunen-Loève expansion, converges absolutely and uniformly to $\omega(\mathbf{x}, \theta)$ in the mean square

sense. For practical implementation, the series in the expansion is truncated:

$$\tilde{\omega}(\mathbf{x},\theta) = \overline{\omega}(\mathbf{x}) + \sum_{i=1}^{N} \xi_i(\theta)\sqrt{\lambda_i} f_i(\mathbf{x}).$$

The number of terms in the truncation, N, can be specified based on the desired encapsulation of information. For example, to retain 90% of the information, N should be chosen so that $\lambda_N/\lambda_1 = 0.1$. This N will be larger for covariance kernels with smaller correlation lengths. The Karhunen-Loève expansion is advantageous over other spectral representations as its bi-orthonormal property (i.e. the orthonormal deterministic basis functions and the orthonormal, or uncorrelated, random coefficients) ensures that the expansion optimally encapsulates the information of the process defined by the set of random variables [47]; the mean square error of the truncation is minimized. Additionally, the Karhunen-Loève expansion can be used to compute higher order moments of the solution without computing the solution directly.

The existence and uniqueness of the Karhunen-Loève expansion of a stochastic process depends on several properties of the corresponding covariance function, as well as the abilty to determine its eigendecomposition.

4.2.2.1 Covariance Functions for a Stochastic Process

In the Karhunen-Loève expansion, realizations of a stochastic process are determined by functions of the process's covariance function. The covariance function $C(\mathbf{x}_1, \mathbf{x}_2)$ of a stochastic process describes the linear relationship between pairs of random variables. It measures the expectation of the product of deviations of two random variables from their respective means (4.1).

The covariance is positive when values of the first random variable above its respective mean ($\omega_1 - \mu_{\omega_1}$ positive) correspond to values of the second random variable above its respective mean ($\omega_2 - \mu_{\omega_2}$ positive) and vice versa. In contrast, the covariance function value is negative when values of the first random variable above its respective mean ($\omega_1 - \mu_{\omega_1}$ positive) correspond to values of the second random variable *below* its respective mean ($\omega_2 - \mu_{\omega_2}$ *negative*). In both cases, a linear relationshiop between the two random variables exists. If the random variables are independent, the covariance is near zero, however the converse is not true. Small covariance does not imply independence, but rather a weakness of a linear realationship. Recall that for the stochastic processes defined in this work, random variables are indexed by values in the set $\mathbf{D}$, the spatial domain of interest. Distinct random variables therefore reference the value of the parameter at distinct points in space, and the covariance function of the stochastic process (the collection of these random variables) is a measure of the relationship between the error in the parameter values at different spatial locations.

In the Karhunen-Loève expansion of a stochastic process, it is assumed that the associated covariance function is known, and additionally that it is symmetric, positive semi-definite, and bounded. A covariance matrix is symmetric and positive semi-definite by definition. However, it is often the case that the covariance function is *unknown*, and thus must first be modeled. One way this can be done is by modifying well known covariance functions to suit the characteristics of a particular problem. Commonly used covariance

functions are often classsified by certain properties, and we will explore some of these properties here.

Stationary covariance functions are those that depend on $\mathbf{x}_1$ and $\mathbf{x}_2$ through $(\mathbf{x}_1 - \mathbf{x}_2)$ only, i.e. $C(\mathbf{x}_1, \mathbf{x}_2) = C(\mathbf{x}_1 - \mathbf{x}_2)$; the functions are translation invariant. Their variances, $C(\mathbf{x} - \mathbf{x}) = C(\mathbf{0})$, are thus constant. A stochastic process is called weakly stationary if it has a finite second moment, a constant mean function, and a stationary covariance function. (It is strictly stationary if *all* of its finite dimensional distributions are translation invariant.) Isotropic covariance functions have the additional property that they depend on $\mathbf{x}_1$ and $\mathbf{x}_2$ through $|\mathbf{x}_1 - \mathbf{x}_2|$ only. They are invariant to all rigid motions and for that reason are also sometimes known as radial basis functions. A weakly isotropic stochastic process has a finite second moment, a constant mean function, and an isotropic covariance function. All weakly isotropic stochastic processes are weakly stationary, and for Gaussian processes, weak stationarity/isotropy implies strict stationarity/isotropy.

The continuity of the covariance function does not have a direct relationship to the continuity of the associated stochastic process, however for stationary stochastic processes, it can be related to the mean square continuity. A stochastic process $\omega(\mathbf{x}, \theta)$ with a finite second moment is mean square continuous at $\mathbf{x}_1$ if

$$E(\omega_1 - \omega_2)^2 \to 0 \quad \text{as} \quad \omega_2 \to \omega_1$$

where again we use the notation ω_i to denote $\omega(\mathbf{x}_i, \theta)$. If a stationary co-

variance function, $C(\mathbf{x}_1 - \mathbf{x}_2)$, is continuous at $\mathbf{0}$, (i.e. when $\mathbf{x}_1 = \mathbf{x}_2$), it is continuous for all (directional) distances $(\mathbf{x}_1 - \mathbf{x}_2)$ since, by the Cauchy-Schwarz inequality,

$$\begin{aligned}
|C(\mathbf{x}_1 - \mathbf{x}_2) - C(\mathbf{x}_1 - \mathbf{x}_3)| &= |C(\mathbf{x}_1 - \mathbf{x}_2 - \mathbf{0}) - C(\mathbf{x}_1 - \mathbf{x}_3 - \mathbf{0})| \\
&= |C(\mathbf{x}_1 - \mathbf{x}_2, \mathbf{0}) - C(\mathbf{x}_1 - \mathbf{x}_3, \mathbf{0})| \\
&= |C(\mathbf{x}_3 - \mathbf{x}_2, \mathbf{0})| \\
&\leq [C(\mathbf{x}_3 - \mathbf{x}_2, \mathbf{x}_3 - \mathbf{x}_2)C(\mathbf{0}, \mathbf{0})]^{1/2} \\
&= [(C(\mathbf{x}_3, \mathbf{x}_3) + C(\mathbf{x}_2, \mathbf{x}_2) - 2C(\mathbf{x}_3, \mathbf{x}_2))C(\mathbf{0}, \mathbf{0})]^{1/2} \\
&= [2(C(\mathbf{0}) - C(\mathbf{x}_3 - \mathbf{x}_2))C(\mathbf{0})]^{1/2} \\
&\to 0
\end{aligned}$$

as $\mathbf{x}_3 \to \mathbf{x}_2$ (i.e. as the directional distance converges to $(\mathbf{x}_1 - \mathbf{x}_2)$). The corresponding weakly stationary stochastic process is mean square continuous since

$$\begin{aligned}
E(\omega_1 - \omega_2)^2 &= C(\mathbf{x}_1, \mathbf{x}_1) + C(\mathbf{x}_2, \mathbf{x}_2) - 2C(\mathbf{x}_1, \mathbf{x}_2) \\
&= 2[C(\mathbf{0}) - C(\mathbf{x}_1, \mathbf{x}_2)] \\
&\to 0
\end{aligned}$$

as $\omega_2 \to \omega_1$ (i.e. as $\mathbf{x}_2 \to \mathbf{x}_1$ since $C(\mathbf{x}_1, \mathbf{x}_2) \to C(\mathbf{0})$ in this case). This is also true for general stochastic processes; a stochastic process is mean square continuous at $\mathbf{x}$ if (and only if) its covariance function is continuous at $\mathbf{x}_1 = \mathbf{x}_2 = \mathbf{x}$. In the above proofs we have assumed $\mu_1 = \mu_2 = 0$. It should be noted that the mean square continuity of the stochastic process does not

imply continuity of a *realization* of the stochastic process (it implies that the expectation, $\mu(\mathbf{x})$, is continuous). Consequently, a continuous covariance function can be used to model a highly variable spatial parameter such as a field of Manning's n coefficients.

The mean square derivative of a stochastic process in the ith direction of $\mathbf{D}$ is defined in terms of a limit in the mean square,

$$\frac{\partial \omega(\mathbf{x},\theta)}{\partial x_i} := \quad \text{l.i.m.} \quad \frac{\omega(\mathbf{x}+\mathrm{h}\mathbf{e}_\mathrm{i},\theta)-\omega(\mathbf{x},\theta)}{\mathrm{h}} \quad \text{as} \quad \mathrm{h}\to 0,$$

and the respective covariance function is

$$\frac{\partial^2 C(\mathbf{x}_1,\mathbf{x}_2)}{\partial x_{1i}\partial x_{2i}}.$$

This definition can be extended to higher order derivatives. For stationary processes, if the $2k$th-order partial derivative of the covariance function exists and is finite at $\mathbf{x}=\mathbf{0}$, then the kth order partial derivative of the respective stochastic process exists for all $\mathbf{x}\in\mathbf{D}$, i.e. the differentiability of the covariance function has implications on the continuity of the process.

In this work, we will assume that the covariance function of the stochastic process that defines the field of Manning's n values is isotropic, i.e. we make a simplifying assumption that the relationship between the Manning's n values (i.e. land characteristics) at two points depend only on the distance between them. While it would appear, e.g. from Figure 2.1, that correlations between Manning's n values decrease closer to the coastline, for stochastic processes with a nonzero mean the covariance function is an expression for correlation

in *deviations* from the mean. For the purposes of this work we will see that the assumption of an isotropic covariance function is sufficient.

There are many examples of isotropic covariance functions. The exponential covariance function is

$$C(\mathbf{x}_1, \mathbf{x}_2) = \exp\left(-\frac{|\mathbf{x}_1 - \mathbf{x}_2|}{\ell}\right),$$

where ℓ defines the characteristic length scale, a measure of how quickly influences between random variables decrease with distance. The corresponding stochastic process is mean square continuous, however it is not mean square differentiable; a realization of the process is very rough.

Another common isotropic covariance function is the squared exponential covariance function,

$$C(\mathbf{x}_1, \mathbf{x}_2) = \exp\left(-\frac{|\mathbf{x}_1 - \mathbf{x}_2|^2}{2\ell^2}\right),$$

in fact it is one of the most widely used [76]. It is infinitely differentiable; the associated stochastic process has mean square derivatives of all orders and is thus very smooth. Stein argues that it is *too* smooth, and cannot realistically model a physical process [86].

The γ-exponential covariance functions are defined as

$$C(\mathbf{x}_1, \mathbf{x}_2) = \exp\left(-\left[\frac{|\mathbf{x}_1 - \mathbf{x}_2|}{\ell}\right]^\gamma\right),$$

where $0 < \gamma \leq 2$ is a constant that parameterizes the continuity of the stochastic process. This class includes both the exponential and squared exponential

covariance functions as special cases. These functions are continuous, however they are not mean square differentiable except in the aforementioned case when $\gamma = 2$.

All of the covariance functions above can be considered as members of the Matèrn class [66]. These functions have the form

$$C(\mathbf{x}_1, \mathbf{x}_2) = \frac{2^{1-\nu}}{\Gamma(\nu)} \left(\frac{\sqrt{2\nu}|\mathbf{x_1} - \mathbf{x}_2|}{\ell} \right)^{\nu} K_\nu \left(\frac{\sqrt{2\nu}|\mathbf{x_1} - \mathbf{x}_2|}{\ell} \right).$$

Here, ν is a smoothness parameter (corresponding to $\gamma/2$ in the γ-exponential covariance functions), Γ is the gamma function, and K_ν is a modified Bessel function of the second kind. These functions have the same number of paramaters as the γ-exponential functions, but allow for a larger range of local behavior of the stochastic process. The stochastic process is very rough for small values of ν, but becomes increasingly smooth as $\nu \to \infty$, when the covariance function converges to the squared exponential function. The functions are continuous, however, they are not mean square differentiable, again with the exception of the squared exponential. Their respective stochastic processes are k-times mean square differentiable for $\nu > k$. When ν is a positive half integer, $\nu = n + 1/2$ for n a nonnegative integer, the covariance function is considerably simplified to a product of an exponential and a polynomial of order n. For example, for $\nu = 1/2$, the covariance function is the exponential covariance function, and for $\nu = 3/2$, the covariance function is

$$C(\mathbf{x}_1, \mathbf{x}_2) = \left(1 + \frac{\sqrt{3}|\mathbf{x}_1 - \mathbf{x}_2|}{\ell} \right) \exp \left(-\frac{\sqrt{3}|\mathbf{x}_1 - \mathbf{x}_2|}{\ell} \right).$$

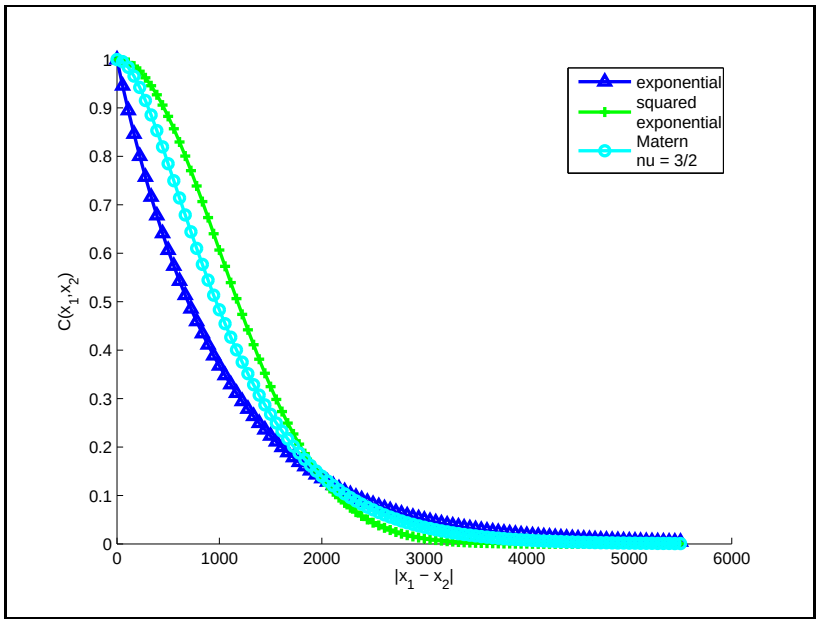

Figure 4.1: Three examples of isotropic covariance functions, with $\ell = 1{,}000$

All of these covariance functions have been normalized so that the stochastic process has unit variance, i.e. $C(x, x) = 1$. When this is not the case, the covariance functions should be multiplied by the respective variances of each random variable. Additional examples of stationary covariance functions can be found in [86, 76].

In modeling the covariance function of a stochastic process, the physical problem that the stochastic process represents should be considered. Any of the covariance functions highlighted above may be selected if it reflects the properties of the process, e.g. stationarity, continuity, and correlation length. Covariance functions can also be modified and/or combined to create new functions. Specifically, the sum, product, and convolution of two covariance

functions defined over the same domain $\mathbf{D}$ are also valid covariance functions (i.e. symmetric and positive semi-definite). For a product space, $\mathbf{D}_1 \times \mathbf{D}_2$ where $\mathbf{D}_i$ is the index set of the respective stochastic process, the direct sum and tensor product of the respective covariance functions also form valid covariance functions.

In addition to the physical problem, the numerical problem should be taken into account. We seek to model the covariance function so that its eigenfunctions can be determined and then used to express realizations of the stochastic process (4.5). For purposes of computational storage, the variation in the process should be adequately represented by a minimum number of these eigenfunctions, i.e. we desire a covariance function that is many times differentiable, as the rate of convergence of the sum in (4.4) is dependent on the differentiability of $C(\mathbf{x}_1, \mathbf{x}_2)$ [78]. Furthermore, the sensitivity of the model to increased variability of the process should be explored, particularly when using a covariance function that is *not* many times differentiable. The advantages of using a less differentiable covariance function, i.e. increasing the number of terms in the Karhunen-Loève expansion, should balance the additional costs incurred.

4.2.2.2 The Eigendecomposition of the Covariance Function

In the Karhunen-Loève expansion, the stochastic process is represented as a linear combination of deterministic basis functions (4.5). The basis functions are chosen to be the eigenfunctions and eigenvalues of the associated

covariance function, which are the solutions to the homogenous Fredholm integral equation of the second kind (4.2). When the exact eigendecomposition of $C(\mathbf{x}_1, \mathbf{x}_2)$ is known, the Karhunen-Loève expansion is the most efficient method of representing a stochastic process, i.e. it minimizes the mean square error of the truncation. However, analytical solutions to this problem only exist for a limited number of covariance functions; in general, it must be solved numerically.

Analytical solutions to the Fredholm integral equation can be found for certain covariance matrices such as those of stationary processes with rational spectra, band limited stationary processes, and a specific class of non-stationary processes [47]. In these cases, (4.2) can be differentiated twice with respect to $\mathbf{x}_2$, and the resulting differential equation can be solved analytically [93].

When (4.2) cannot be solved analytically, numerical solutions can be obtained using integration formulae-based methods such as quadrature and product integration methods, or expansion methods, such as collocation and Galerkin methods.

In this work, we compute the eigendecomposition of $C(\mathbf{x}_1, \mathbf{x}_2)$ using an expansion method. Expansion methods are best suited for integral equations where the kernel (i.e. the covariance function) is analytically defined, e.g. as those described in 4.2.2.1. In these methods, each unknown eigenfunction, $f_i(\mathbf{x})$, is approximated by an expansion in terms of a complete set of basis

functions, $\phi_k \in \chi_M$, and unknown coefficients, d_{ik}:

$$\tilde{f}_i(\mathbf{x}) = \sum_{k=1}^{M} d_{ik}\phi_k(\mathbf{x}). \tag{4.6}$$

Here we let χ_M be an M-dimensional subspace of a Banach space, χ, where M is finite. For sufficiently large M, the expansion, $\tilde{f}_i(\mathbf{x})$, approximates the eigenfunction $f_i(\mathbf{x})$ as accurately as desired, nevertheless, the truncation will result in some error in the integral equation. We define this error as $r(\mathbf{x})$:

$$\begin{aligned} r(\mathbf{x}) &:= \int_{\mathbf{D}} C(\mathbf{x}_1, \mathbf{x}_2)\tilde{f}_i(\mathbf{x}_1)\ \mathrm{d}\mathbf{x}_1 - \lambda_i \tilde{f}_i(\mathbf{x}_2) \\ &= \sum_{k=1}^{M} d_{ik}\left[\int_{\mathbf{D}} C(\mathbf{x}_1, \mathbf{x}_2)\phi_k(\mathbf{x}_1)\ \mathrm{d}\mathbf{x}_1 - \lambda_i \phi_k(\mathbf{x}_2)\right]. \end{aligned}$$

The coefficients of $\tilde{f}_i(\mathbf{x})$, d_{ik}, are chosen so that the error function, $r(\mathbf{x})$, is approximately zero. Expansion methods are characterized by the way that "approximately zero" is defined.

In the Galerkin method, χ is chosen to be a Hilbert space, and the d_{ik} are chosen so that $r(\mathbf{x})$ is orthogonal to each of the basis functions; $\tilde{f}_i(\mathbf{x})$ is the best approximation of $f_i(\mathbf{x})$ in χ_M:

$$\begin{aligned} \langle r(\mathbf{x}), \phi_j(\mathbf{x})\rangle &= \left\langle \int_{\mathbf{D}} C(\mathbf{x}_1, \mathbf{x}_2)\tilde{f}_i(\mathbf{x}_1)\ \mathrm{d}\mathbf{x}_1 - \lambda_i \tilde{f}_i(\mathbf{x}_2), \phi_j(\mathbf{x})\right\rangle \\ &= \sum_{k=1}^{M} d_{ik}\left[\int_{\mathbf{D}}\left[\int_{\mathbf{D}} C(\mathbf{x}_1, \mathbf{x}_2)\phi_k(\mathbf{x}_1)\mathrm{d}\mathbf{x}_1\right]\phi_j(\mathbf{x}_2)\mathrm{d}\mathbf{x}_2\right] \\ &\qquad -\lambda_i \sum_{k=1}^{M} d_{ik}\left[\int_{\mathbf{D}} \phi_i(\mathbf{x}_2)\phi_j(\mathbf{x}_2)\mathrm{d}\mathbf{x}_2\right] \\ &= 0. \end{aligned} \tag{4.7}$$

Letting

$$\begin{aligned} A_{kj} &= \int_{\mathbf{D}}\int_{\mathbf{D}} C(\mathbf{x}_1,\mathbf{x}_2)\phi_k(\mathbf{x}_1)\phi_j(\mathbf{x}_2)\ \mathrm{d}\mathbf{x}_1\mathrm{d}\mathbf{x}_2, \\ D_{ik} &= d_{ik}, \\ \Lambda_{ij} &= \delta_{ij}\lambda_i, \\ B_{ij} &= \int_{\mathbf{D}} \phi_i(\mathbf{x}_2)\phi_j(\mathbf{x}_2)\ \mathrm{d}\mathbf{x}_2, \end{aligned} \tag{4.8}$$

the Galerkin method results in a generalized eigenvalue problem,

$$\mathbf{AD} = \Lambda\mathbf{BD}. \tag{4.9}$$

Note that when the basis functions, ϕ_k, used to expand the eigenfunctions of the covariance function are orthonormal, $\mathbf{B} = \mathbf{I}$ and the generalized eigenvalue problem becomes the standard eigenvalue problem. The generalized or standard eigenvalue problem is then solved for $\mathbf{D}$ and Λ, and using the d_{ik} to approximate each eigenfunction (4.6), we obtain the numerical solution of the Fredholm integral equation (4.2).

In order to analyze the error that results from estimating the eigenfunctions of $C(\mathbf{x}_1,\mathbf{x}_2)$ using the Galerkin method, we express the orthogonality condition of $r(\mathbf{x})$ (4.7) as a condition on its projection into χ_M. Letting $\mathcal{P}_M$ be an orthogonal projection operator from $\chi \rightarrow \chi_M$, we have that if $\langle r(\mathbf{x}), \phi_k(\mathbf{x})\rangle = 0$ for all of the basis functions of χ_M (i.e. if the error is orthogonal to the space χ_M), then $\mathcal{P}_M r(\mathbf{x}) = 0$:

$$\mathcal{P}_M(\mathcal{K} - \lambda_i)\tilde{f}_i = 0,$$

where for simplification we have dropped the argument, $\mathbf{x}$, and define $\mathcal{K}$ to denote the integral operator in $r(\mathbf{x})$, $\int_{\mathbf{D}} C(\mathbf{x}_1, \mathbf{x}_2)(\cdot)\, \mathrm{d}\mathbf{x}_1$. For the $\tilde{f}_i \in \chi_M \subset \chi$ that solves this problem, $\tilde{f}_i$ also solves

$$(\mathcal{P}_M \mathcal{K} - \lambda_i)\tilde{f}_i = 0. \tag{4.10}$$

Now suppose $\mathcal{K} : \chi \to \chi$ is bounded, $||\mathcal{K} - \mathcal{P}_M \mathcal{K}|| \to 0$ as $M \to \infty$, and $(\lambda_i - \mathcal{K} : \chi \to \chi)$ is one-to-one and onto. Then the operator $(\lambda_i - \mathcal{P}_M \mathcal{K})^{-1}$ is a bounded operator from χ to χ for suffenciently large M, and it is uniformly bounded:

$$\sup_M ||(\mathcal{P}_M \mathcal{K} - \lambda_i)^{-1}|| < \infty.$$

From (4.2) and (4.10)

$$f_i - \tilde{f}_i = \lambda_i (\mathcal{P}_M \mathcal{K} - \lambda_i)^{-1}(f_i - \mathcal{P}_M f_i), \quad \text{and}$$

$$\frac{|\lambda_i|}{\|\mathcal{P}_M \mathcal{K} - \lambda_i\|} \|f - \mathcal{P}_M f\| \leq \|f_i - \tilde{f}_i\| \leq |\lambda_i| \|(\mathcal{P}_M \mathcal{K} - \lambda_i)^{-1}\| \|f - \mathcal{P}_M f\|.$$

Thus, the approximation of the eigenfunction, $\tilde{f}_i(\mathbf{x})$, converges to the true eigenfunction, $f_i(\mathbf{x})$, and it does so at the rate that $\mathcal{P}_M f_i(\mathbf{x})$ converges to $f_i(\mathbf{x})$. The proof of this theorem is shown in [7].

Regarding the error in the eigenvalues, the estimates of the eigenvalues are far more accurate than those of the eigenfunctions. Also, the computed eigenvalues are lower bounds of the corresponding true eigenvalues; the convergence of each eigenvalue is monotonic in M [24]. Ignoring the quadrature error that arises from (4.8) and numerical round off error, the accuracy of the eigendecomposition obtained by the Galerkin method is dependent on the

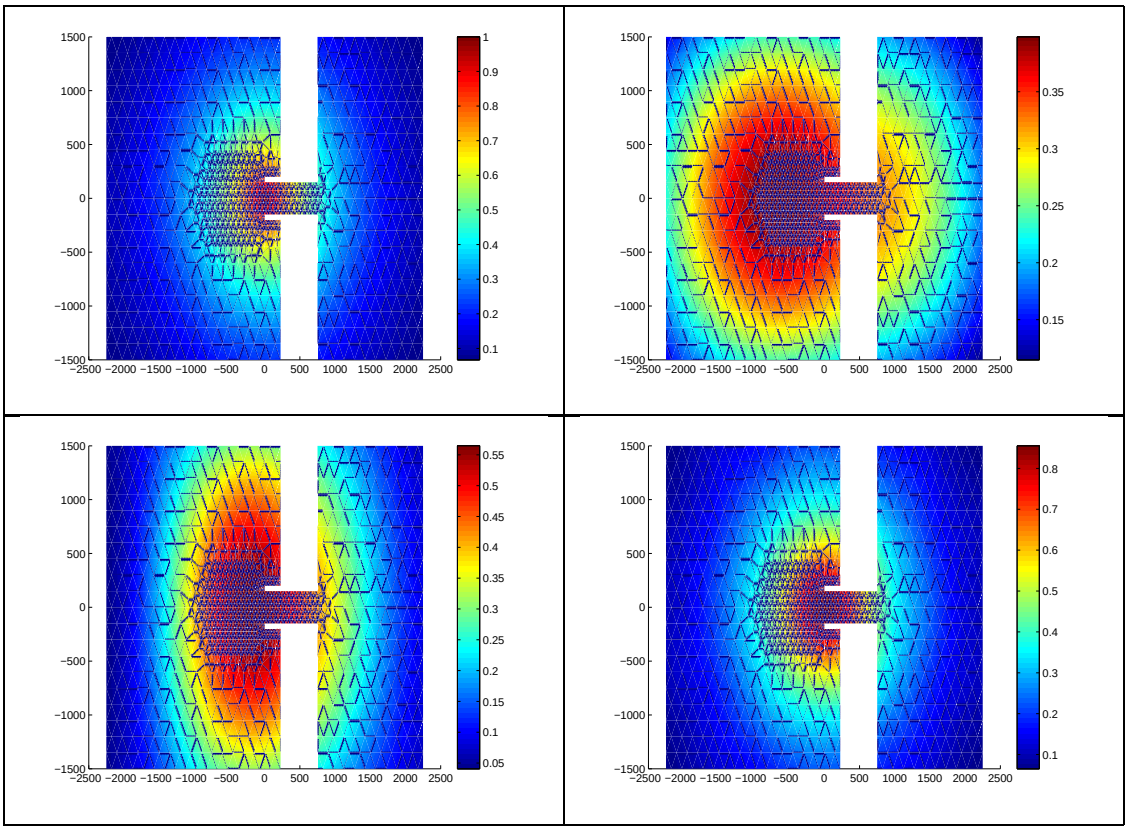

Figure 4.2: The exponential covariance function evaluated for the point (0,0), i.e. $C(\mathbf{x}_1, \mathbf{x}_2)$ where $\mathbf{x}_1 = \mathbf{0}$ (top left), and the same covariance function in terms of its spectral decomposition (4.4) using 1 (top right), 5 (bottom left), and 50 (bottom right) terms

space spanned by the basis functions ϕ_k, not the basis functions themselves. It is the most common expansion method for eigenvalue problems and is the method chosen in this work. Examples of a Galerkin approximation of the exponential covariance function is shown for 1, 5, and 50 eigenpairs in Figure 4.2.

It is useful to represent highly variable spatial parameters as a stochas-

tic process. Doing so significantly reduces the dimension of a parameter vector defining parameter values at each vertex of a computational domain, saving computational costs associated with storage and, of most importance for our interests, parameter estimation. For practical implementation, there are many methods of representing a stochastic process, including the Karhunen-Loève expansion, which is the most efficient in the sense that it minimizes mean square truncation error. The Karhunen-Loève expansion requires the eigen-decomposition of the covariance function of the stochastic process. It is often necessary that the covariance function first be modeled, and then decomposed into its eigenvalues and eigenfunctions numerically. A linear combination of the eigenpairs with random coefficients is used to express realizations of the stochastic process. We generate realizations of the stochastic process that represent a field of Manning's n values in this way. We then proceed with the goal of correctly determining the random coefficients of a given realization by using the parameter estimation methods described in Chapter 3 to invert water elevation data.

Chapter 5

Numerical Results

In this chapter, we test the effectiveness of our proposed method of parameter estimation in determining the bottom stress coeffiecients in the shallow water equations. We implement the Singular Interpolated Evolutive Kalman (SEIK) filter, described in section 3.2.4.2, to estimate the Manning's n coefficients used to define the bottom stress in the Advanced Circulation (ADCIRC) model. We assimilate synthetic water elevation data into ADCIRC model simulations of the coastal ocean under moderate conditions to recover parameters defining various fields of Manning's n coefficients. For our computational domain, we use both a simple test problem, an idealized inlet with an ebb shoal, as well as a coarse representation of a true domain of interest, Galveston Bay.

5.1 The Advanced Circulation Model

The Advanced Circulation (ADCIRC) model [62] is a widely used coastal ocean model [8, 12, 26, 41]. The continuity equation in the SWEs (2.1) is replaced by what is known as the generalized wave continuity equation (GWCE) [56, 63]. The GWCE is a second-order, hyperbolic equation, obtained in sev-

eral steps. The continuity equation is first differentiated with respect to time, and then multiplied by a user-defined constant, $\tau_0 \geq 0$. (In this work, we let $\tau_0 = 0.04$.) Then, it is assumed that the bathymetric depth is constant, i.e. $\frac{\partial H}{\partial t} = \frac{\partial \zeta}{\partial t}$. Substituting the momentum equations into this equation completes the derivation:

$$\begin{aligned}
&\frac{\partial^2 \zeta}{\partial t^2} + \tau_0 \frac{\partial \zeta}{\partial t} \\
&\quad + \frac{\partial}{\partial x}\Bigg(- \frac{\partial U Q_x}{\partial x} - \frac{\partial V Q_x}{\partial y} + f Q_y - gH \frac{\partial [\zeta + P_s/g\rho_0 - \alpha\eta]}{\partial x} \\
&\qquad + \frac{\tau_{sx}}{\rho_0} - \frac{\tau_{bx}}{\rho_0} + M_x - D_x - B_x + \tau_0 Q_x \Bigg) \\
&\quad + \frac{\partial}{\partial y}\Bigg(- \frac{\partial U Q_y}{\partial x} - \frac{\partial V Q_y}{\partial y} + f Q_x - gH \frac{\partial [\zeta + P_s/g\rho_0 - \alpha\eta]}{\partial y} \\
&\qquad + \frac{\tau_{sy}}{\rho_0} - \frac{\tau_{by}}{\rho_0} + M_y - D_y - B_y + \tau_0 Q_y \Bigg) \\
&\quad - UH \frac{\partial \tau_0}{\partial x} - VH \frac{\partial \tau_0}{\partial y} = 0.
\end{aligned} \tag{5.1}$$

The variable definitions are listed in Section 2.1. Use of the GWCE reduces the occurrence of spurious oscillations often associated with the numerical solution of the original form [22]. Together, the GWCE (5.1) and the momentum equations (2.2) define the modified form of the SWEs solved by the ADCIRC model.

In the version of the ADCIRC model used in this work, the GWCE and the momentum equations are discretized in space by a first-order continuous Galerkin finite element method. The elements which make up the computational domain are triangular. The time derivatives are approximated

using centered finite differences in the GWCE (5.1) and forward differences in the momentum equations (2.2). The ADCIRC model has been verified and validated extensively for modeling both tides [100, 11] and hurricane storm surges, e.g. through hindcast studies of hurricanes that have occured in the Gulf of Mexico. These studies compare common quantities of interest computed from the model solution (e.g. maximum water elevations at various locations along the Gulf Coast of the United States) to data collected from actual storms. Storms used for hindcasting include Hurricanes Betsy (1965), Ivan (2004), Dennis (2004), Katrina (2005), Rita (2005) [14, 25, 99], Gustav (2008) [27], and Ike (2008) [54]. A fully parallel version of the ADCIRC model has been developed [87]. For parameter estimation, we have utilized both the serial and parallel versions, however, for the results shown in this work, we have utilized the serial version.

The ADCIRC model allows for the implementation of multiple formulations of the bottom stress. A linear or quadratic bottom friction law can be used, as well as a hybrid law that implements a constant friction coefficient in deep water and a quadratic friction law everywhere else. A Chezy or Manning's n formulation of the bottom stress is supported. Each vertex (node) of the computational spatial domain can be assigned a constant friction coefficient, or, alternatively, given distinct values, which are specified in an input file. In this work we utilize the quadratic friction coefficient, with the coefficient determined using the Manning's n formulation.

The Manning's n coefficient specified at each node is updated through-

out the data assimilation cycles. We implement the SEIK filter to the ADCIRC model using Matlab. We initialize the ensemble of parameters by using a random distribution to sample around the expected value. The ensemble is then used to create input files defining the Manning's n coefficients, and this file is read in by multiple instances of the ADCIRC model following an initial ramp up period. Each instance of the ADCIRC model is run until the data assimilation time (i.e. when data is available). At this point, Matlab is used to read in each of the model state variables (i.e. water elevations defined at each node of the domain) output by the instances of the ADCIRC model, and the residual between the modeled and "true" state data is used to update the expected value of the parameter using the SEIK filter. A new ensemble is created from this update, and the ADCIRC model run/ SEIK filtering cycle is repeated until the end of the parameter estimation.

5.2 Observation Simulation System Experiments

We test the SEIK filter for parameter estimation by performing observation simulation system experiments (OSSEs). In OSSEs, synthetic data is generated from a model simulation where all of the input values (e.g model parameters) are "correct." For our experiments, water elevation data is generated using the parameters that define the "true" field of Manning's n values we wish to estimate. The synthetic data is then assimilated into a model simulation that uses uncertain input values commonly used in the model. The assimilation is performed in an effort to recover the correct model state and/or

parameters. In our cases, we begin a model simulation with an incorrect estimate of the field of Manning's n coefficients and then use statistical data assimilation to essentially invert the "true" water elevation data and recover the true field. Additionally, we seek to improve the accuracy of the model output or forecasts (i.e. water elevations). Performing the OSSEs allows the effect of the data assimilation to be directly quantified.

5.2.1 Computational Domains

For our OSSEs, we estimate several fields of Manning's n coefficients for two computational domains, a simple idealized inlet with an ebb shoal and a coarse representation of Galveston Bay.

5.2.1.1 Idealized Inlet with Ebb Shoal

The first computational domain is an idealized inlet with an ebb shoal. It consists of a bay that is connected to the open ocean on the west side via an inlet with twin jetties. Immediately to the west of the inlet is an ebb shoal. This models a realistic situation, as the formation of an ebb shoal is a common occurrence at coastal inlets. An ebb shoal forms due to the deceleration of water as it exits the inlet, which results in the deposition of large amounts of sediment that have been transported by the flow [57].

The computational grid for the idealized inlet contains 1,518 nodes and 2,828 elements, and covers an area that is 4500 m wide and 3000 m long (Figure 5.1). The bathymetry is measured positive downward from the geoid,

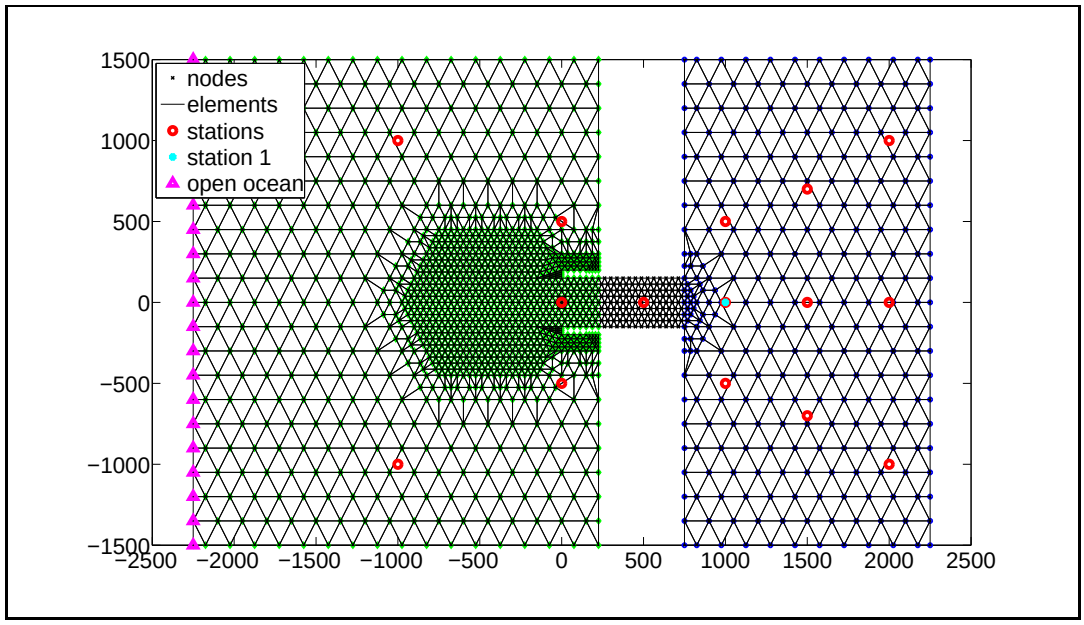

Figure 5.1: Idealized inlet with ebb shoal domain

and slopes linearly from 3.8 m on the open ocean boundary to 1 m at the mouth of the inlet on the west side of the domain. The remaining, landlocked portion of the domain on the east side of the inlet has a constant bathymetry of 1 m. The ebb shoal at the mouth of the channel is 750 m in diameter and has a maximum height of 0.4 m in the center.

5.2.1.2 Galveston Bay

The second computational domain is Galveston Bay, a large estuary located on the upper Texas coast in the Gulf of Mexico. It is a densely populated, large metropolitan area, and it is also home to the Port of Houston, one of the world's busiest ports. It is vital to the U.S. economy. Unfortunately, the location of Galveston Bay makes it particularly susceptible to hurricane

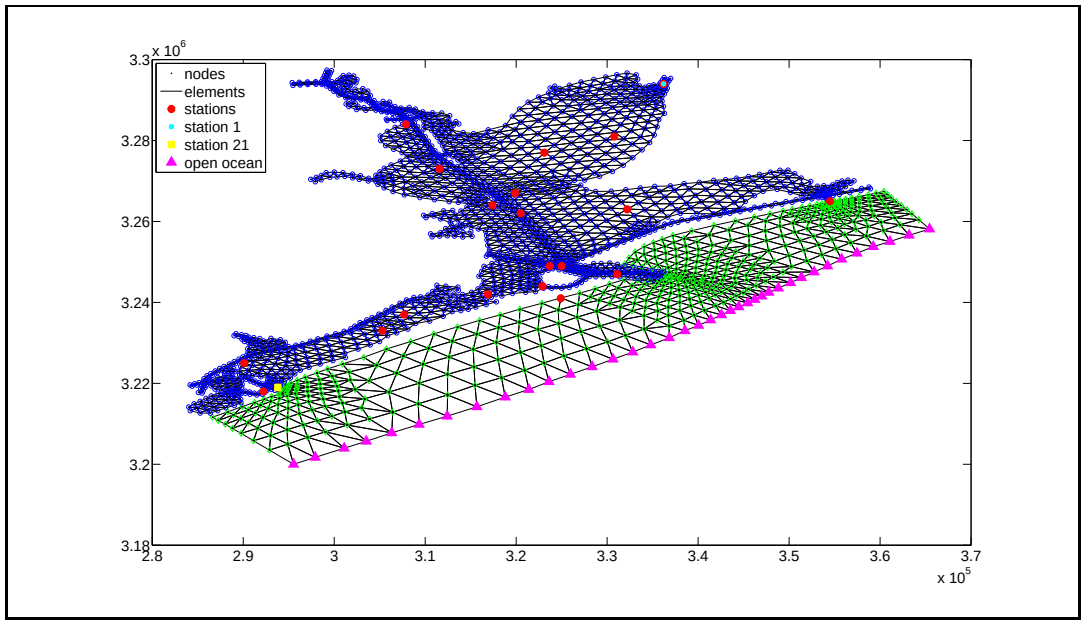

Figure 5.2: Galveston Bay domain

storm surge. The Great Galveston Hurricane destroyed the region in 1990, and in 2008, Hurricane Ike devastated the area again in what has since been estimated as the third costliest hurricane in U.S. history [9].

We use a relatively coarse mesh to represent Galveston Bay, with a grid containing 2,113 nodes and 3,397 elements (Figure 5.2). There is an open ocean boundary on the southeast side of the domain, and land boundaries surrounding the remaining sides. There are also island boundaries surrounding 17 small islands located within the bay. The bathymetry of the domain ranges from 0.354 m inside the bay to 17.244 m in the Gulf of Mexico.

5.2.2 Parameterizing a field of Manning's n Coefficients

To estimate a field of Manning's n coefficients, rather than estimating the value of the coefficient at each node of the computational domains described above, we first model the field using low-dimensional parameterizations. Then the parameter estimation problem reduces to estimating the few parameters that result.

5.2.2.1 A Field of (Piecewise) Constant Manning's n Coefficients

We first aim to estimate a field of Manning's n coefficients parametrically defined by one value. For this, we initially use the simplest parameterization, and let the value of the Manning's n coefficient equal a constant at every node of the domain. This represents a field that is constant in space, and is the implementation of the Manning's n friction coefficient most often used in coastal ocean modeling.

We also aim to estimate two model parameters, α and β, which parametrically define a 2-D field of Manning's n coefficients. We will denote this field by $n_{\alpha,\beta}$. For this case, we will parameterize the field as two piecewise constants, letting α be the value of the Manning's n coefficient on the open ocean side of the domain, and β be the value of the Manning's n coefficient within the inlet and the bay. We will use this configuration for both of the computational domains.

5.2.2.2 A Realization of a Stochastic Process

In an effort to model a more realistic field of Manning's n coefficients, we also represent the field as a stochastic process, which we parameterize using the Karhunen-Loève expansion (section 4.2.2). For both the idealized inlet and Galveston Bay cases, we use the exponential covariance function (section 4.2.2.1). We have chosen this covariance function because realizations of the corresponding processes are allowed to be rough, which is representative of the fields of Manning's n coefficients we generally expect to find in practice. For the idealized inlet, we let the correlation length of the covariance functions equal 1,000 m and 25,000 m, respectively. These lengths are chosen as approximately 1/4 of the diameter of each computational domain in large part so that the covariance can be adequately represented by just a few eigenfunctions. The eigendecomposition of the covariance function is computed using a first order Galerkin method with triangular elements. We choose to use the same basis functions and spatial discretization for the Karhunen-Loève expansion that we use to spatially discretize the shallow water equations in the ADCIRC model. We use the built-in Lanczos algorithm in Matlab to solve the generalized eigenvalue problem that results. The first six computed eigenpairs, i.e. the deterministic functions of the Karhunen-Loève expansion (4.5), for the idealized inlet are shown in Figure 5.3. The eigenpairs for Galveston Bay are shown in Figure 5.4. Several examples of the fields that result from varying the random coefficients in a five-term expansion are shown in Figures 5.5 and 5.6 for the idealized inlet and Galveston Bay, respectively.

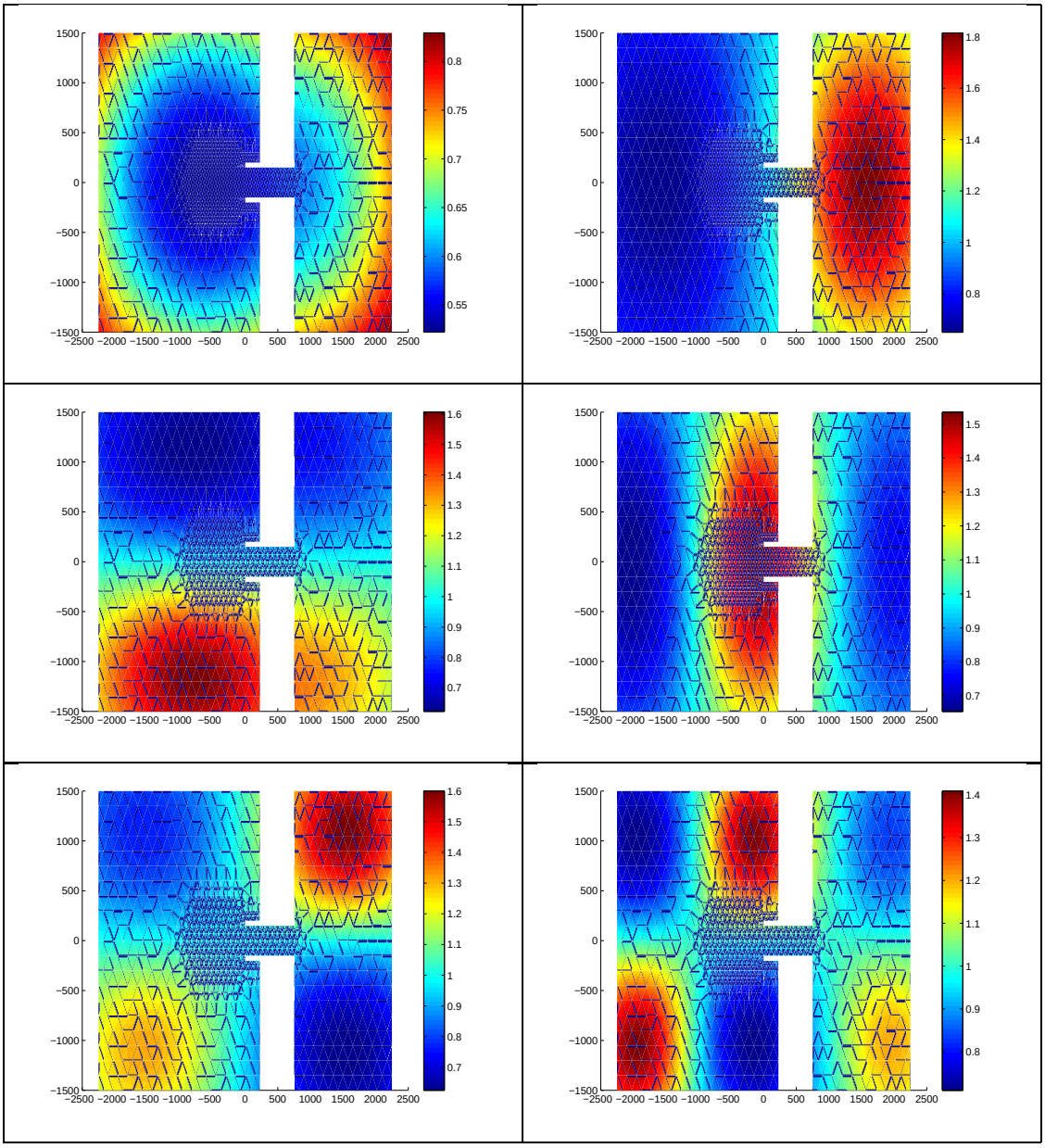

Figure 5.3: The first six eigenpairs (from left to right, top to bottom) of the exponential covariance function, with $\ell = 1{,}000$, for the idealized inlet domain

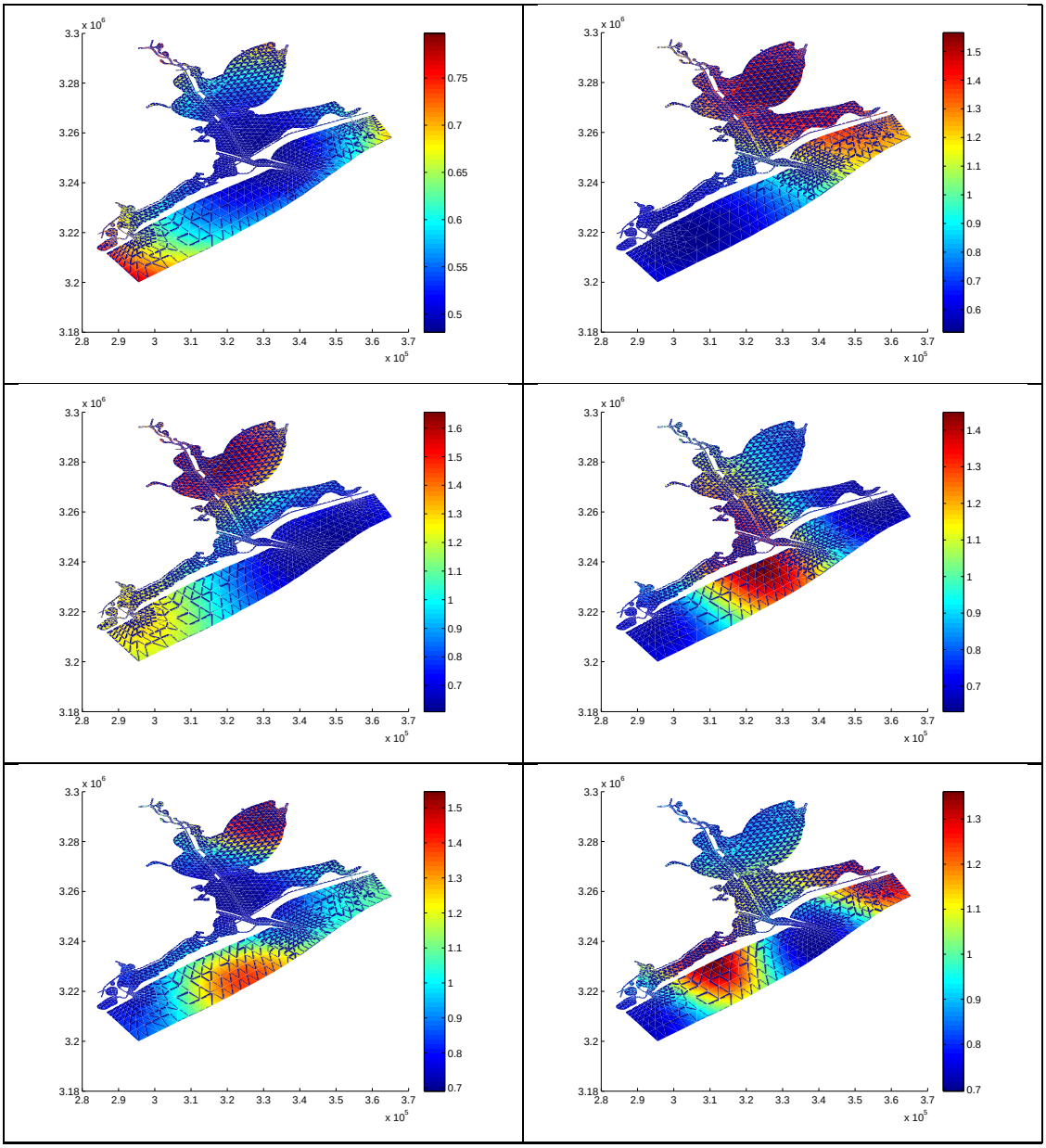

Figure 5.4: The first six eigenpairs (from left to right, top to bottom) of the exponential covariance function, with $\ell = 25{,}000$, for the Galveston Bay domain

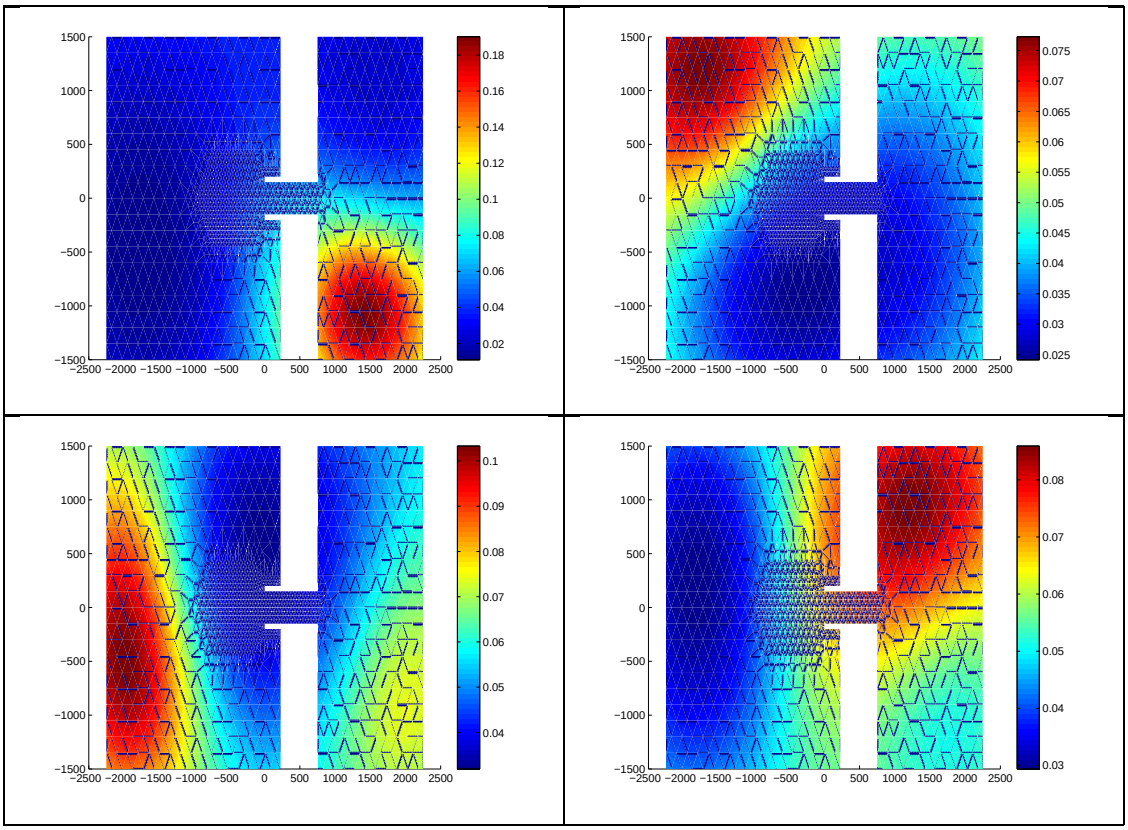

Figure 5.5: Various fields of Manning's n coefficients for the idealized inlet domain defined by varying the random coefficients in a Karhunen-Loève expansion with five terms

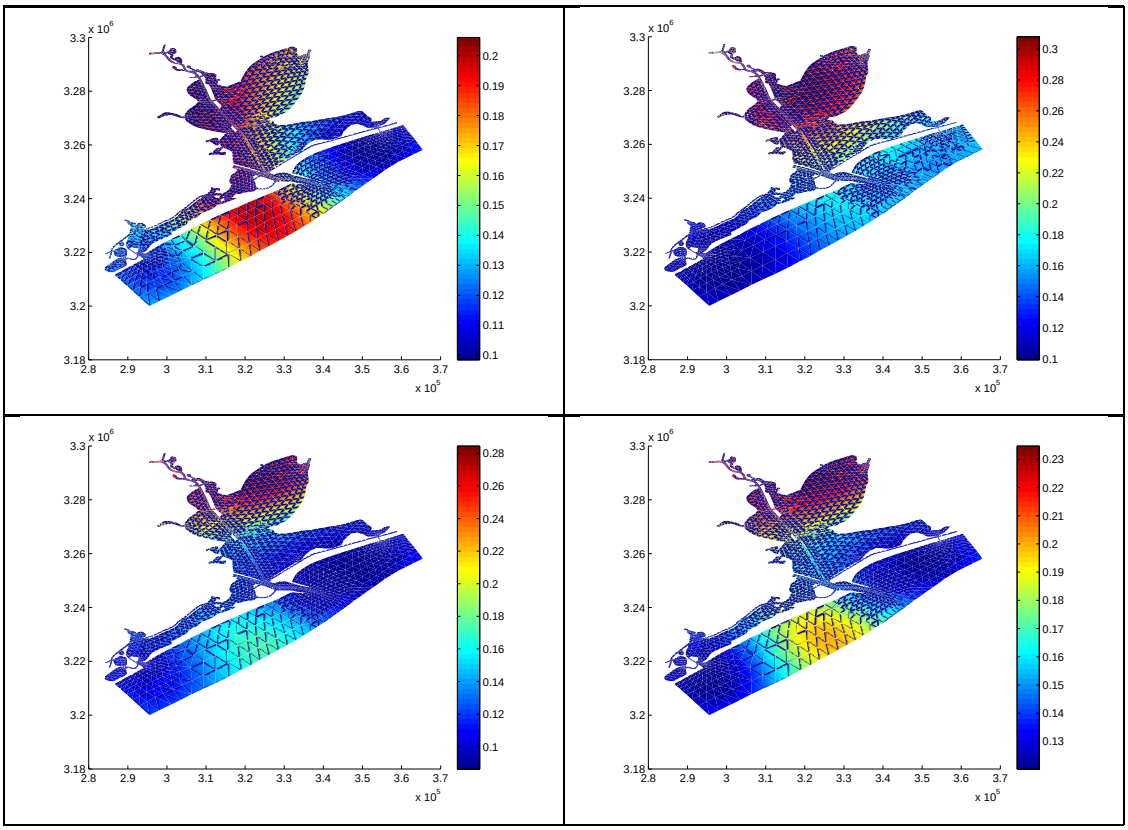

Figure 5.6: Various fields of Manning's n coefficients for the Galveston Bay domain defined by varying the random coefficients in a Karhunen-Loève expansion with five terms

For simplicity, we choose to estimate only one term of the Karhunen-Loève expansion. We also find that the level of detail resulting from including additional terms does not significantly affect the ADCIRC model solution in our test cases. Model sensitivity should always be considered when formulating a parameter estimation problem. Thus, in this work, the parameterization of the field of Manning's n coefficients represented as a stochastic process is also 1-D.

5.2.3 Parameter Estimation Methodology

We use a systematic approach in formulating our OSSEs in order to effectively determine the impact of using the SEIK filter for parameter estimation. In general, parameter estimation problems are approached with an attempt to exactly recover a model parameter that produces model output closely matching observed data. However, for complex computational models, these problems are often ill-posed, with various parameter values resulting in very similar model output. Thus, the aforementioned approach is not necessarily the most effective. Instead, our efforts may be better spent attempting to recover parameter estimates that produce the desired model output. In the experiments that follow, we seek to recover true Manning's n coefficients with the goal of improving forecasts of water elevations. We find that forecasted water elevations are generally not influenced by small perturbations in the value used for the Manning's n coefficient. Thus, rather than attempting to estimate the Manning's n coefficient exactly, it suffices to recover a value that

produces very similar water elevation data.

In the case of the field of constant Manning's n coefficients, we can do this by first classifying the values based on the water elevations they produce. We can then generate synthetic water elevation data from each of the classes, and use the parameter estimation to recover the correct class from an incorrect initial guess. We describe this procedure below.

5.2.3.1 Classifying Manning's n coefficients

To begin, we divide a spectrum of Manning's n coefficients, ranging from 0.005 to 0.2 and incremented by 0.005, into five classes. These values represent those often found in empirically defined tables, e.g. Table 2.1. The classes are defined by simulating tides using the ADCIRC model, with the smallest Manning's n coefficient, 0.005, defining the bottom stress. The smallest Manning's n coefficient is used because in the Manning's n formulation, smaller friction coefficients generate larger water elevations (i.e. tides with larger amplitudes). ADCIRC is forced using the principal lunar semi-diurnal (M_2) tidal constituent, with an amplitude of 0.25 m for the idealized inlet, and 0.1 m for Galveston Bay where the amplitude is measured relative to the geoid. The tides are simulated for 5 days, which includes a 12 hour ramp up period, using a 2 s time step. The largest mean amplitude of the tides generated at several locations throughout the domain is computed, and the Manning's n coefficients that generate tides with mean amplitudes less than 20%, 40%, 60%, 80%, and 100% of this value are divided into five classes. For

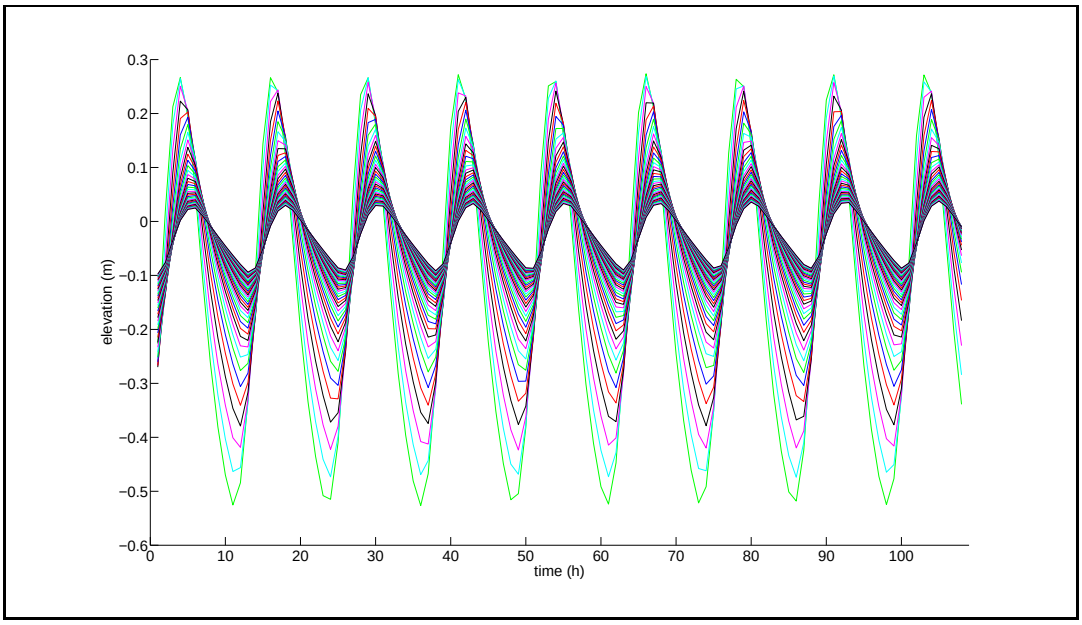

Figure 5.7: Water elevations modeled at station 1 of the idealized inlet domain for various Manning's n coefficients, with larger tidal amplitudes corresponding to smaller Manning's n coefficients

the idealized inlet, the largest tidal amplitudes are generated at station 1. The mean amplitude at this station is 0.267989 m, and the resulting classifications of the Manning's n coefficients are defined in Table 5.1.

For Galveston Bay, the mean amplitude at station 1 is 0.099569 m. The Manning's n coefficients are classified as shown in Table 5.2.

For both computational domains it is clear that the tides are more sensitive to variations in smaller Manning's n coefficients than they are to those in larger coefficients, as the classes become larger (i.e. they contain more coefficients) as the values of the coefficients increase.

Class	Mean of tidal amplitude (m)	Manning's n
A	0.267989 - 0.214391	0.005 - 0.025
B	0.214391- 0.160793	0.03 - 0.04
C	0.160793 - 0.107195	0.045 - 0.07
D	0.107195 - 0.053598	0.075 - 0.135
E	0.053598 - 0	0.14 - 0.2

Table 5.1: Manning's n coefficients in the idealized inlet classified by amplitude of corresponding tidal data at station 1

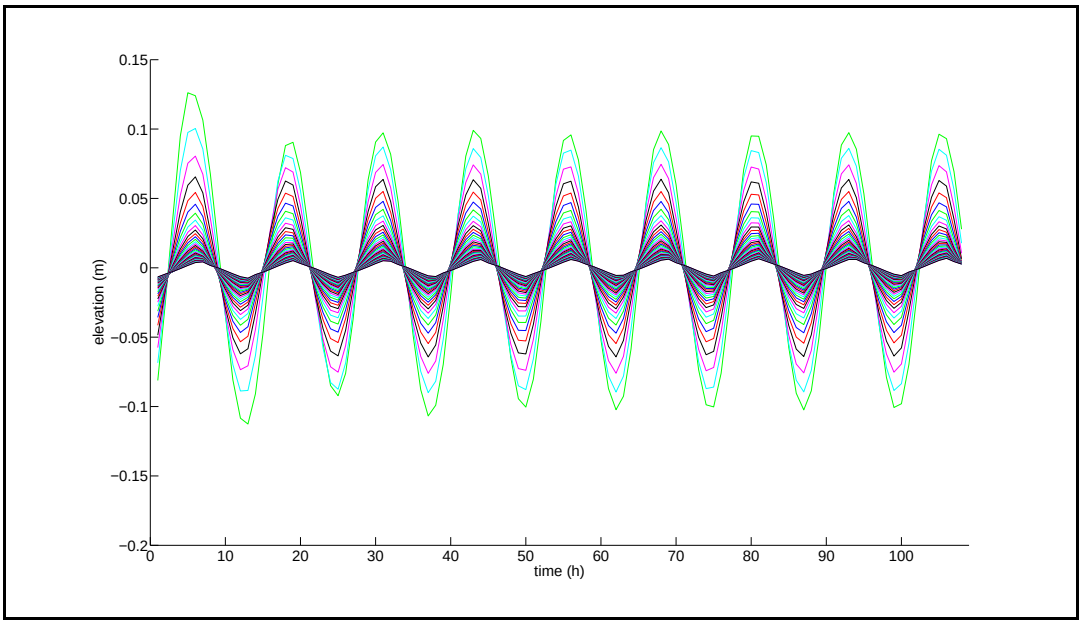

Figure 5.8: Water elevations modeled at station 1 of the Galveston Bay domain for various Manning's n coefficients, with larger tidal amplitudes corresponding to lower Manning's n coefficients

Class	Mean of tidal amplitude (m)	Manning's n
A	0.099569 - 0.079655	0.005 - 0.01
B	0.079655 - 0.059742	0.015-0.02
C	0.059742 - 0.039828	0.025 - 0.035
D	0.039828 - 0.019914	0.04 - 0.075
E	0.019914 - 0	0.08 - 0.2

Table 5.2: Manning's n coefficients in Galveston Bay classified by amplitude of corresponding tidal data at station 1

5.2.3.2 Simulating synthetic water elevation data

Once the five classes are defined, we generate synthetic water elevation data to be assimilated in the OSSEs. We simulate tides using the same configuration of the ADCIRC model described above, and set the constant Manning's n coefficient to a value from the center of each of the predefined classes. We use values of 0.015, 0.035, 0.06, 0.105, and 0.17 for the idealized inlet. For Galveston Bay, we use the constant values 0.01, 0.02, 0.03, 0.06, and 0.14. The data generated from these model runs are considered "truth" in the respective OSSEs.

5.2.3.3 Recovering the true class of Manning's n coefficients

Using the water elevations generated by the "true" parameters, we attempt to recover a Manning's n coefficient that lies within the correct class from an incorrect initial guess by applying the SEIK filter for parameter estimation to the ADCIRC model. We begin a model simulation using an initial guess of the Manning's n coefficient that comes from each of the four remaining classes. After the 12 hour ramp up period, we assimilate the synthetic water

sta.	x	y	h (m)	sta.	x	y	h (m)
1	1000	0	1.000	9	1500	700	1.000
2	1000	500	1.000	10	1500	0	1.000
3	1000	-500	1.000	11	1500	-700	1.000
4	2000	0	1.000	12	0	500	1.004
5	2000	-1000	1.000	13	0	-500	1.004
6	500	0	1.000	14	-1000	1000	2.389
7	0	0	0.995	15	-1000	-1000	2.389
8	2000	1000	1.000				

Table 5.3: x- and y-coordinates and bathymetry at the 15 observation stations in the idealized inlet

elevation data every hour over the 5 days for which we have simulated data. We only assimilate the data at several locations throughout the domain, which we label as observation stations. For the idealized inlet, we use 15 observation stations throughout the domain, denoted by the red circles in Figure 5.1. The locations and coordinates of these stations are listed in Table 5.3. We use an ensemble size of 10 and a value of $\sigma = 0.01$ (recall that σ^2 is the standard deviation in the initial estimate of the parameter). We have experimented with other values of σ, ranging from 0.001 to 0.1, however, for estimating a constant (or piecewise constant) field of Manning's n coefficients, the value of this filter parameter seems to have little influence on our parameter estimation results. For Galveston Bay, we use 21 observation stations (Figure 5.2). Data for these stations are listed in Table 5.4. Because of the increase in the number of observation stations, we also increase the ensemble size to 20 and we again let $\sigma = 0.01$.

To estimate two parameters, α and β, that define a field of Manning's

sta.	x (10^5 m)	y (10^6 m)	h (m)	sta.	x	y	h (m)
1	3.362	3.294	1.573	12	3.311	3.247	6.388
2	3.308	3.281	2.524	13	3.229	3.244	10.670
3	3.231	3.277	2.793	14	3.545	3.265	1.875
4	3.116	3.273	2.797	15	3.169	3.242	3.439
5	3.199	3.267	1.946	16	3.077	3.237	1.878
6	3.079	3.284	3.547	17	3.249	3.241	1.405
7	3.174	3.264	1.827	18	3.053	3.233	0.895
8	3.205	3.262	8.086	19	2.901	3.225	0.845
9	3.322	3.263	2.183	20	2.922	3.218	0.963
10	3.250	3.249	7.446	21	2.938	3.219	4.239
11	3.237	3.249	4.876				

Table 5.4: x- and y-coordinates and bathymetry at the 21 observation stations in Galveston Bay

n coefficients described by piecewise constants, we perform OSSEs in a similar manner as described above. We generate synthetic water elevation data by simulating tides using a field of Manning's n coefficients specified by "true" parameters, and then attempt to recover these parameters from incorrect initial guesses through data assimilation. However, for this case we cannot create classes as we did when estimating a single parameter without significant computation. Instead, we let the "true" parameterization equal $n_{0.005,0.1}$; the coefficient is set to 0.005 in the deep water of the open ocean (highlighted in green in Figures 5.1 and 5.2), and 0.1 in the shallow bay area (highlighted in blue). For the idealized inlet, we let the value of the coefficient increase linearly from α to β within the inlet (highlighted in purple). This field is reflective of Manning's n coefficients commonly used for these types of domains. Then, using various initial guesses, we seek to obtain parameterizations of Manning's

n coefficients that produce maximum tidal amplitudes that are within 20% of those amplitudes that result when the tides are simulated using the "true" bottom stress parameters. For the idealized inlet case, we use initial guesses equal to $n_{0.005,0.005}$, $n_{0.1,0.1}$, $n_{0.06,0.06}$, and $n_{0.1,0.005}$. Thus we see the results of incorrectly estimating either α or β, as well as incorrectly estimating both α and β. We also see the effect of estimating a field that is not constant from one that is constant. The initial guesses used in the Galveston Bay case are influenced by a sensitivity analysis of the ADCIRC model respective to the 2-D parameterization and we will discuss this further in the next section. Again we force the ADCIRC model with an M_2 tidal constituent with an amplitude of 0.25 m for the idealized inlet and 0.1 m for Galveston Bay. We assimilate the true water elevation data every hour following a 12 hour ramp up period in a 5 day simulation for the idealized inlet. For Galveston Bay, we use a total simulation time of 30 days.

For our final experiments, we estimate the random variable in the first term of a Karhunen-Loève expansion. For a fixed random variable, the Karhunen-Loève expansion represents a realization of the stochastic process that defines the field of Manning's n coefficients. Rather than estimating the field of coefficients directly, we instead estimate the natural log of the field. We take this approach primarily because it allows us to simulate fields of Manning's n coefficients that are physical. The Manning's n coefficient is a positive value that, as indicated by the classifications above, nonlinearly affects the modeled water elevations. By modeling the natural log of the stochastic

process, we enforce positivity of the estimated coefficients. Furthermore, the Gaussian assumptions in the Kalman filter equations translate to an assumption of a log normal distribution of Manning's n coefficients. If we consider each model state to be equally probable, this more accurately represents the distribution of the coefficients.

To determine the "true" parameters to be estimated we utilize the classes defined in the first OSSEs (Tables 5.1 and 5.2). The Gaussian assumption of the (log of the) process allows us to define the field of Manning's n coefficients completely through its mean and covariance. We let the expectation of the field equal a value from the middle class, class C. As previously discussed, we choose the exponential covariance function to define the underlying stochastic process. Various realizations of the process, i.e. fields of Manning's n coefficients to be estimated, are then modeled by fixing the random variable, $\xi_1(\theta)$, in the first term of the expansion (4.2.2).

We choose our "true" parameters in such a way that the resulting fields are realistic (i.e. Manning's n coefficients do not significantly exceed 0.2) and span the values of the remaining classes. We do this through the specification of the parameter variance. For these experiments we will denote the spatially varying field by $n(\mathbf{x})$. Thus, in terms of the Karhunen-Loève expansion,

$$n(\mathbf{x}) = \exp\left[\overline{\omega}(\mathbf{x}) + \xi_1(\theta)\sqrt{\lambda_1} f_1(\mathbf{x})\right].$$

For the idealized inlet, we choose $\overline{\omega}(\mathbf{x})$ so that the expectation of the field is equal to 0.06, i.e. $n(\mathbf{x}) = 0.06$ when $\xi_1(\theta) = 0$. We then define the pa-

rameter variance so that values from classes B and D are within one standard deviation of the mean; we let $\exp\left[\overline{\omega}(\mathbf{x}) - \xi_1(\theta)\sqrt{\lambda_1}f_1(\mathbf{x})\right] = 0.035$ and $\exp\left[\overline{\omega}(\mathbf{x}) + \xi_1(\theta)\sqrt{\lambda_1}f_1(\mathbf{x})\right] = 0.105$. Considering the ranges of Manning's n coefficients defined by the eigenpairs for the exponential covariance function, we determine that the value of σ, the standard deviation in the initial estimate of the parameter, should be $0.851 \leq \sigma \leq 2.695$. We follow the same procedure for the Galveston Bay domain, letting the expectation of the field equal 0.02. We determine that σ should be specified so that $0.764 \leq \sigma \leq 3.060$.

Using this estimate of the standard deviation, we let the true random coefficients in the Karhunen-Loève expansion range from -3 to +3 and generate true fields of Manning's n coefficients using each nonzero integer in this range (Figures 5.11 and 5.12). For the idealized inlet, we force the ADCIRC model in the same manner that we have described in the other two experiments, i.e. with an M_2 tidal constituent with a 0.25 m amplitude. However, for Galveston Bay we increase the amplitude of the M_2 tidal constituent to 0.5 m. Using the larger amplitude allows for more variation in the water elevations generated by the different parameters, which is essential for the statistical data assimilation for parameter estimation to be effective. Then, for the parameter estimation, we assimilate the "true" water elevation data into a model simulation where the initial guess of the field is equal to the mean field, i.e. the initial guess of the parameter is zero. For the idealized inlet, the tides are simulated for 30 days, including a 12 hour ramp up period, and data is assimilated every hour. For this case, we let $\sigma = 2.695$, since this is the standard deviation in

ξ that corresponds to a distribution of physical Manning's n fields. For the Galveston Bay case, we let $\sigma = 3.060$. The length of the assimilation time is discussed below.

We again approach the parameter estimation problem with the goal of recovering those bottom stress parameters, ξ, corresponding to Manning's n coefficients that produce maximum tidal amplitudes that are within 20% of those amplitudes that result when the tides are simulated using the "true" parameters. For the idealized inlet, we compute the tidal amplitudes at station 15, as the water elevations are some of the largest here. For Galveston Bay, we compute the tidal amplitudes at station 21.

For each of the OSSEs, in addition to the data assimilation experiments, we run a baseline case, where no data is assimilated, to quantify the impact of the SEIK filter. It should be noted that in all of our test cases we use the same model to generate synthetic data that we use to perform data assimilation experiments. We do this deliberately in order to isolate the source of error in the water elevations; the parameter estimates are not overcompensating for other sources of model error. Additionally, the ADCIRC coastal ocean model has been verified and validated extensively. It gives reliable data provided the model parameters are accurate and the spatial domain is adequately resolved. Accurately prescribing parameters is the focus of this work, and with regard to the spatial resolution, refining the model domain used to generate synthetic data introduces only negligible changes to the numerical results presented below.

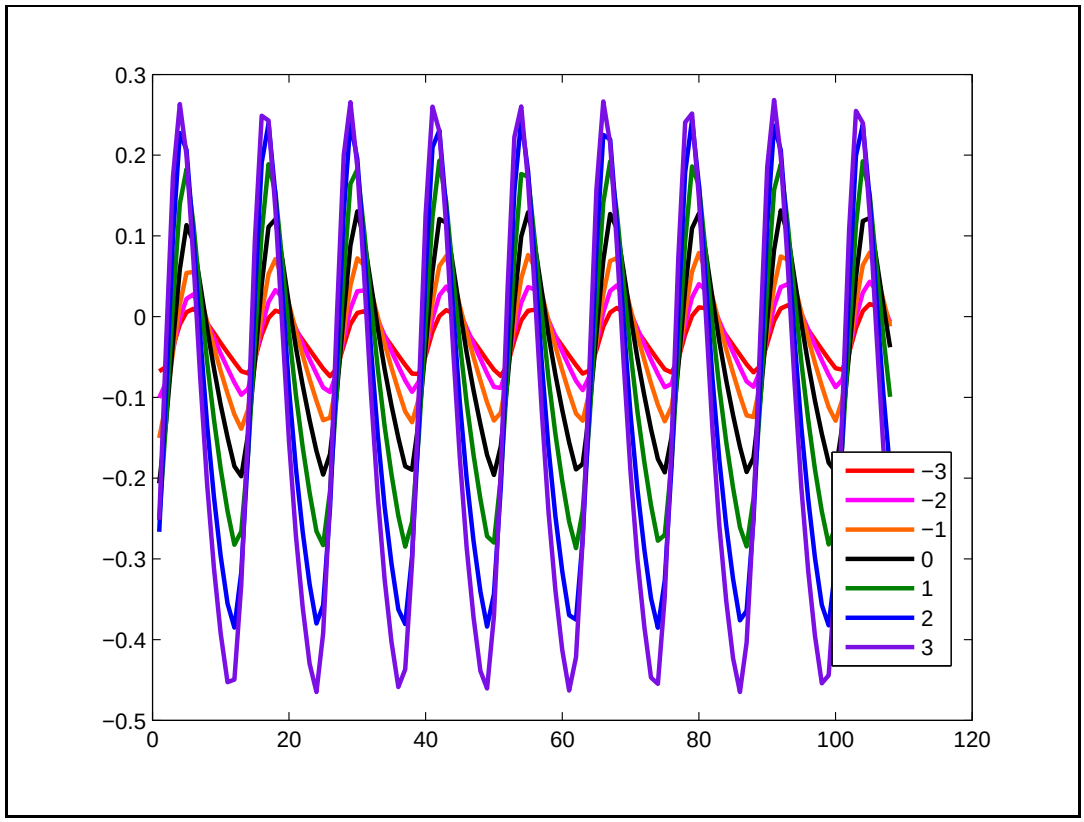

Figure 5.9: Water elevations modeled at station 1 in the idealized inlet for seven parameters used to define different fields of Manning's n coefficients

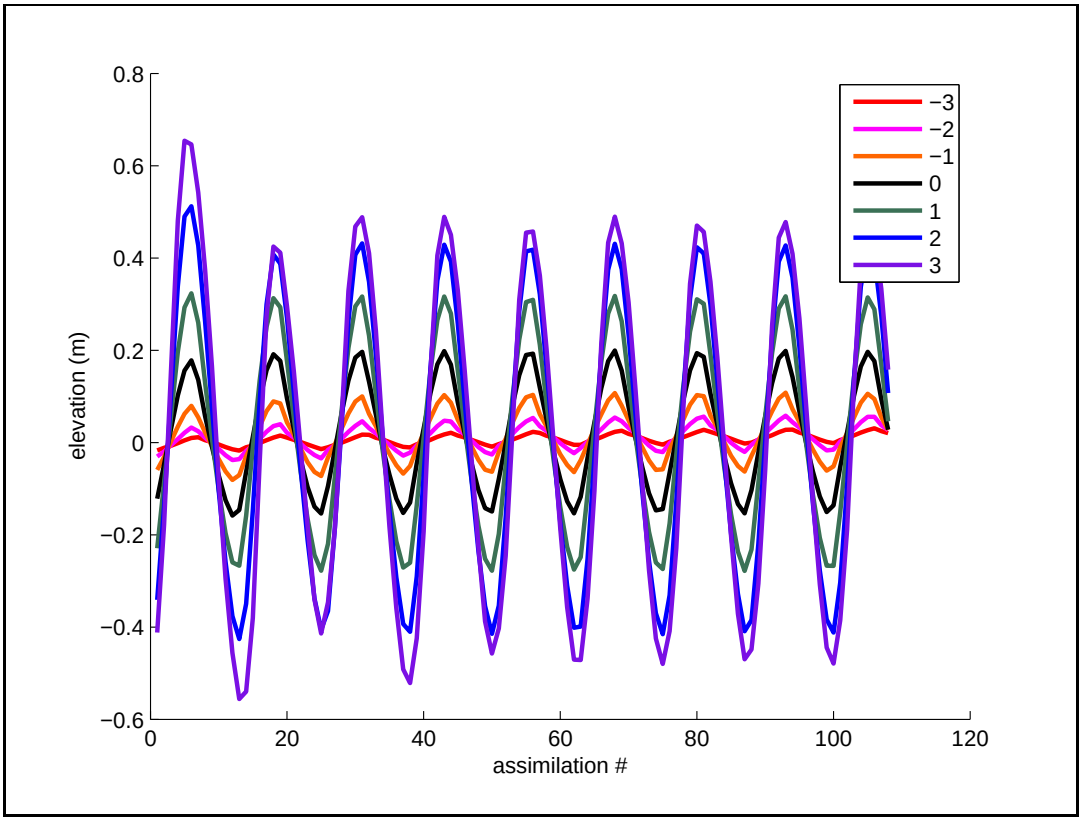

Figure 5.10: Water elevations modeled at station 1 in Galveston Bay for seven parameters used to define different fields of Manning's n coefficients

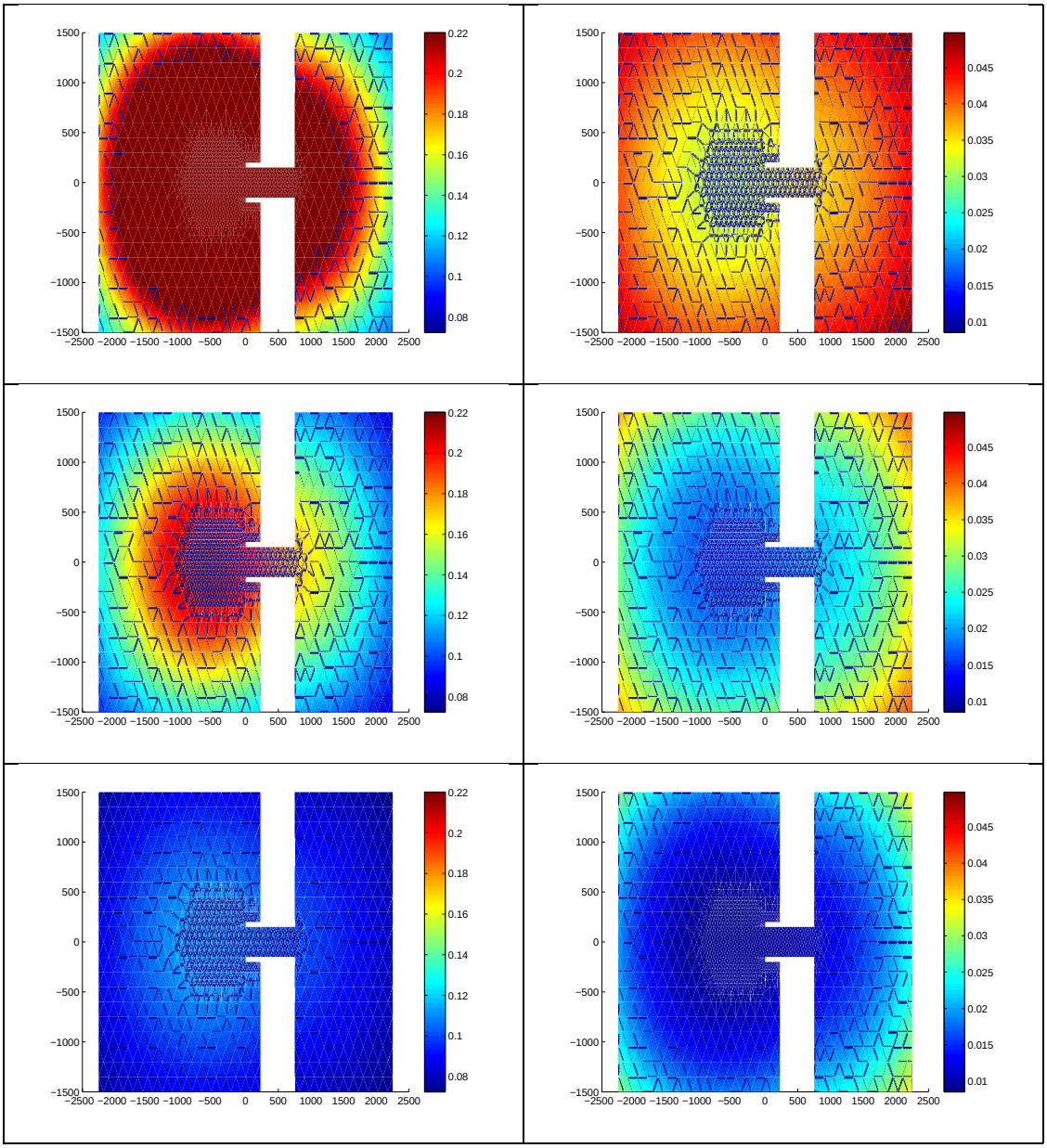

Figure 5.11: Realizations of the stochastic process defining a field of Manning's n coefficients on the idealized inlet domain. From top to bottom, left to right, $\xi = -3, -2, -1, 1, 2$, and 3

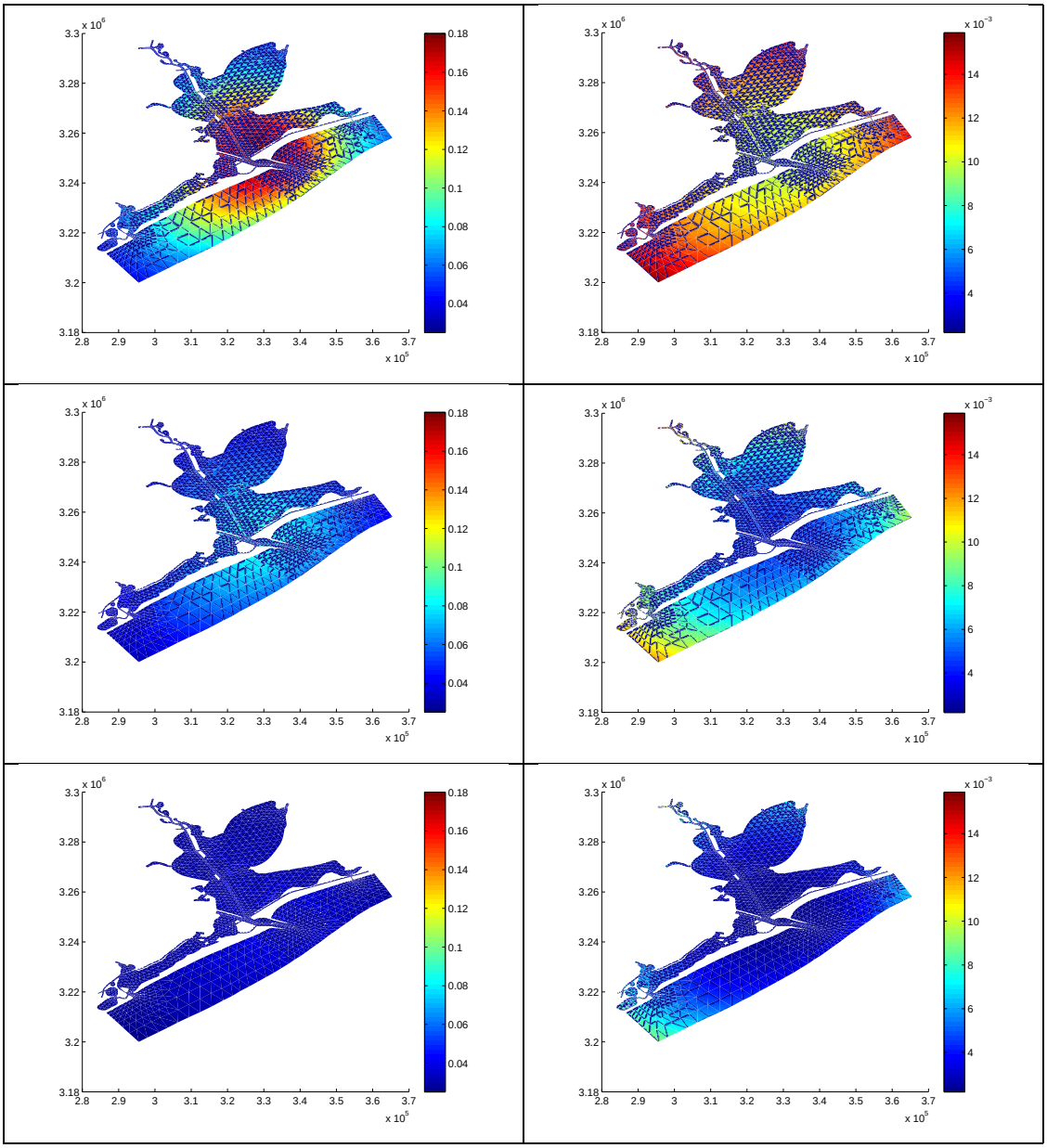

Figure 5.12: Realizations of the stochastic process defining a field of Manning's n coefficients on the Galveston Bay domain. From top to bottom, left to right, $\xi = -3, -2, -1, 1, 2$, and 3

5.3 Numerical Results and Discussion

In this section we present the results of the OSSEs described above. A summary of the results is provided in Tables 5.17-5.19.

5.3.1 A Field of Constant Manning's n Coefficients

Using the SEIK filter for parameter estimation, we find that for the field of constant Manning's n coefficients, we are able to accurately estimate the correct class of parameters for the three smallest classes A, B, and C, no matter which of the four incorrect initial guesses we choose, i.e. the final estimate of the coefficient lies in the same class as that of the true value (Table 5.5). In estimating the field of Manning's n coefficients parameterized by 0.105 (i.e. class D), final estimates belonging to class D were obtained from all but the smallest of the initial guesses. In estimating the field of Manning's n coefficients parameterized by 0.17 (i.e. class E), an estimate belonging to class E was obtained from the largest initial guess. Because we incremented the Manning's n coefficients by 0.005 when defining the classes, there are Manning's n coefficients that do not lie within a class, i.e. they lie between two classes (Table 5.1). In these cases, we consider the parameter estimation a success if the final estimate of the Manning's n coefficient lies in one of the intervals adjacent to the "true" class. With this consideration, a correct final estimate of 0.17 was also obtained from an initial guess from class B. In both of these cases (the estimates of 0.105 and 0.17), "correct" final estimates were recovered from the initial guesses that were from classes

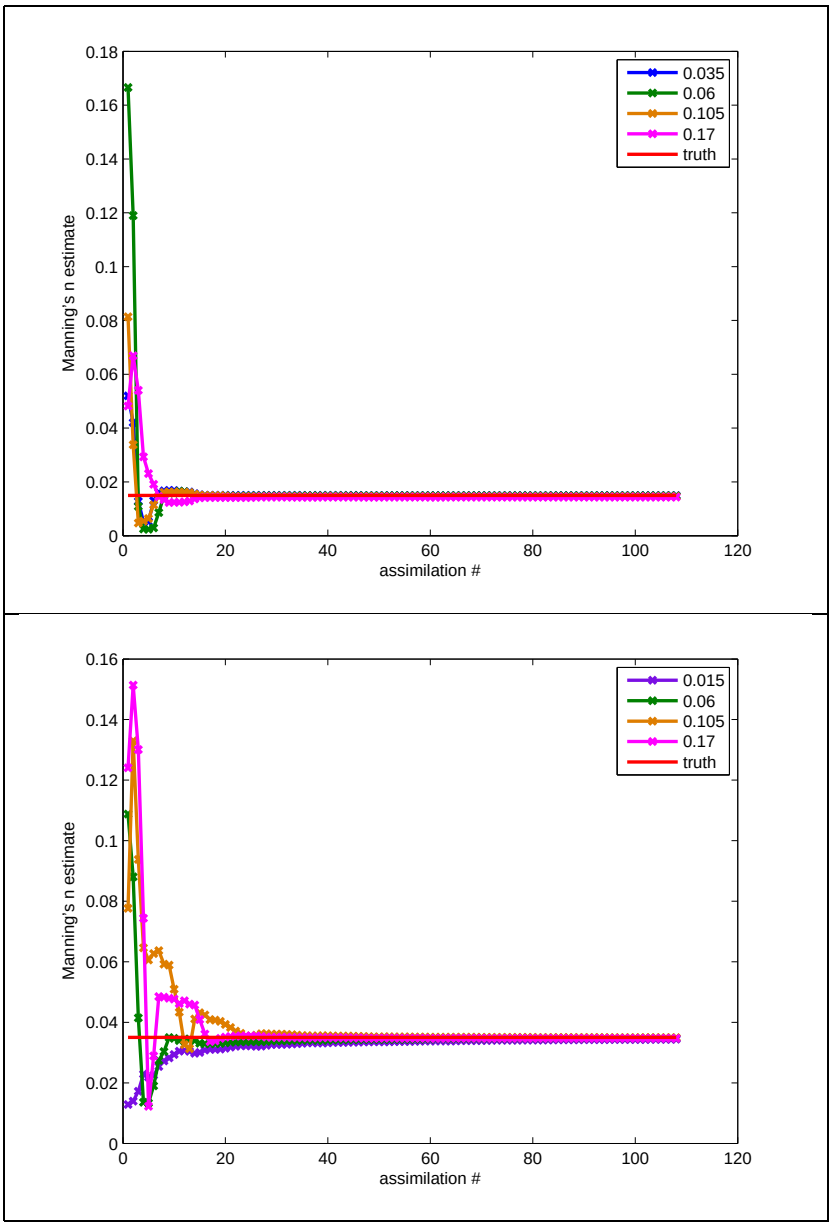

Figure 5.13: Estimates of various "true" Manning's n fields parameterized by a single value for the idealized inlet case. The "true" Manning's n value is 0.015 (class A) in the top figure and 0.035 (class B) in the bottom figure.

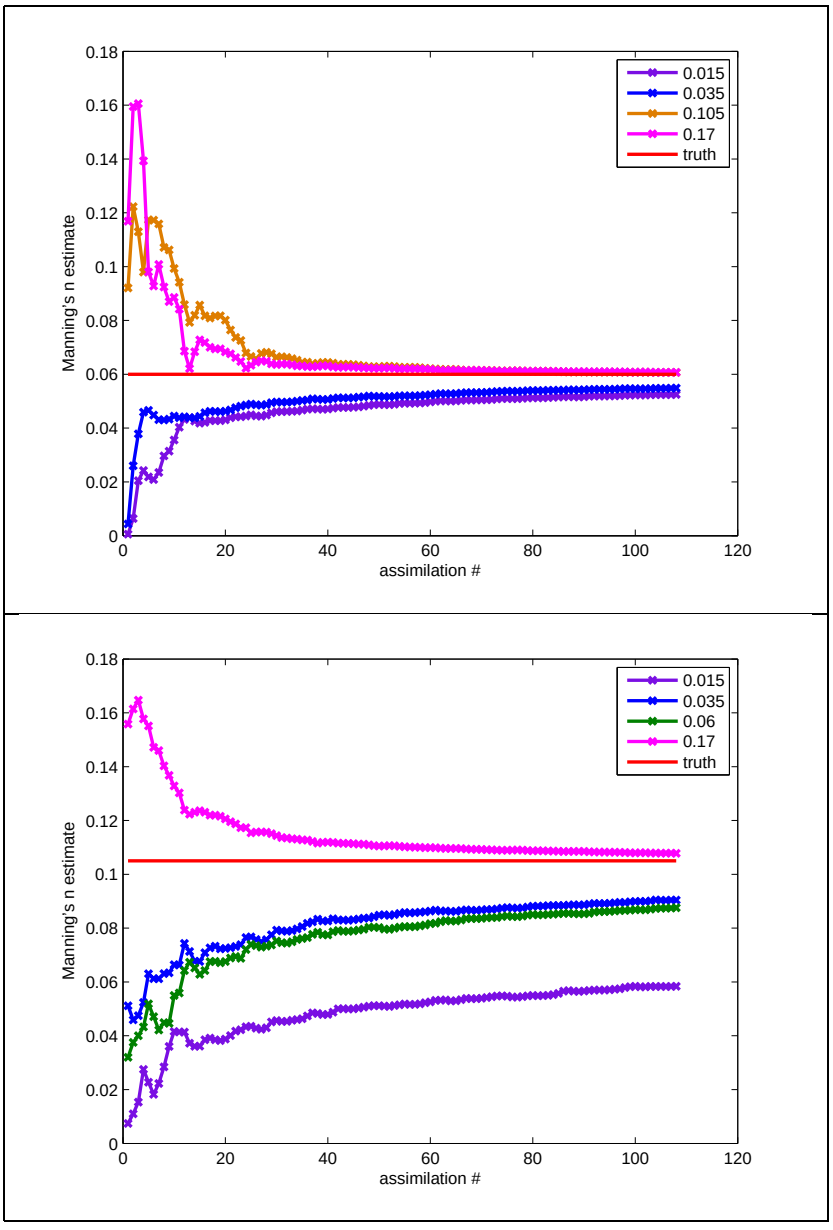

Figure 5.14: Estimates of various "true" Manning's n fields parameterized by a single value for the idealized inlet case. The "true" Manning's n value is 0.06 (class C) in the top figure and 0.105 (class D) in the bottom figure.

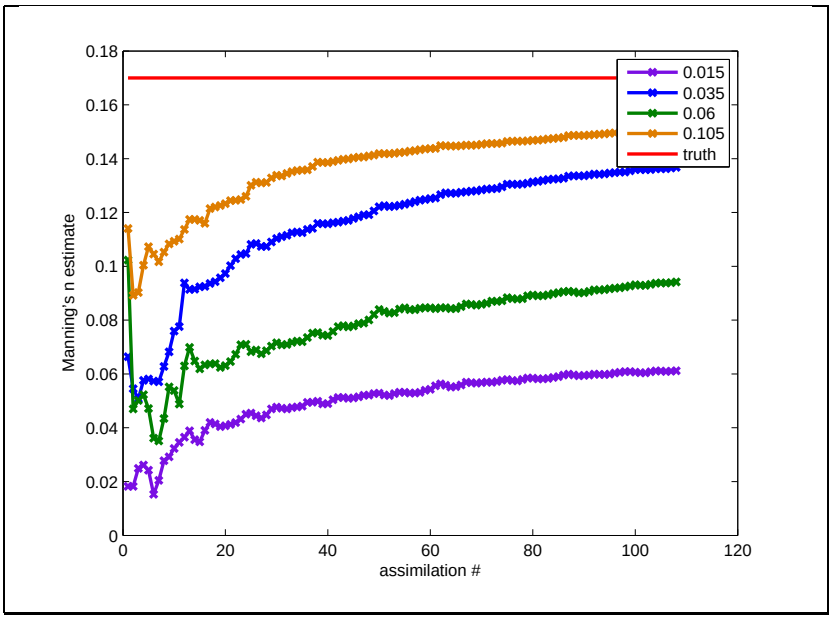

Figure 5.15: Estimates of various "true" Manning's n fields parameterized by a single value for the idealized inlet case. The "true" Manning's n value is 0.17 (class E).

Idealized Inlet with Ebb Shoal				
initial guess of 0.015	**0.035**	**0.06**	**0.105**	**0.17**
Final estimate	0.014948	0.014840	0.014622	0.014353
Relative error	0.003460	0.010640	0.025180	0.043134
RMSE (SEIK)	0.014790	0.022188	0.011590	0.017258
RMSE (baseline)	0.076792	0.115541	0.140996	0.157038
initial guess of 0.035	**0.015**	**0.06**	**0.105**	**0.17**
Final estimate	0.034406	0.034739	0.034930	0.034684
Relative error	0.016967	0.007469	0.002011	0.009015
RMSE (SEIK)	0.018030	0.014338	0.017707	0.018068
RMSE (baseline)	0.076792	0.042259	0.072842	0.094232
initial guess of 0.06	**0.015**	**0.035**	**0.105**	**0.17**
Final estimate	0.052506	0.054884	0.060664	0.060719
Relative error	0.124892	0.085252	0.011067	0.011977
RMSE (SEIK)	0.035843	0.023266	0.013747	0.013204
RMSE (baseline)	0.115541	0.042259	0.032302	0.056430
initial guess of 0.105	**0.015**	**0.035**	**0.06**	**0.17**
Final estimate	0.058388	0.090433	0.087582	0.107812
Relative error	0.443927	0.138733	0.165878	0.026781
RMSE (SEIK)	0.058573	0.018113	0.024664	0.007318
RMSE (baseline)	0.140996	0.072843	0.032302	0.025872
initial guess of 0.17	**0.015**	**0.035**	**0.06**	**0.105**
Final estimate	0.061195	0.136759	0.094165	0.151548
Relative error	0.640027	0.195536	0.446086	0.108542
RMSE (SEIK)	0.076949	0.028322	0.046545	0.014223
RMSE (baseline)	0.157038	0.094232	0.056430	0.025872

Table 5.5: Final estimate errors of various "true" Manning's n fields parameterized by a single value for the idealized inlet case. The RMSEs are of forecasted water elevations for the parameter estimation (SEIK filter) and baseline cases.

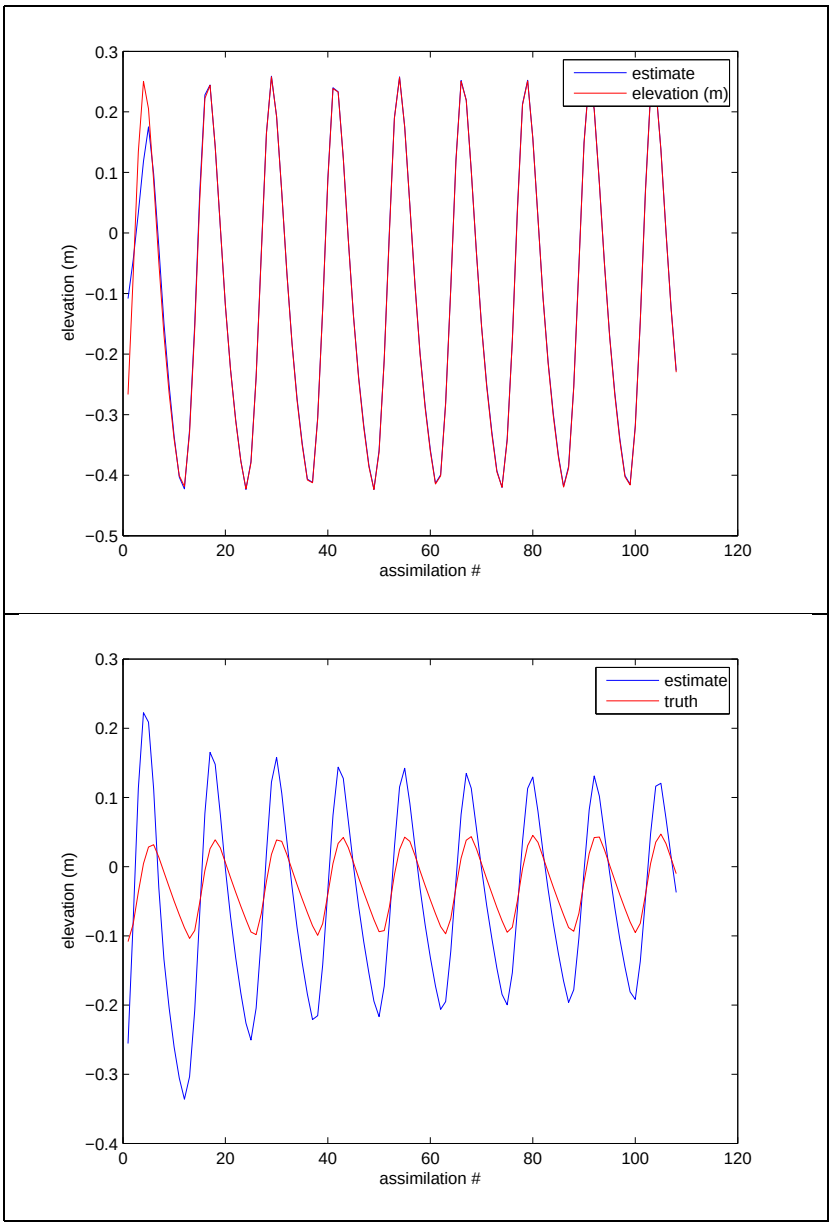

Figure 5.16: Estimates of the "true" state at station 1 from the initial guess $n = 0.17$ of the "true" value of $n = 0.015$ (top) and from the initial guess $n = 0.015$ of the "true" value of $n = 0.17$ (bottom).

closest to that of the true coefficient. In general, the correct coefficient is underestimated, particularly in the case when the initial guess is less than the true value. Also, the relative error in the estimate of the Manning's n coefficient generally increases with the true value. Here, it is appropriate to consider relative error as the model output is more sensitive to variations in the smaller coefficients than it is to variations in the larger coefficients. We discuss the aforementioned trend in the relative error below.

In addition to estimating the model parameters, we seek to improve forecasts of the model state. We compute the global root mean square error (RMSE) in the water elevations across all nodes of the domain at every assimilation time. As a result, this error is influenced by the (inaccurate) initial guess of the Manning's n coefficient (e.g. see Figure 5.16), but we find that it is significantly improved by the SEIK filtering over the baseline case in every instance. We note that the largest RMSE in the SEIK filtering case is 0.076949, and by comparison the baseline case has a corresponding RMSE that is over 100% larger (Table 5.5).

As previously noted, the size of the classes of Manning's n coefficients (Table 5.1) generally increases with the values of the coefficients, indicating that the ADCIRC model is not as sensitive to small variations in the larger Manning's n coefficients as it is to small variations in the smaller coefficients. This idea is supported by noting that the baseline RMSEs in the water elevations generally decrease with increasing values of the true Manning's n coefficients. The result is that smaller model/data discrepancies, and thus

smaller subsequent filter updates, occur when larger Manning's n coefficients are estimated from classes with smaller values. We thus expect to experience more difficulty in recovering larger coefficients. For the case of 0.105, the filter only failed to attain an estimate in the desired class (class D) when the initial guess was from the class furthest from that of the true value (class A). We see similar behavior in the case of 0.17. Thus, for larger coefficients, the filter might simply require a more accurate initial guess or more time to attain the correct value. This idea is reflected in Figures 5.13 - 5.15, as the variation in the estimates of each Manning's n coefficient after 40 assimilation cycles increases with the true value; the parameter estimate requires more time to converge for larger values.

For Galveston Bay, we again find that we are able to accurately estimate nearly all of the Manning's n coefficients from any initial guess (Table 5.6). The only exception occurs in the estimation of 0.14. In this case, final estimates belonging to the correct class are obtained from all but the smallest of the initial guesses, 0.01 and 0.02; "correct" estimates are recovered from the two larger initial guesses, which come from the classes that are closest to the true coefficient (classes C and D).

In addition to estimating the model parameters, we again aim to improve forecasts of the model state. We compute the global RMSE in the water elevations across all nodes of the domain at every assimilation time and find that it is significantly improved by the SEIK filtering over the baseline case in every instance. The largest RMSE is 0.015166. This is the error in the case

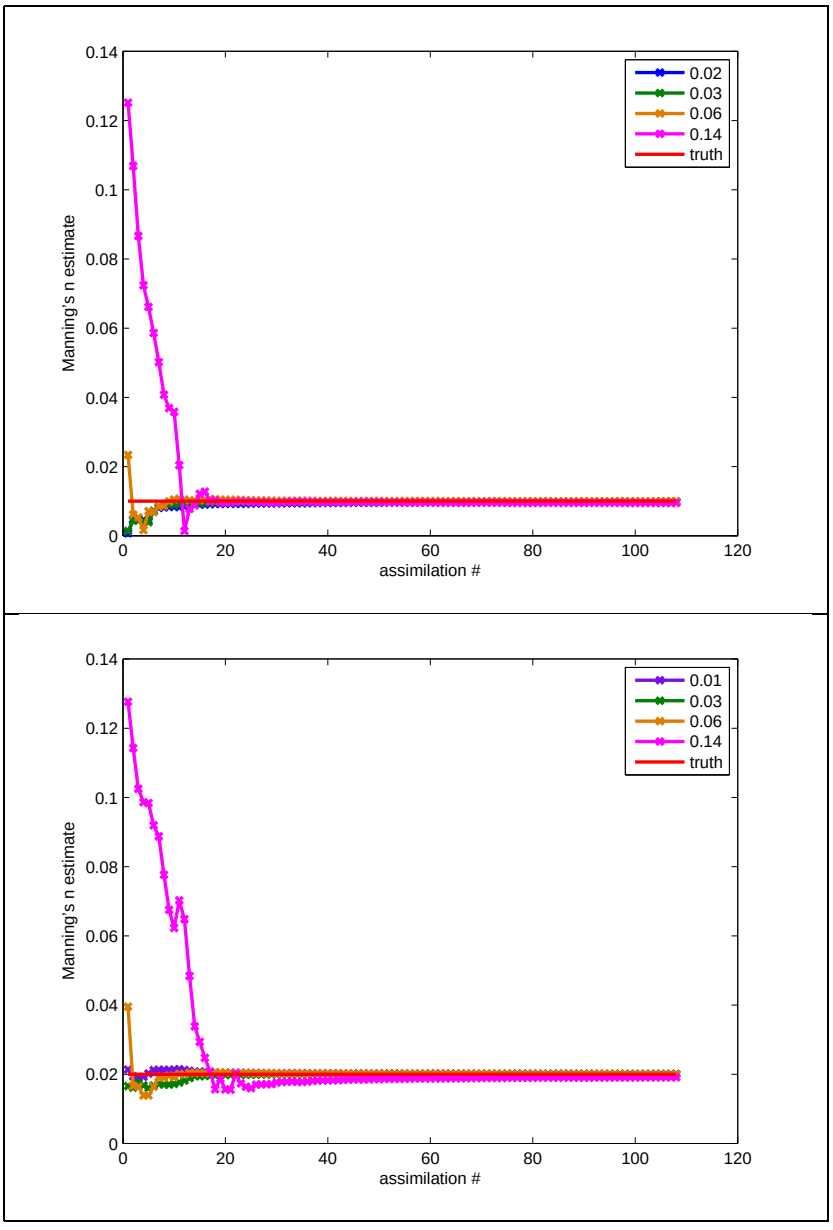

Figure 5.17: Estimates of "true" Manning's n fields parameterized by a single value for the Galveston Bay case. The "true" Manning's n value is 0.01 (class A) in the top figure and 0.02 (class B) in the bottom figure.

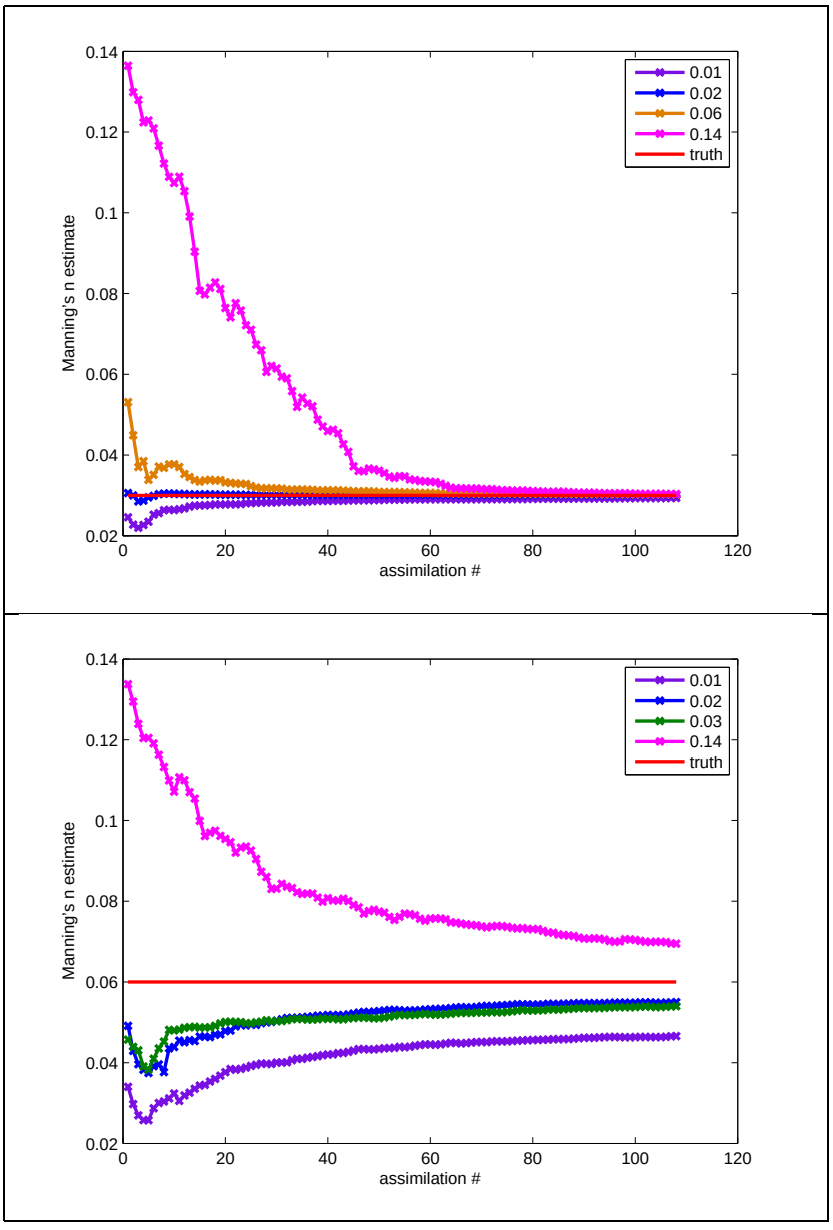

Figure 5.18: Estimates of "true" Manning's n fields parameterized by a single value for the Galveston Bay case. The "true" Manning's n value is 0.03 (class C) in the top figure and 0.06 (class D) in the bottom figure.

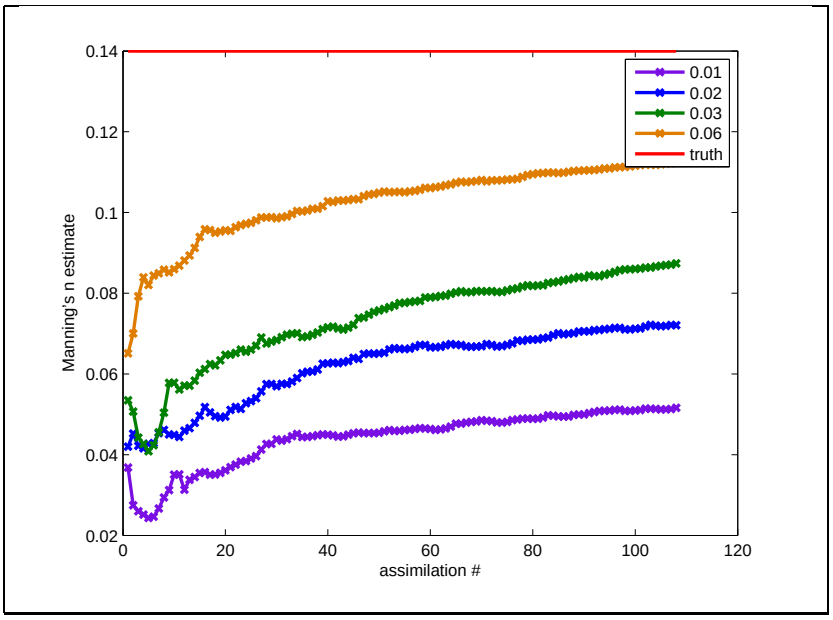

Figure 5.19: Estimates of a "true" Manning's n field parameterized by a single value for the Galveston Bay case. The "true" Manning's n value is 0.14 (class E).

Galveston Bay				
initial guess of 0.01	**0.02**	**0.03**	**0.06**	**0.14**
Final estimate	0.009776	0.009903	0.009921	0.009479
Relative error	0.022383	0.009720	0.007877	0.052067
RMSE (SEIK)	0.003502	0.004191	0.007290	0.015166
RMSE (baseline)	0.016351	0.024598	0.033514	0.038380
initial guess of 0.02	**0.01**	**0.03**	**0.06**	**0.14**
Final estimate	0.020069	0.019979	0.019948	0.019101
Relative error	0.003440	0.001044	0.002582	0.044947
RMSE (SEIK)	0.002411	0.001935	0.003781	0.009337
RMSE (baseline)	0.016351	0.008966	0.019577	0.026017
initial guess of 0.03	**0.01**	**0.02**	**0.06**	**0.14**
Final estimate	0.029357	0.030051	0.030207	0.030323
Relative error	0.021433	0.001706	0.006885	0.010777
RMSE (SEIK)	0.003870	0.001264	0.002745	0.009045
RMSE (baseline)	0.024598	0.008966	0.011161	0.018304
initial guess of 0.06	**0.01**	**0.02**	**0.03**	**0.14**
Final estimate	0.046579	0.055006	0.053981	0.069481
Relative error	0.223687	0.083235	0.100310	0.158009
RMSE (SEIK)	0.007690	0.004010	0.002911	0.003770
RMSE (baseline)	0.033514	0.019577	0.011161	0.007729
initial guess of 0.14	**0.01**	**0.02**	**0.03**	**0.06**
Final estimate	0.051604	0.072078	0.087391	0.112387
Relative error	0.631399	0.485155	0.375777	0.197233
RMSE (SEIK)	0.013696	0.008704	0.006591	0.002847
RMSE (baseline)	0.038380	0.026017	0.018304	0.007729

Table 5.6: Final estimates and estimate errors of various "true" Manning's n fields parameterized by a single value for the Galveston Bay case. The RMSEs are of forecasted water elevations for parameter estimation (SEIK filter) and baseline cases.

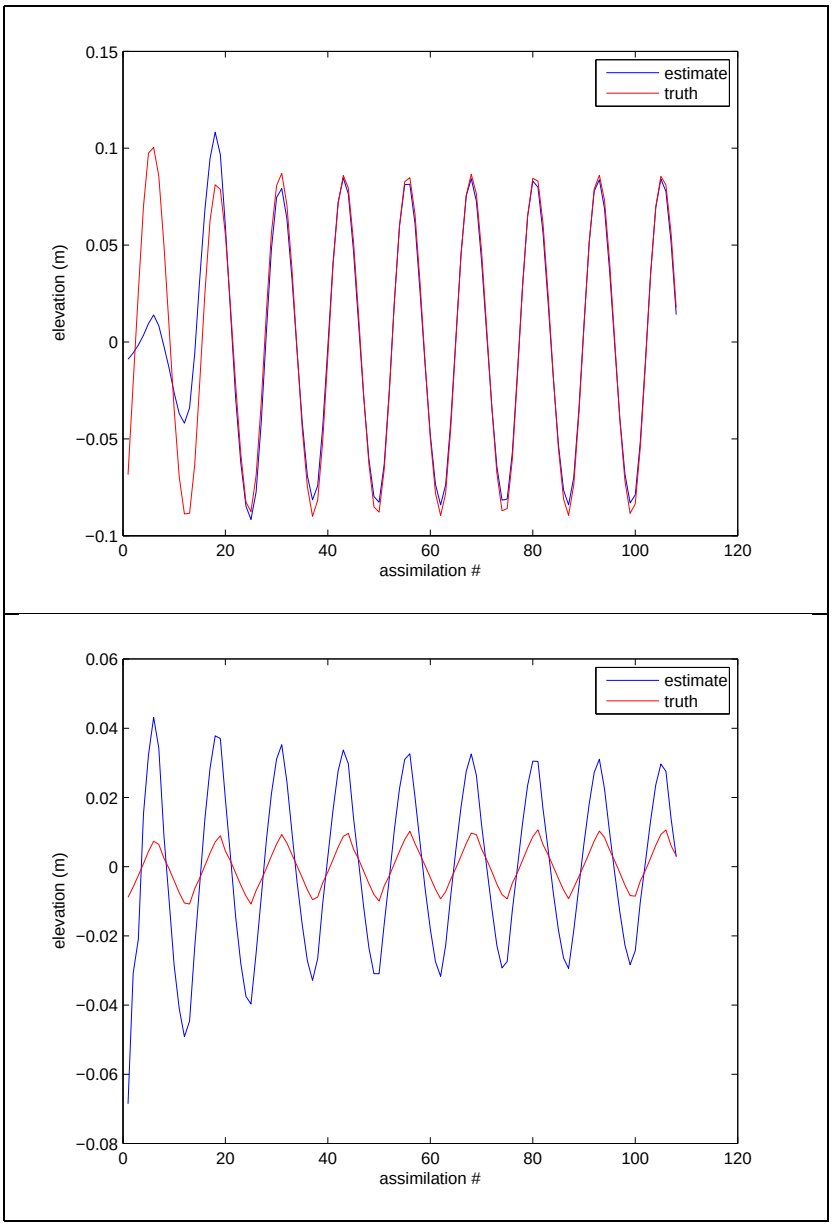

Figure 5.20: Estimates of the "true" state at station 1 from the initial guess $n = 0.14$ of the "true" value of $n = 0.01$ (top) and from the initial guess $n = 0.01$ of the "true" value of $n = 0.14$ (bottom).

when the smallest Manning's n coefficient (0.01) is estimated from the largest initial guess (0.14). Consequently this RMSE is inflated from the initial error in the water elevations. Nevertheless, the error is reduced by over 60 % over the baseline case, and it is small in comparison to the mean tidal amplitudes generated using Manning's n coefficients in this class.

We observe the same trends in estimating a constant field of Manning's n coefficients in Galveston Bay that we did when estimating a constant field in the idealized inlet. Again, we note that the size of the classes of Manning's n coefficients (Table 5.2) increases with the values, supporting the idea that the ADCIRC model is not as sensitive to small variations in the larger Manning's n coefficients. We expect that for larger values of the Manning's n coefficients, the SEIK filter will make smaller updates to the model parameters and thus require more time to converge to final estimates that lie within the desired class. This is observed in Figures 5.17 - 5.19, as the variation in the final estimates of each Manning's n coefficient increases with the magnitude of the true value, noticeably for the estimates of the largest values, 0.06 and 0.14. The small baseline RMSEs in the computed water elevations again support the idea that the updates made to the parameters are small. In the two cases where the Manning's n coefficients are not accurately recovered (i.e. when 0.14 is estimated from 0.01 and 0.02), the RMSEs are less than 0.015. Because this error is computed globally over space and time, the elevation errors at the later assimilation times are smaller than those at earlier times (e.g. see Figure 5.20), and the updates made to the estimates of the Manning's n coefficients in the

initial guess	$\boldsymbol{n_{0.005,0.005}}$	$\boldsymbol{n_{0.1,0.1}}$	$\boldsymbol{n_{0.06,0.06}}$	$\boldsymbol{n_{0.1,0.005}}$
Manning's n	0.006633	0.005721	0.005004	0.005325
estimate of $n_{0.005,0.1}$	0.087819	0.100251	0.098679	0.097747
ℓ_2 error (SEIK)	0.012290	0.000764	0.001321	0.002276
ℓ_2 error (baseline)	0.095000	0.095000	0.068007	0.134350
Relative error (α)	0.326543	0.144290	0.000852	0.065053
Relative error (β)	0.121809	0.002512	0.013206	0.022526
RMSE (SEIK)	0.027044	0.010573	0.004613	0.008532
RMSE (baseline)	0.156683	0.082921	0.068212	0.106257
Mean tidal amplitude (sta. 1)	0.155605	0.115380	0.128850	0.132544
Relative error	0.196570	0.083531	0.029745	0.056787

Table 5.7: Final estimate errors of various "true" Manning's n fields parameterized by two values for the idealized inlet domain. The RMSEs are of forecasted water elevations for the parameter estimation (SEIK filter) and baseline cases.

final assimilation cycles are minor. Relative to the idealized inlet cases, here, the parameter estimates require a longer time to converge to the true value. For the estimates of 0.06 and 0.14, there is still a notable amount of variation in the estimates of the coefficients even through the fifth day of assimilation.

5.3.2 A Field of Piecewise Constant Manning's n Coefficients

Next we attempt to estimate the values defining a 2-D parameterization of a field of Manning's n coefficients. For the idealized inlet case, we find that we are able to do so accurately from each of the four initial guesses (Table 5.7). In each experiment, the ℓ_2 error (i.e., the Euclidean norm of the error) of the final estimate of the pair of parameters is less than 0.013. This is a significant reduction in the ℓ_2 error of the initial guesses, which is as high

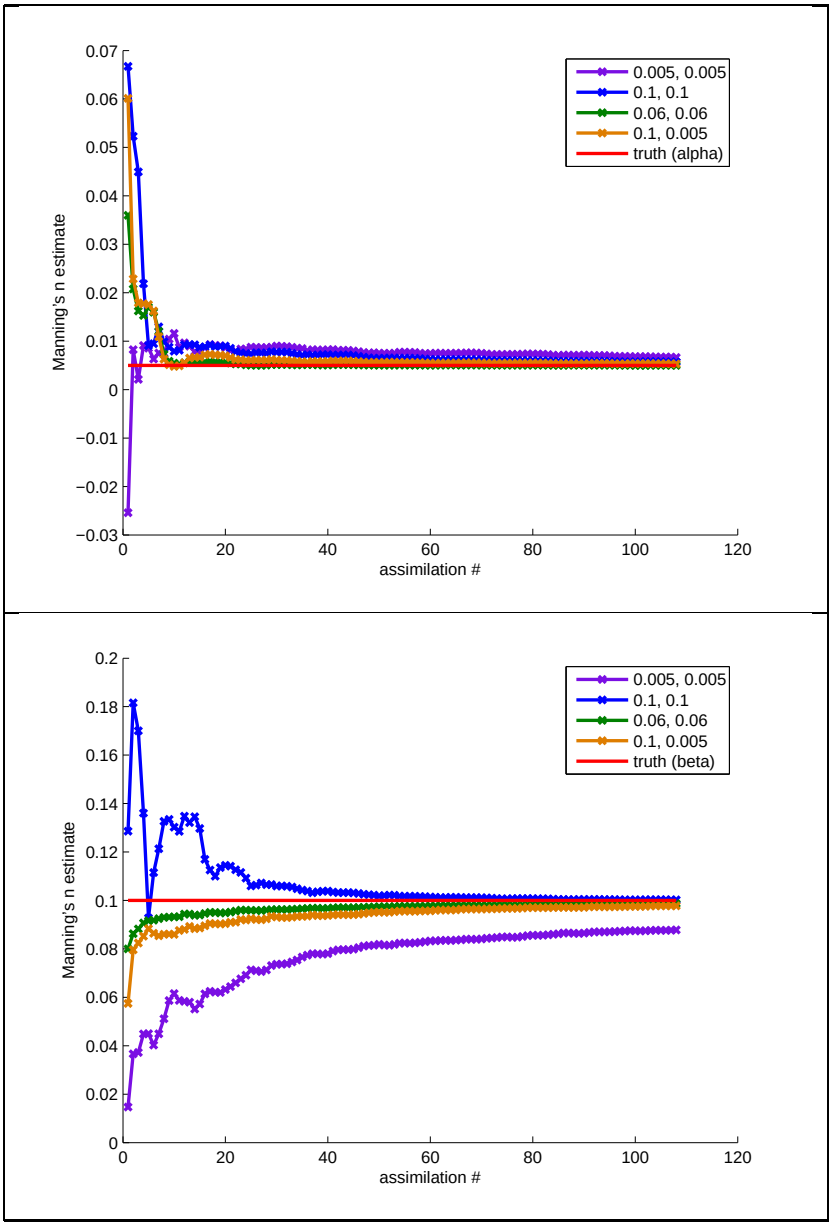

Figure 5.21: Estimates of α (top) and β (bottom), parameters that define a "true" 2-D parameterization of a Manning's n field defined on idealized inlet

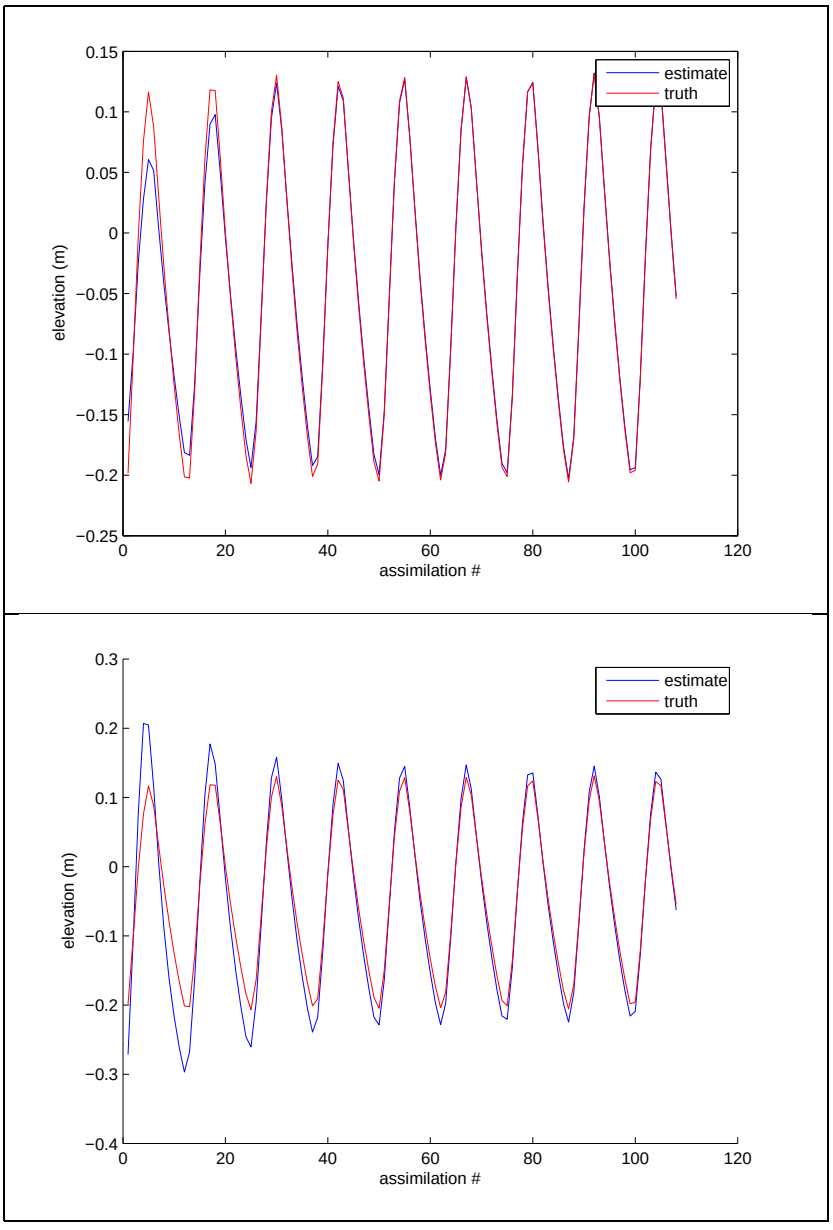

Figure 5.22: Estimates of the "true" state at station 1 from the initial guess $n = 0.14$ of the "true" value of $n = 0.01$ (top) and from the initial guess $n = 0.01$ of the "true" value of $n = 0.14$ (bottom).

as 0.134. For each individual instance, the initial errors are reduced by at least 87%. The final estimates of each distinct Manning's n coefficient, α and β, are also accurate with respect to the classes defined in the first set of OSSEs (Table 5.1). Generally speaking, $\alpha = 0.005$ is slightly overestimated and $\beta = 0.1$ is slightly underestimated. The exception to this is the experiment with an initial guess of $n_{0.005,0.005}$. Here, it appears that the underestimation of β is compensated for through a more pronounced overestimation of α (nearly 33%).

We find that smaller ℓ_2 errors in the initial guesses of the parameter vector do not necessarily result in smaller ℓ_2 errors in the final estimates. However, we see varying trends for the relative error of the individual components of the parameter vector. We see correlation between the error in the initial guess of the second parameter, $\beta = 0.1$, and the error in the final estimate; a more accurate initial guess produces a more accurate final estimate. This is not the case for the estimation of $\alpha = 0.005$, the Manning's n coefficient assigned to the portion of the domain in the deep water.

With regard to estimating the model state, the RMSEs of the water elevations obtained when using the SEIK filter for parameter estimation is an 82% decrease of the RMSEs obtained for the respective baseline cases. We also find that we are able to accurately forecast the mean of the tidal amplitude (0.125018 m). In each case, the relative error of the estimated tidal amplitude is less than 20%, as desired (Figure 5.22).

In estimating $\beta = 0.1$, we see the same trend that was observed when

initial guess	$\boldsymbol{n_{0.005,0.01}}$	$\boldsymbol{n_{0.005,0.02}}$	$\boldsymbol{n_{0.005,0.03}}$	$\boldsymbol{n_{0.005,0.06}}$
Manning's n estimate of $\beta = 0.1$	0.069189	0.082208	0.081744	0.093426
Relative error (β)	0.308112	0.177918	0.182555	0.065742
RMSE (SEIK)	0.005968	0.003506	0.003380	0.001313
RMSE (baseline)	0.036703	0.024333	0.016423	0.005416
Mean tidal amplitude (sta. 21)	0.100471	0.100696	0.100684	0.100858
Relative error	0.004738	0.002519	0.002635	0.000905

Table 5.8: Final estimate errors of various "true" Manning's n fields defined in Galveston Bay parameterized by two values. The RMSEs are of forecasted water elevations for the parameter estimation (SEIK filter) and baseline cases.

estimating a field of constant Manning's n coefficients, i.e. in the sense of absolute error, larger Manning's n coefficients are more difficult to reproduce and are generally underestimated. The results also give us some intuition about the model sensitivity of the ADCIRC model. If we hold the Manning's n coefficient on the west side of the inlet constant with $\alpha = 0.005$ and vary β, the coefficient on the east side, we see far more variation in the resulting tidal amplitudes than we do if we hold the coefficient on the east side constant at β =0.1 and vary the coefficient α on the west side (Figure 5.23). The variation in the amplitudes in the former case is 0.197915 m whereas the variation in the latter case is only 0.078774 m. Based on these results, we presume that the model is less sensitive to the value of the Manning's n coefficient on the west side of the domain, α. This is reasonable since, although this side of the domain contains more nodes (1,073), it also has deeper bathymetry, reducing the value of the drag law coefficient, c_f in equation (2.5).

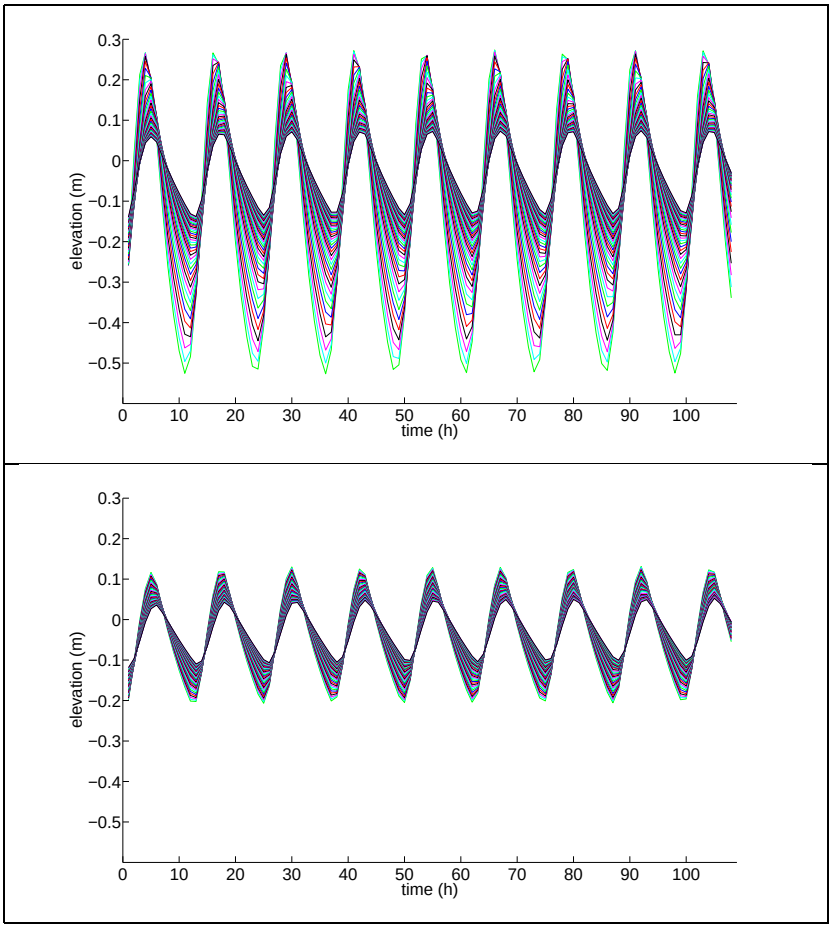

Figure 5.23: Water elevations that result at station 1 when one of the two parameters that define a piecewise constant field of Manning's n coefficients for the Idealized inlet is fixed while the other is varied from 0.005 to 0.2 (fixed $\alpha = 0.005$ and varying β (top), fixed $\beta = 0.2$ and varying α (bottom)). Larger tidal amplitudes correspond to lower Mannings n coefficients.

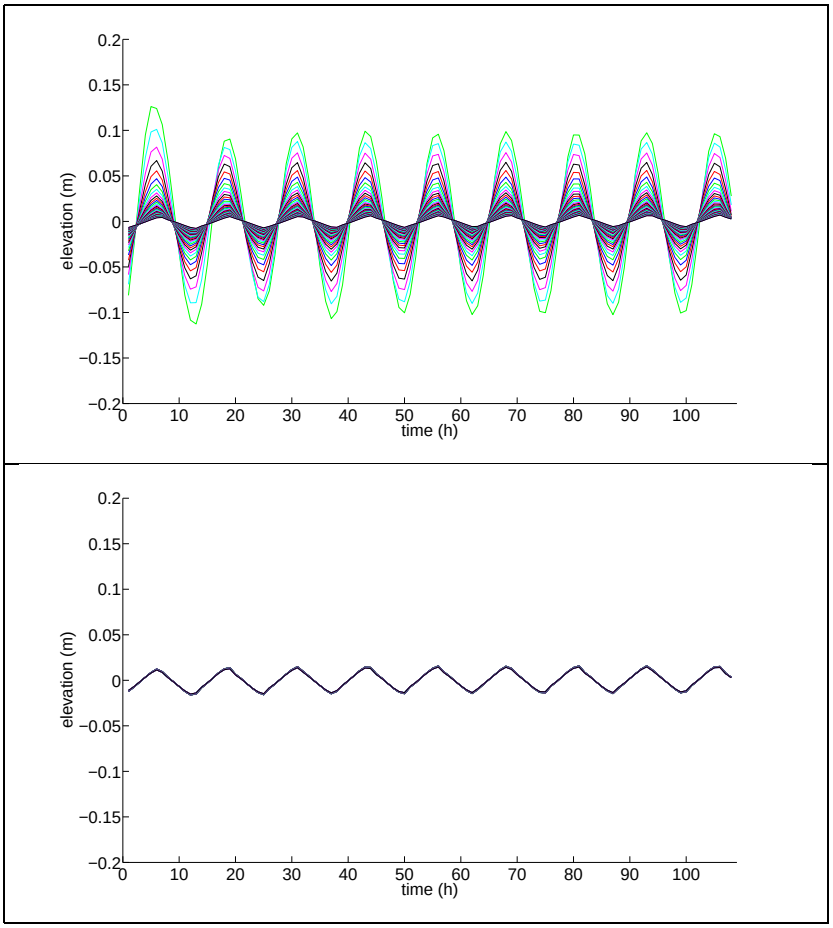

Figure 5.24: Water elevations that result at station 1 when one of the two parameters that define a piecewise constant field of Manning's n coefficients for Galveston Bay is fixed while the other is varied from 0.005 to 0.2 (fixed $\alpha = 0.005$ and varying β (top), fixed $\beta = 0.2$ varying α (bottom)). Larger tidal amplitudes correspond to lower Mannings n coefficients.

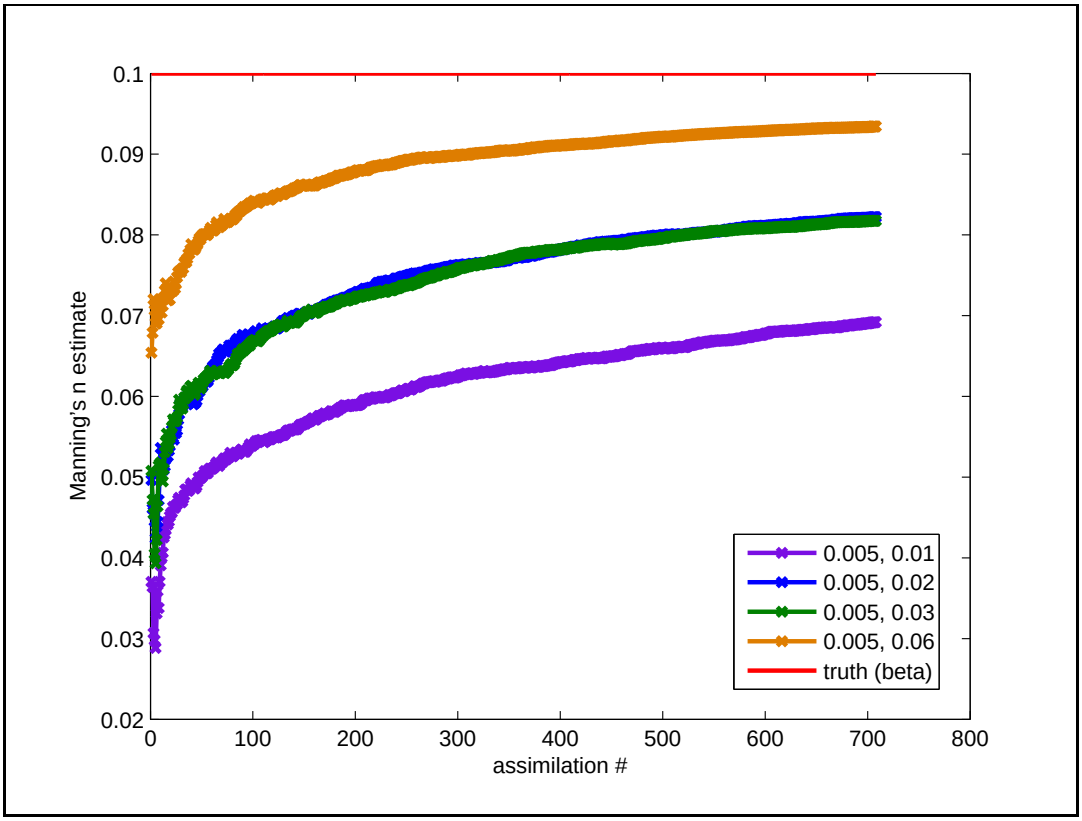

Figure 5.25: Estimates of β, a parameter that partially defines a "true" Manning's n field defined on Galveston Bay

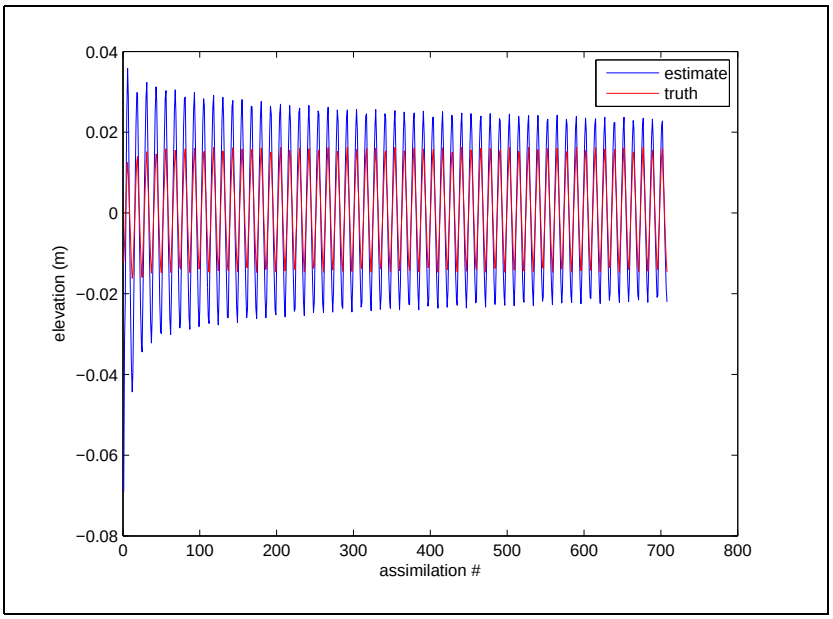

Figure 5.26: Estimates of the "true" state at station 1 from the initial guess $n_{0.005,0.01}$ of the "true" value of $n_{0.005,0.1}$.

When estimating the field $n_{0.005,0.1}$ for the Galveston Bay domain, we observe that while varying the value of β significantly impacts the water elevations computed at the observation stations, varying the value of α does not cause notable variation in the water elevations at all; for this case, the ADCIRC model is not sensitive to variations in the value of the Manning's n coefficient in the deep water of the Gulf of Mexico (Figure 5.24). For this reason, we choose to begin the data assimilation with the assumption that $\alpha = 0.005$ is known, and use the SEIK filter to estimate the parameter β only. We assimilate data at the 20 observation stations located in Galveston Bay, discarding data collected from the station located in the Gulf of Mexico (station 17) since we have chosen not to estimate the Manning's n coefficient

there. Including a 12 hour ramp up period, we perform the data assimilation over 30 days, as we find that the parameter estimation requires longer than 5 days to converge to the correct value. We begin with the initial guesses $n_{0.005,0.01}$, $n_{0.005,0.02}$, $n_{0.005,0.03}$, and $n_{0.005,0.6}$. These fields are chosen so that the initial guess of β comes from an incorrect class (in reference to Table 5.2), as we have found that initial guesses close to 0.1 (i.e. from class E) quickly converge to 0.1 as expected.

We are able to accurately estimate β from each of the initial guesses with the exception of the smallest initial guess, $\beta = 0.01$. However, we find that the relative error of the final estimate of β is significantly reduced from that of the initial guess in each of the four experiments. In the worst case, the error is still reduced by more than 73%. We see some correlation between the accuracy of the initial guesses and that of the final estimates, i.e. better initial guesses result in better final estimates. Also in each of the four cases, the parameter is underestimated. This is consistent with our findings from the previous OSSEs.

We see the impact of the SEIK filter on the estimates of the model state (e.g. see Figure 5.26). The RMSEs of the estimated water elevations is significantly reduced in every case respective to the baseline cases. Overall, the RMSEs of the estimated elevations are small, with the largest RMSE in the four experiments being less than 0.006. We see the direct correlation between model input and output (i.e. model response), as the accuracy of the estimated Manning's n coeffecients directly relates to the accuracy of the

estimated elevations. We obtain the mean tidal amplitude at station 21 (Figure 5.2), as this station has the largest water elevations (0.100950 m) for the true field of Manning's n coefficients. The mean tidal amplitude that results when estimating the Manning's n coefficient in Galveston Bay is always very close to this value, with the relative error less than 0.005 in every case.

In these experiments, significantly more assimilation cycles are required to accurately estimate the Manning's n coefficient in the bay. With respect to the classes determined in the first set of OSSEs (Table 5.2), acceptable estimates are nearly attained after 108 updates, but more time is required for convergence to the true value as conjectured above. By the thirtieth day, final estimates within the correct class result from each of the initial guesses except for $\beta = 0.01$, the initial guess that comes from class A, the class furthest from the true class (class E). Again we emphasize that class E is the largest of the classes; Manning's n coefficients ranging from 0.08 to 0.2 all produce similar elevation output. Thus the incremental updates made to the parameter estimate by the SEIK filter are small, and the longer convergence times are expected. This idea is also supported by the water elevation data (Table 5.8). The RMSEs in the elevations for the baseline cases are small even though the Manning's n coefficients in the bay are as much as 90% inaccurate. Finally, with this experiment we again find that ADCIRC is less sensitive to α, the value of the Manning's n coefficient in deep water. The deep water of this domain has a significantly larger bathymetric depth than that of the idealized inlet (e.g. see Tables 5.3 and 5.4), and as a result we see a much smaller effect

of the depth-dependent bottom stress coefficient defined in this region on the water elevations.

5.3.3 A Realization of a Stochastic Process

When estimating the random variable in the Karhunen-Loève expansion for the idealized inlet domain, we are able to accurately estimate the correct field of Manning's n coefficients for every experiment using the SEIK filter (Tables 5.9 and 5.10). The estimates of the positive random variables are notably better than the estimates of the negative variables, nevertheless the largest absolute error in any of the experiments is still less than 0.828. Here, we look at the absolute error as we have already accounted for the nonlinear dependence of the water elevation on the Manning's n coefficients by estimating the natural log of the field. In addition to accurately estimating the random variable of the expansion, we are also able to accurately estimate the true values of the Manning's n coefficients; the RMSEs of all of the estimated fields are small, particularly for those parameterizations that use positive values (the RMSEs are less than 0.002 in these cases), and they are always significantly reduced relative to the baseline RMSEs (by at least 45% and by as much as 97%).

The parameter estimation also improves the estimates of the model state. The baseline RMSE in the forecasts of the water elevation is not more than 0.14 m, however, the RMSE when the SEIK filter is applied is only about 0.04 m for half of the cases, with a maximum RMSE of 0.073 m over all of

the experiments. The error in the mean tidal amplitude at station 15 (where the tidal amplitudes are some of the largest) is less than 20% in every case, and thus the parameter estimation is successful by the standards we have set forth. The data for the tidal amplitudes at station 1, where the estimation of the model state is not quite as succesful, are shown in Tables 5.11 and 5.12). The estimated tidal amplitudes are within 20 % of the truth for the positive parameters, however, this is not the case for the negative parameters. For $\xi = -1$, the error in the estimate is slightly more than 20%, and for $\xi = -2$ and $\xi = -3$, the errors are more than 50%. Of course these numbers are influenced by the initial error in the tides (e.g. see Figure 5.28).

For most of the observation stations, the negative values of ξ correspond to smaller tidal amplitudes whereas the positive values of ξ correspond to larger ones. Thus, an initial guess of $\xi = 0$ corresponds to an initial *over*estimate of the true state when the true ξ is negative, and an initial *under*estimate of the state when the true ξ is positive. This is seen in the hydrographs in Figure 5.28. This gives some intuition regarding the difficulty in estimating $\xi < 0$ (in comparison to estimating $\xi > 0$), as physically, the process of reducing the fluid in the system by increasing the magnitude of the bottom stress is more difficult than the process of increasing the fluid in the system by decreasing the bottom stress when the tidal forcing at the boundary is not changed.

We encountered an instability in the forward model when estimating the random variables used to define the various fields of Manning's n coefficients for the Galveston Bay domain. As was the case in the other OSSEs, we

found that more time is required to estimate the field for Galveston Bay than is required to estimate the field for the idealized inlet. For the idealized inlet domain, the parameter estimates converge within 30 days of model simulation. It seems that for the Galveston Bay domain, more than 60 days of simulation is required for the parameters to converge to accurate estimates. Unfortunately, the ADCIRC model encounters some instability at day 53 of simulation, which we were unable to eliminate despite implementing common approaches to this problem including increasing the temporal resolution and the eddy viscosity. We have reason to believe that the grid itself may play a role in the problem, as difficulties have been encountered previously for this model domain.

We attempted to circumvent the model instability by increasing the frequency with which we performed the SEIK filtering. It was our hope that this would allow the true parameters to be attained prior to the 53rd day of simulation. We assimilated data every .25 h and every .5 h only to find that the more frequent assimilation times did not provide the model with enough time to respond to the new field of bottom stress terms between updates. As a result, the parameter estimates routinely overshot the true values. However, through our efforts we gained additional insight into the ADCIRC model response to an evolving bottom stress. The results obtained after 53 days of assimilation cycles are shown in Tables 5.13 and 5.14.

Though we expect that the parameter estimates require more time to converge to the true parameter, we find that within the 53 days before the model instability occurs the estimates do begin to approach the correct values

(Figure 5.29). The absolute errors in the parameters range from 0.311 to 1.315, and the RMSEs of the estimated fields of Manning's n coefficients computed over all of the nodes are reduced by at least 33% in every case. The global RMSE is reduced by over 87% for the case when the true parameter is $\xi = 3$.

Again we see improvement in the estimates of the water elevations. The maximum global RMSE of all of the cases is 0.096 m, and the average reduction of the global RMSE is 43% relative to the baseline cases. At many locations in the domain, the error in the estimated tidal amplitude is within 20% of the truth despite the fact that the parameter estimation has not converged. We see this behavior at station 21, where the magnitude of the tidal amplitudes is the largest of all of the stations. For the estimates of the negative parameters, the relative error is less than 0.011. The relative error in the estimates of the positive values is as large as 0.047, however, this is still considerably small. This is partly due to the reduced sensitivity of the ADCIRC model to variations in the bottom stress parameters at these locations. The errors are larger at stations where the model is more sensitive. For example, at station 1, where we have shown that there is significant variation in the water elevations that result from the various parameters (Figure 5.12), the estimated tidal amplitudes are not within 20% of the true ones after 53 days (Tables 5.15 and 5.16). However, these are not the locations of maximum water elevations, and again these errors are influenced by the large initial errors (e.g. see Figure 5.30).

As was the case for the idealized inlet, we find that the estimation of positive parameters is more accurate than that of negative, however, as we

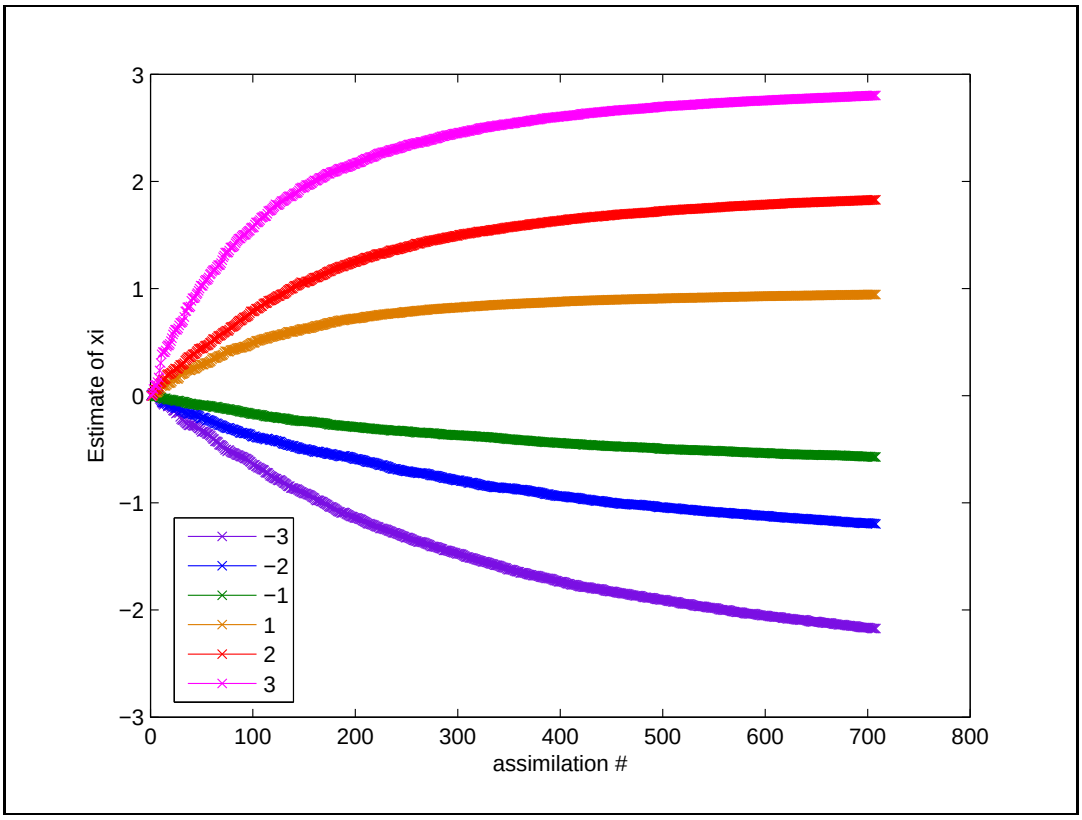

Figure 5.27: Estimates of various "true" values of ξ from an initial guess of $\xi = 0$ where ξ defines a field of Manning's n coefficients on an idealized inlet

discussed above, these values generally correspond to larger tidal amplitudes (i.e. an initial underestimate of the water elevations), and we expect to more accurately recover the parameters in these cases.

We have implemented the SEIK filter for the estimation of model parameters defining several fields of Manning's n coefficients in the SWEs. We have tested our methodology on two computational domains that both represent a bay connected to the open ocean through one or several channels.

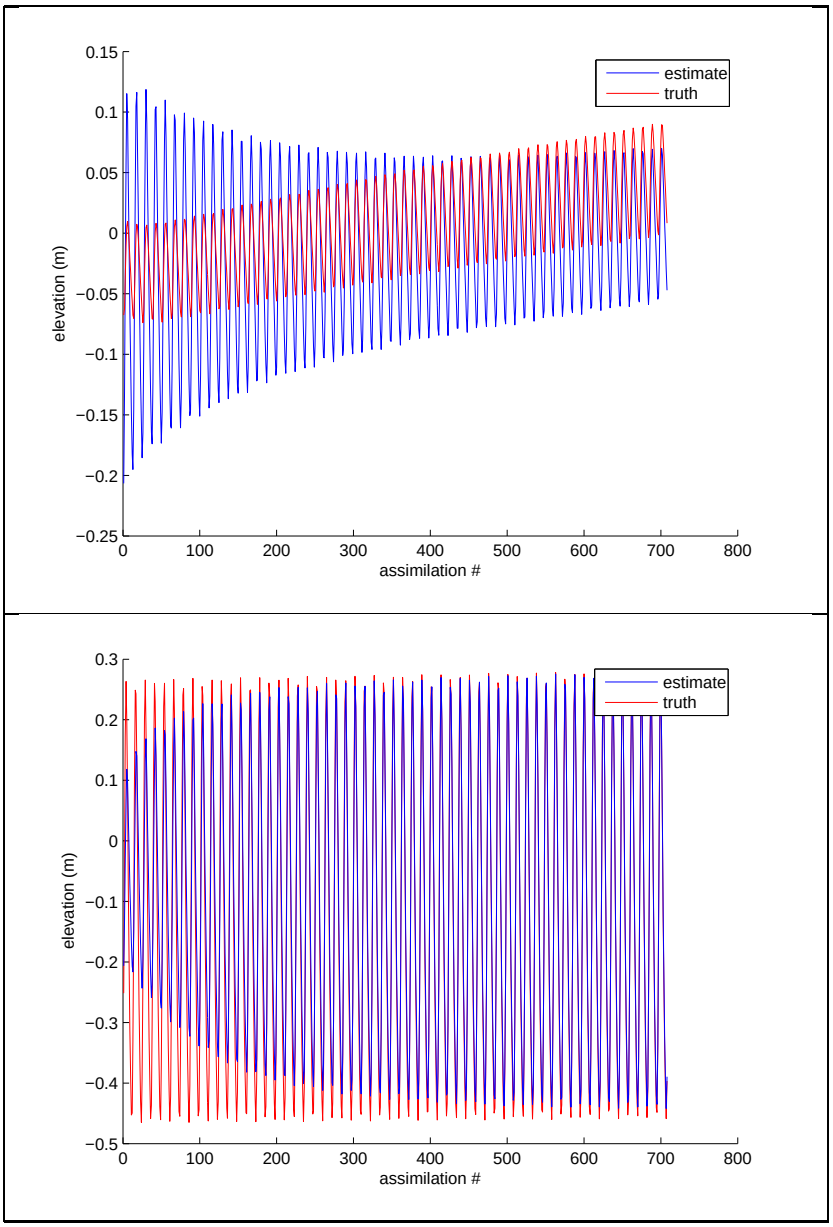

Figure 5.28: Estimates of the "true" state at station 1 from the initial guess ξ = 0 of the "true" values of ξ = -3 (top) and ξ = 3 (bottom).

Idealized Inlet with Ebb Shoal			
true value of ξ	**-3**	**-2**	**-1**
Final estimate	-2.172928	-1.196583	-0.572610
Absolute error	0.827072	0.803417	0.427390
RMSE of field (SEIK)	0.128589	0.068921	0.022481
RMSE of field (baseline)	0.274264	0.126232	0.044977
RMSE (SEIK)	0.072748	0.042743	0.025117
RMSE (baseline)	0.109536	0.065723	0.035674
True mean tidal amplitude (sta. 15)	0.506692	0.475501	0.457686
Est. mean tidal amplitude (sta. 15)	0.457814	0.445177	0.436127
Relative error	0.096465	0.063773	0.047104

Table 5.9: Final estimates and estimate errors of various "true" Manning's n fields parameterized by a single, negative value for the idealized inlet case. The RMSEs are of forecasted water elevations for parameter estimation (SEIK filter) and baseline cases.

Idealized Inlet with Ebb Shoal			
true value of ξ	**1**	**2**	**3**
Final estimate	0.944737	1.827173	2.802159
Absolute error	0.055263	0.172827	0.197841
RMSE of field (SEIK)	0.001048	0.001941	0.001311
RMSE of field (baseline)	0.025158	0.039408	0.047596
RMSE (SEIK)	0.016517	0.041199	0.045742
RMSE (baseline)	0.046427	0.098558	0.139466
True mean tidal amplitude (sta. 15)	0.395054	0.346886	0.300999
Est. mean tidal amplitude (sta. 15)	0.404665	0.376470	0.334992
Relative error	0.024331	0.085285	0.112935

Table 5.10: Final estimates and estimate errors of various "true" Manning's n fields parameterized by a single, positive value for the idealized inlet case. The RMSEs are of forecasted water elevations for parameter estimation (SEIK filter) and baseline cases.

Idealized Inlet			
true value of ξ	**-3**	**-2**	**-1**
True mean tidal amplitude (sta. 1)	0.048472	0.062558	0.095086
Est. mean tidal amplitude (sta. 1)	0.073903	0.096428	0.114201
Relative error	0.524662	0.541420	0.201024

Table 5.11: The relative error in the average tidal amplitudes computed at station 1 of the idealized inlet domain

Idealized Inlet			
true value of ξ	**1**	**2**	**3**
True mean tidal amplitude (sta. 1)	0.192761	0.242182	0.266649
Est. mean tidal amplitude (sta. 1)	0.178343	0.211527	0.246550
Relative error	0.074796	0.126579	0.075378

Table 5.12: The relative error in the average tidal amplitudes computed at station 1 of the idealized inlet domain

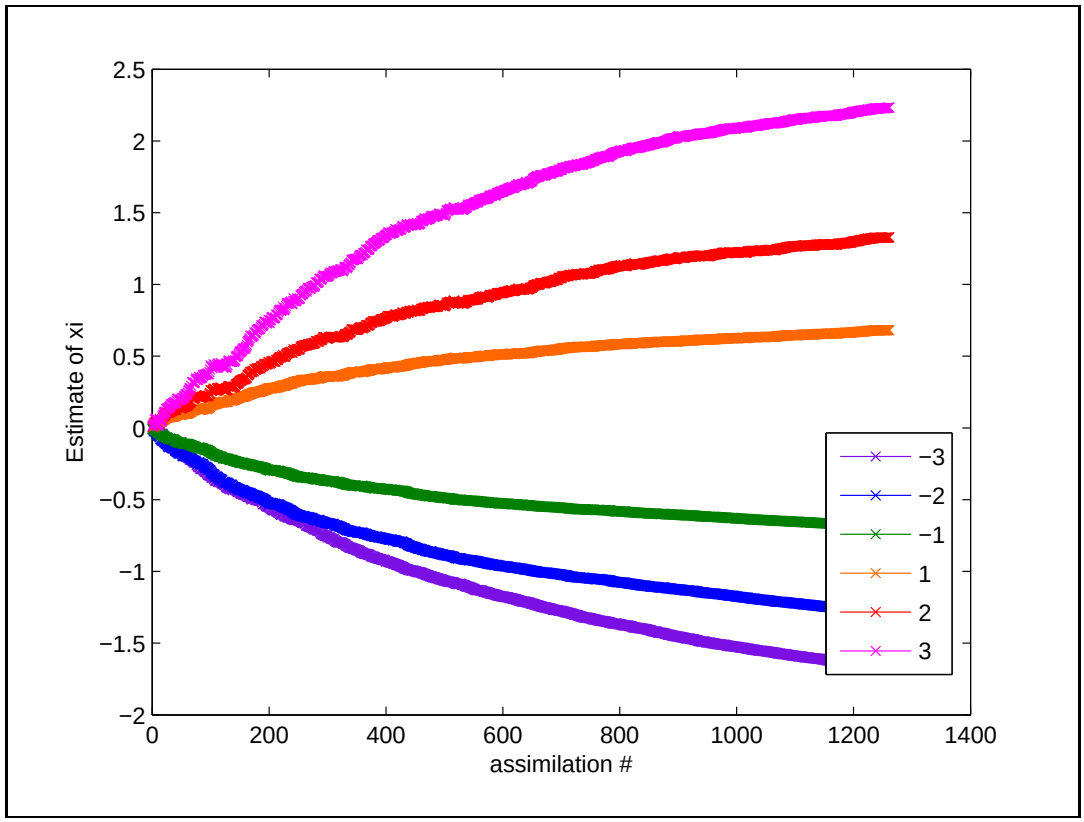

Figure 5.29: Estimates of various "true" values of ξ from an initial guess of $\xi = 0$ where ξ defines a field of Manning's n coefficients on Galveston Bay

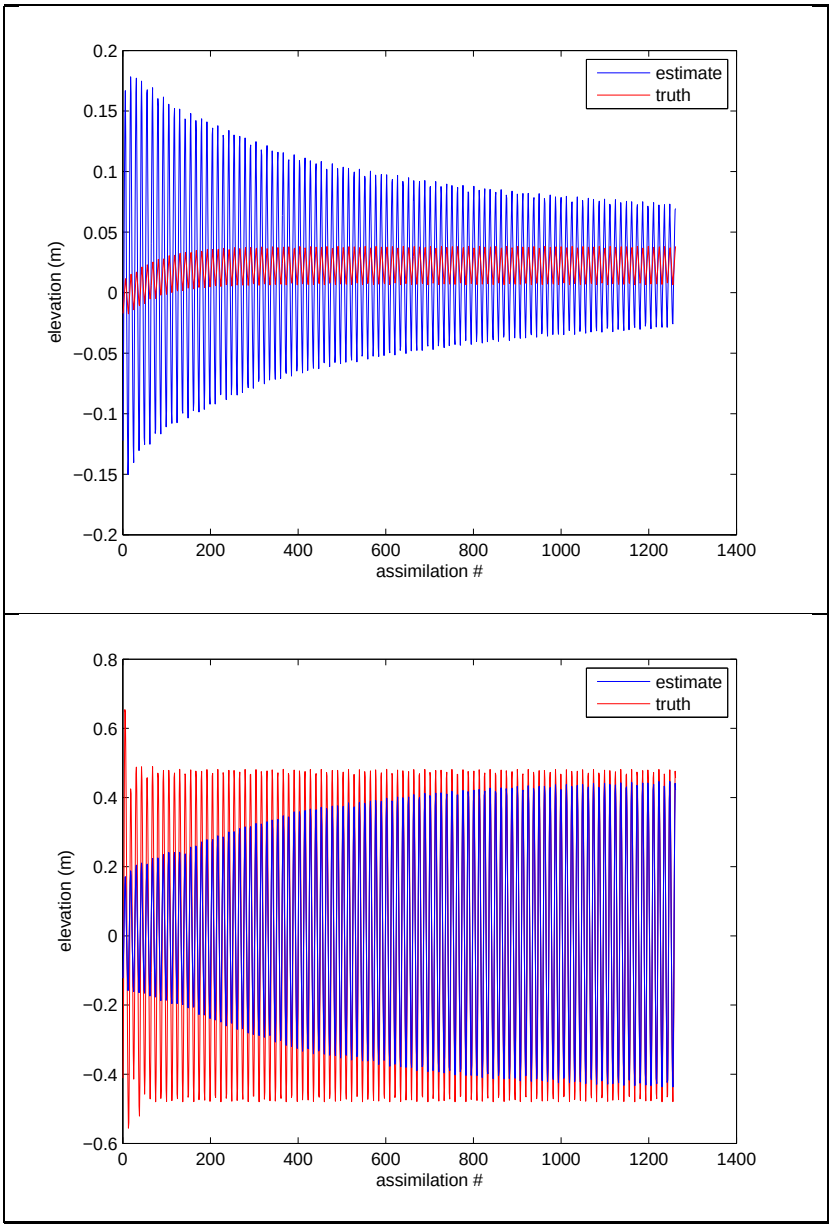

Figure 5.30: Estimates of the "true" state at station 1 from the initial guess ξ = 0 of the "true" values of ξ = -3 (top) and ξ = 3 (bottom).

Galveston Bay			
true value of ξ	**-3**	**-2**	**-1**
Final estimate	-1.685021	-1.291645	-0.688881
Absolute error	1.314979	0.708355	0.311119
RMSE of field (SEIK)	0.064870	0.021822	0.005746
RMSE of field (baseline)	0.097173	0.043412	0.015152
RMSE (SEIK)	0.042183	0.031062	0.019371
RMSE (baseline)	0.076811	0.061863	0.038296
True mean tidal amplitude (sta. 21)	0.454999	0.457729	0.459872
Est. mean tidal amplitude (sta. 21)	0.459810	0.460257	0.461209
Relative error	0.010575	0.005523	0.002909

Table 5.13: Final estimates and estimate errors of various "true" Manning's n fields parameterized by a single, negative value for the Galveston Bay case. The RMSEs are of forecasted water elevations for parameter estimation (SEIK filter) and baseline cases.

Galveston Bay			
true value of ξ	**1**	**2**	**3**
Final estimate	0.681886	1.330059	2.233303
Absolute error	0.318114	0.669941	0.766697
RMSE of field (SEIK)	0.002142	0.002857	0.001980
RMSE of field (baseline)	0.008314	0.012992	0.015695
RMSE (SEIK)	0.033347	0.077179	0.096246
RMSE (baseline)	0.056041	0.118499	0.165191
True mean tidal amplitude (sta. 21)	0.471059	0.488450	0.504228
Est. mean tidal amplitude (sta. 21)	0.465814	0.470396	0.480717
Relative error	0.011135	0.036960	0.046628

Table 5.14: Final estimates and estimate errors of various "true" Manning's n fields parameterized by a single, positive value for the Galveston Bay case. The RMSEs are of forecasted water elevations for parameter estimation (SEIK filter) and baseline cases.

Galveston Bay			
true value of ξ	**-3**	**-2**	**-1**
True mean tidal amplitude (sta. 1)	0.037139	0.059919	0.106235
Est. mean tidal amplitude (sta. 1)	0.104240	0.115451	0.143944
Relative error	1.806791	0.926774	0.354965

Table 5.15: The relative error in the average tidal amplitudes computed at station 1 of the Galveston Bay domain

Galveston Bay			
true value of ξ	**1**	**2**	**3**
True mean tidal amplitude (sta. 1)	0.314011	0.425812	0.476666
Est. mean tidal amplitude (sta. 1)	0.244365	0.298773	0.370225
Relative error	0.221793	0.298346	0.223303

Table 5.16: The relative error in the average tidal amplitudes computed at station 1 of the Galveston Bay domain

We simulated data to be assimilated using tidal forcing on the open ocean boundaries, and then performed OSSEs, using incorrect initial guesses of the true bottom stress parameters. In all of our experiments, we use the ADCIRC model as the state forecast model (i.e. as the parameter observation operator). A summary of our results is provide in Tables 5.17 - 5.19.

Idealized Inlet			Galveston Bay		
Truth	Initial Guess	Parameter Recovered	Truth	Initial Guess	Parameter Recovered
0.015	0.035	y	0.01	0.02	y
0.015	0.06	y	0.01	0.03	y
0.015	0.105	y	0.01	0.06	y
0.015	0.17	y	0.01	0.14	y
0.035	0.015	y	0.02	0.01	y
0.035	0.06	y	0.02	0.03	y
0.035	0.105	y	0.02	0.06	y
0.035	0.17	y	0.02	0.14	y
0.06	0.015	y	0.03	0.01	y
0.06	0.035	y	0.03	0.02	y
0.06	0.105	y	0.03	0.06	y
0.06	0.17	y	0.03	0.14	y
0.105	0.015	n	0.06	0.01	y
0.105	0.035	y	0.06	0.02	y
0.105	0.06	y	0.06	0.03	y
0.105	0.17	y	0.06	0.14	y
0.17	0.015	n	0.14	0.01	n
0.17	0.035	y	0.14	0.02	n
0.17	0.06	n	0.14	0.03	y
0.17	0.105	y	0.14	0.06	y

Table 5.17: A summary of the results for the SEIK filter for parameter estimation of a constant field of Manning's n coefficients

Idealized Inlet			Galveston Bay		
Truth	Initial Guess	Parameter Recovered	Truth	Initial Guess	Parameter Recovered
$n_{0.005,0.1}$	$n_{0.005,0.005}$	y	$n_{0.005,0.1}$	$n_{0.005,0.01}$	y
$n_{0.005,0.1}$	$n_{0.1,0.1}$	y	$n_{0.005,0.1}$	$n_{0.005,0.02}$	y
$n_{0.005,0.1}$	$n_{0.06,0.06}$	y	$n_{0.005,0.1}$	$n_{0.005,0.03}$	y
$n_{0.005,0.1}$	$n_{0.1,0.005}$	y	$n_{0.005,0.1}$	$n_{0.005,0.06}$	y

Table 5.18: A summary of the results for the SEIK filter for parameter estimation of a piecewise constant field of Manning's n coefficients

Idealized Inlet			Galveston Bay		
Truth	Initial Guess	Parameter Recovered	Truth	Initial Guess	Parameter Recovered
-3	0	y	-3	0	y
-2	0	y	-2	0	y
-1	0	y	-1	0	y
1	0	y	1	0	y
2	0	y	2	0	y
3	0	y	3	0	y

Table 5.19: A summary of the results for the SEIK filter for parameter estimation of a field of Manning's n coefficients defined as a realization of a stochastic process

Chapter 6

Conclusions

The bottom stress of a physical problem domain significantly impacts the hydrodynamics of a system under moderate and extreme conditions alike. In modeling phenomena such as sea level, tides, and storm surge, the representation of the bottom stress terms in the momentum equations becomes an important research area. With sufficient observations of the model state, this problem can be formulated as an inverse problem; efforts can be focused on determining those bottom stress terms that produce model output matching the observed data. The Manning's n formulation of the bottom stress is one that is often implemented. This formulation is advantageous, as it describes the dependence of the bottom stress in terms of the height of the water column above it. However, it contains an empirically defined constant, the Manning's n coefficient of roughness, which contains a large amount of uncertainty for most problems. Thus, the accurate representation and estimation of bottom friction is an ongoing research problem.

In this work, we have approached this research problem using statistical data assimilation methods. This is a novel approach to parameter estimation, as typically variational methods are used. We have used our method to esti-

mate several fields of Manning's n coefficients. Specifically, we inverted synthetic water elevation data by implementing the singular interpolated evolutive Kalman (SEIK) filter to the Advanced Circulation (ADCIRC) coastal ocean model. Water elevations were simulated using tidal forcing on two domains, a bay connected to an open ocean via an idealized inlet with an ebb shoal, and a coarse representation of Galveston Bay, an estuary located along the upper Texas coast. We estimated three bottom stress fields. The first was defined by a Manning's n coefficient held constant across the domain. The second was defined by two Manning's n coefficients, where the bottom stress in the bay was defined by one constant value, and the bottom stress in the open ocean was defined by the other. Finally, the third field was spatially variable. We defined it as a stochastic process, which we parameterized using a single term of the Karhunen-Loève expansion. We performed observation simulation system experiments to test the effectiveness of our method of parameter estimation.

For all of our cases, we were generally able to accurately recover the true field of Manning's n coefficients. We were also able to improve the accuracy of forecasted water elevations in every experiment. When estimating the values of the Manning's n coefficients directly (i.e. the first two fields), we found that in general, smaller values could be recovered from nearly any initial guess. In estimating larger values, however, either a relatively accurate initial guess or many data assimilation cycles (updates using data) were required for the method to converge to the true parameter value. This is likely because our model output, water elevation data, is not as sensitive to variations in larger

values of the Manning's n coefficient; the number of coefficients that produce similar water elevation data increases with the value of the coefficient, which we also showed, resulting in moderate updates to the parameter estimates. Larger values are generally underestimated, particularly when the initial guess is much less than the true value.

When estimating two model parameters, where the Manning's n coefficient was set to a small value in deep water of the domain and a larger value in shallow water, we found that the bathymetry to be a significant factor in the sensitivity of the model to the bottom stress parameters. For areas with large bathymetric depths, the value of the Manning's n coefficient had a significantly smaller of an effect on the corresponding water elevation.

Finally, in estimating parameters used to define a spatially variable field of Manning's n coefficients, we found that more data assimilation cycles were required to achieve accurate final estimates due to the indirect relationship between the parameter to be estimated and the data being observed. In these cases, we also experienced more difficulty in recovering negative parameters than positive parameters. However, we found that for our parameterization of the field, negative parameters mostly corresponded to initial overestimates of the state (at observation locations), and thus it can be conjectured that the difficulty in the parameter estimation was related to the difficulty of reducing the amount of fluid in the system through an increase of the bottom stress alone.

The results of this study show that statistical data assimilation is a

promising approach to parameter estimation. By using statistical data assimilation methods, we were able to efficiently estimate model parameters using modest computational resources. Furthermore, we were able to achieve these results without the development of an adjoint model. There are several ways in which this work can be extended. Future research will include more complex configurations of bottom stress parameters. In this work, we explored estimating a spatially variable field of bottom stress terms using the Karhunen-Loève expansion, however including additional terms in the series will allow even more variation in the field to be represented. Additionally, we are interested in investigating the effect of our parameter estimation methodology on hurricane storm surge forecasting, i.e. for a hydrodynamic model forced by hurricane wind data, which is the first step in improving the accuracy of real-time forecasts of hurricane storm surges. The methodology will also be used to estimate other parameters important to coastal ocean modeling.

Appendix

Appendix 1

The Reformulation of the Manning's n Formula

Robert Manning's empirical formula describing flow in an open channel is generally expressed

$$U = \frac{s^{1/2} R^{2/3}}{n},$$

where U is the mean velocity of the fluid, s is the slope of the channel, R is the hydraulic radius of the cross section of the channel, and n is the Manning's n coefficient of roughness. This expression can be used to define the bottom stress terms in the momentum equations in the shallow water equations (2.2) [38].

Using the quadratic drag law defined in (2.4), the standard friction coefficient, c_f, can be expressed in terms of the magnitude of the bottom stress:

$$\begin{aligned} \left(\frac{\tau_{bx}}{\rho_0}\right)^2 + \left(\frac{\tau_{by}}{\rho_0}\right)^2 &= \frac{|\boldsymbol{\tau}_b|^2}{\rho_0^2} \\ &= c_f^2 |\mathbf{U}|^2 \left(U^2 + V^2\right) \\ &= c_f^2 |\mathbf{U}|^4, \end{aligned}$$

and so we have

$$c_f = \frac{|\boldsymbol{\tau}_b|}{\rho_0 |\mathbf{U}|^2}.$$

The magnitude of the bottom stress can be approximated as $|\boldsymbol{\tau}_b| = \rho_0 Rgs$ [37], and thus

$$\begin{aligned} c_f &= \frac{|\boldsymbol{\tau}_b|}{\rho_0 |\mathbf{U}|^2} \\ &= \frac{Rgs}{|\mathbf{U}|^2} \\ &= \frac{Rgsn^2}{|s^{1/2} R^{2/3}|^2} \\ &= \frac{gn^2}{R^{1/3}}, \end{aligned}$$

where we have used the Manning's n formula to obtain the third equality. In the shallow water equations, the hydraulic radius, R, is equal to the total water column height, H. Thus we have that

$$c_f = \frac{gn^2}{H^{1/3}}.$$

Bibliography

[1] A. Aksoy, F. Zhang, and J.W. Nielsen-Gammon. Ensemble-based simultaneous state and parameter estimation in a two-dimensional sea-breeze model. *Monthly weather review*, 134(10):2951–2970, 2006.

[2] Francisco Alcrudo and Fayssal Benkhaldoun. Exact solutions to the riemann problem of the shallow water equations with a bottom step. *Computers & Fluids*, 30(6):643–671, 2001.

[3] MU Altaf, T Butler, X Luo, C Dawson, T Mayo, and I Hoteit. Improving short range ensemble kalman storm surge forecasting using robust adaptive inflation. *Monthly Weather Review*, (2013), 2013.

[4] J.L. Anderson. An ensemble adjustment kalman filter for data assimilation. *Monthly weather review*, 129(12):2884–2903, 2001.

[5] JD Annan, JC Hargreaves, NR Edwards, and R. Marsh. Parameter estimation in an intermediate complexity earth system model using an ensemble kalman filter. *Ocean Modelling*, 8(1):135–154, 2005.

[6] Genadii A Atanov, Elena G Evseeva, and Ehab A Meselhe. Estimation of roughness profile in trapezoidal open channels. *Journal of Hydraulic Engineering*, 125(3):309–312, 1999.

[7] Kendall E.. Atkinson. *The Numerical Solution of Integral Equations of the Second Kind*. Cambridge University Press, 1997.

[8] Peter Bacopoulos, Scott C Hagen, Andrew T Cox, William R Dally, and Steven M Bratos. Observation and simulation of winds and hydrodynamics in st. johns and nassau rivers. *Journal of Hydrology*, 420:391–402, 2012.

[9] R. Berg. *Tropical cyclone report: Hurricane ike (al092008), 1-14 september 2008*. National Hurricane, Center, 2009.

[10] Craig H Bishop, Brian J Etherton, and Sharanya J Majumdar. Adaptive sampling with the ensemble transform kalman filter. part i: Theoretical aspects. *Monthly weather review*, 129(3):420–436, 2001.

[11] Cheryl A Blain and WE Rogers. Coastal tide prediction using the adcirc-2ddi hydrodynamic finite element model: Model validation and sensitivity analyses in the southern north sea/english channel. Technical report, DTIC Document, 1998.

[12] Brian Blanton, John McGee, Jason Fleming, Carola Kaiser, Hartmut Kaiser, Howard Lander, Rick Luettich, Kendra Dresback, and Randy Kolar. Urgent computing of storm surge for north carolina's coast. *Procedia Computer Science*, 9:1677–1686, 2012.

[13] WP Budgell. Stochastic filtering of linear shallow water wave processes. *SIAM journal on scientific and statistical computing*, 8(2):152–170, 1987.

[14] S. Bunya, JC Dietrich, JJ Westerink, BA Ebersole, JM Smith, JH Atkinson, R. Jensen, DT Resio, RA Luettich, C. Dawson, et al. A high-resolution coupled riverine flow, tide, wind, wind wave, and storm surge model for southern louisiana and mississippi. part i: Model development and validation. *Monthly Weather Review*, 138(2):345–377, 2010.

[15] G. Burgers, P. Jan van Leeuwen, and G. Evensen. Analysis scheme in the ensemble kalman filter. *Monthly weather review*, 126(6):1719–1724, 1998.

[16] T. Butler, M. U. Altaf, C. Dawson, I. Hoteit, X. Luo, and T. Mayo. Data assimilation within the advanced circulation (adcirc) modeling framework for hurricane storm surge forecasting. *Monthly Weather Review*, 140:22152231, 2012.

[17] Stephen E Cohn and Ricardo Todling. Approximate data assimilation schemes for stable and unstable dynamics. *Journal of the Meteorological Society of Japan*, 74(1):63–75, 1996.

[18] R. Courant and D. Hilbert. *Methods of Mathematical Physics*. Number v. 1 in Methods of Mathematical Physics. Wiley, 2008.

[19] G.T. Csanady. *Circulation in the Coastal Ocean*. Environmental Fluid Mechanics. Springer, 1982.

[20] SK Das and RW Lardner. On the estimation of parameters of hydraulic models by assimilation of periodic tidal data. *Journal of Geophysical*

Research: Oceans (1978–2012), 96(C8):15187–15196, 1991.

[21] Alan M Davies. On formulating two-dimensional vertically integrated hydrodynamic numerical models with an enhanced representation of bed stress. *Journal of Geophysical Research: Oceans (1978–2012)*, 93(C2):1241–1263, 1988.

[22] C. Dawson and J. Proft. Coupled discontinuous and continuous galerkin finite element methods for the depth-integrated shallow water equations. *Computer Methods in Applied Mechanics and Engineering*, 193(3):289–318, 2004.

[23] Caleb M DeChant and Hamid Moradkhani. Examining the effectiveness and robustness of sequential data assimilation methods for quantification of uncertainty in hydrologic forecasting. *Water Resources Research*, 48(4), 2012.

[24] L.M. Delves and J.L. Mohamed. *Computational Methods for Integral Equations*. Cambridge University Press, 1988.

[25] JC Dietrich, S Bunya, JJ Westerink, BA Ebersole, JM Smith, JH Atkinson, R Jensen, DT Resio, RA Luettich, C Dawson, et al. A high-resolution coupled riverine flow, tide, wind, wind wave, and storm surge model for southern louisiana and mississippi. part ii: Synoptic description and analysis of hurricanes katrina and rita. *Monthly Weather Review*, 138(2):378–404, 2010.

[26] JC Dietrich, CJ Trahan, MT Howard, JG Fleming, RJ Weaver, S Tanaka, L Yu, RA Luettich, CN Dawson, JJ Westerink, et al. Surface trajectories of oil transport along the northern coastline of the gulf of mexico. *Continental Shelf Research*, 2012.

[27] JC Dietrich, JJ Westerink, AB Kennedy, JM Smith, RE Jensen, M Zijlema, LH Holthuijsen, C Dawson, RA Luettich Jr, MD Powell, et al. Hurricane gustav (2008) waves and storm surge: Hindcast, synoptic analysis, and validation in southern louisiana. *Monthly Weather Review*, 139(8):2488–2522, 2011.

[28] Y. Ding, Y. Jia, and S. Wang. Identification of manning's roughness coefficients in shallow water flows. *Journal of Hydraulic Engineering*, 130:501–510, 2004.

[29] Ghada YH El Serafy and Arthur E Mynett. Improving the operational forecasting system of the stratified flow in osaka bay using an ensemble kalman filter–based steady state kalman filter. *Water Resources Research*, 44(6), 2008.

[30] G. Evensen. Sampling strategies and square root analysis schemes for the enkf. *Ocean Dynamics*, 54(6):539–560, 2004.

[31] G. Evensen. *Data assimilation: the ensemble Kalman filter*. Springer Verlag, 2009.

[32] Geir Evensen. Sequential data assimilation with a nonlinear quasi-geostrophic model using monte carlo methods to forecast error statistics. *Journal of Geophysical Research: Oceans (1978–2012)*, 99(C5):10143–10162, 1994.

[33] Craig Fischenich. Robert manning (a historical perspective), 2000.

[34] A. Gelb. *Applied Optimal Estimation*. MIT Press, 1974.

[35] Izrail Moiseevich Gel'fand and Georgiui Shilov. *Generalized functions*, volume 2. Academic press New York, 1968.

[36] Kamal Kumar Ghosh and Lokenath Debnath. Some exact solutions of non-linear shallow water equations. *International journal of non-linear mechanics*, 32(3):633–636, 1997.

[37] G Gioia and FA Bombardelli. Scaling and similarity in rough channel flows. *Physical review letters*, 88(1):014501, 2001.

[38] Lindley Graham. Critical review. Critical Review of "Scaling and Similarity in Rough Channel Flows" by Gioia and Bombardelli, November 2012.

[39] Mircea Grigoriu. Evaluation of karhunen–loève, spectral, and sampling representations for stochastic processes. *Journal of engineering mechanics*, 132(2):179–189, 2006.

[40] P Groen and GW Groves. Surges. *The Sea*, 1:611–646, 1962.

[41] Scott C Hagen and Peter Bacopoulos. Coastal flooding in florida's big bend region with application to sea level rise based on synthetic storms analysis. *Terrestrial, Atmospheric and Oceanic Sciences*, 23(5):481–500, 2012.

[42] SJ Hammarling. Numerical solution of the stable, non-negative definite lyapunov equation lyapunov equation. *IMA Journal of Numerical Analysis*, 2(3):303–323, 1982.

[43] CJ Hearn and JR Hunter. A new method of describing bottom stress in two-dimensional hydrodynamical models of shallow homogeneous seas, estuaries, and lakes. *Applied Mathematical Modelling*, 12(6):573–580, 1988.

[44] AW Heemink and H Kloosterhuis. Data assimilation for non-linear tidal models. *International journal for numerical methods in fluids*, 11(8):1097–1112, 1990.

[45] HJ Hendricks Franssen and W Kinzelbach. Real-time groundwater flow modeling with the ensemble kalman filter: Joint estimation of states and parameters and the filter inbreeding problem. *Water Resources Research*, 44(9), 2008.

[46] I. Hoteit, D.T. Pham, and J. Blum. A simplified reduced order kalman filtering and application to altimetric data assimilation in tropical pacific. *Journal of Marine systems*, 36(1):101–127, 2002.

[47] SP Huang, ST Quek, and KK Phoon. Convergence study of the truncated karhunen–loeve expansion for simulation of stochastic processes. *International Journal for Numerical Methods in Engineering*, 52(9):1029–1043, 2001.

[48] Akira Ishii and Mutsuto Kawahara. Parameter identification of manning roughness coefficient using analysis of hydrauric jump with sediment transport. In *Proceeding of the first Asian-Pacific Congress on Computational Mechanics*, volume 2, pages 1071–1076, 2001.

[49] Behnam Jafarpour and Dennis McLaughlin. History matching with an ensemble kalman filter and discrete cosine parameterization. *Computational Geosciences*, 12(2):227–244, 2008.

[50] Chester P Jelesnianski. Numerical computations of storm surges without bottom stress. *Monthly Weather Review*, 94(6):379–394, 1966.

[51] Chester P Jelesnianski. Numerical computations of storm surges with bottom stress. *Monthly Weather Review*, 95(11):740–756, 1967.

[52] M Kac and AJF Siegert. An explicit representation of a stationary gaussian process. *The Annals of Mathematical Statistics*, 18(3):438–442, 1947.

[53] Kari Karhunen. *Über lineare Methoden in der Wahrscheinlichkeitsrechnung*, volume 37. Universitat Helsinki, 1947.

[54] Andrew B Kennedy, Uriah Gravois, Brian C Zachry, Joannes J Westerink, Mark E Hope, J Casey Dietrich, Mark D Powell, Andrew T Cox, Richard A Luettich, and Robert G Dean. Origin of the hurricane ike forerunner surge. *Geophysical Research Letters*, 38(8), 2011.

[55] Rahman H Khatibi, John JR Williams, and Peter R Wormleaton. Identification problem of open-channel friction parameters. *Journal of Hydraulic Engineering*, 123(12):1078–1088, 1997.

[56] Ingemar Kinnmark. *The shallow water wave equations: formulation, analysis, and application*, volume 15. Springer-Verlag Berlin-Heidelberg, 1986.

[57] Ethan J Kubatko, Joannes J Westerink, and Clint Dawson. Discontinuous galerkin methods for advection dominated problems in shallow water flow. *Computer Methods in Applied Mechanics and Engineering*, 196(1):437–451, 2006.

[58] Marc Leisenring and Hamid Moradkhani. Snow water equivalent prediction using bayesian data assimilation methods. *Stochastic Environmental Research and Risk Assessment*, 25(2):253–270, 2011.

[59] Pierre FJ Lermusiaux and AR Robinson. Data assimilation via error subspace statistical estimation. part i: Theory and schemes. *Monthly Weather Review*, 127(7):1385–1407, 1999.

[60] Chun-Ching Li and Armen Der Kiureghian. Optimal discretization of random fields. *Journal of Engineering Mechanics*, 119(6):1136–1154, 1993.

[61] Michel Loève. Fonctions aléatoires de second ordre. *CR Acad. Sci. Paris*, 220:380, 1945.

[62] R.A. Luettich and J.J. Westerink. *Formulation and numerical implementation of the 2D/3D ADCIRC finite element model version 44. XX.* R. Luettich, 2004.

[63] Daniel R Lynch and William G Gray. A wave equation model for finite element tidal computations. *Computers & fluids*, 7(3):207–228, 1979.

[64] Robert Manning, John Purser Griffith, TF Pigot, and Leveson Francis Vernon-Harcourt. *On the flow of water in open channels and pipes.* 1890.

[65] Elizabeth L Mansfield and Peter A Clarkson. Symmetries and exact solutions for a 2+ 1-dimensional shallow water wave equation. *Mathematics and computers in simulation*, 43(1):39–55, 1997.

[66] B. Matérn. *Spatial variation.* Lecture notes in statistics. Springer-Verlag, 1986.

[67] Christopher Michael Mirabito. *Analysis, implementation, and verification of a discontinuous galerkin method for prediction of storm surges*

and coastal deformation. PhD thesis, The University of Texas at Austin, 2011.

[68] IM Navon. Practical and theoretical aspects of adjoint parameter estimation and identifiability in meteorology and oceanography. *Dynamics of Atmospheres and Oceans*, 27(1):55–79, 1998.

[69] L. Nelson and E. Stear. The simultaneous on-line estimation of parameters and states in linear systems. *Automatic Control, IEEE Transactions on*, 21(1):94–98, 1976.

[70] Lars Nerger, Wolfgang Hiller, and Jens Schröter. A comparison of error subspace kalman filters. *Tellus A*, 57(5):715–735, 2005.

[71] Lars Nerger, Tijana Janjic, Jens Schröter, and Wolfgang Hiller. A unification of ensemble square root kalman filters. *Monthly Weather Review*, 140(7):2335–2345, 2012.

[72] Emanuel Parzen. *Statistical inference on time series by Hilbert space methods*. Applied Mathematics and Statistics Laboraotry, Stanford University, 1959.

[73] Dinh Tuan Pham. Dimension, predictability and reduced rank kalman filtering in data assimilation. In *Proc. Third Bilateral French–Russian Conf.: Predictability of Atmospheric and Oceanic Circulations*, pages 255–260. Citeseer, 1997.

[74] D.T. Pham. Stochastic methods for sequential data assimilation in strongly nonlinear systems. *Monthly weather review*, 129(5):1194–1207, 2001.

[75] R Ramesh, Bithin Datta, S Murty Bhallamudi, and A Narayana. Optimal estimation of roughness in open-channel flows. *Journal of Hydraulic Engineering*, 126(4):299–303, 2000.

[76] C.E. Rasmussen and C.K.I. Williams. *Gaussian Processes for Machine Learning*. Adaptative computation and machine learning series. University Press Group Limited, 2006.

[77] AR Robinson, PFJ Lermusiaux, and N.Q. Sloan III. Data assimilation. *The sea*, 10:541–594, 1998.

[78] Christoph Schwab and Radu Alexandru Todor. Karhunen–loève approximation of random fields by generalized fast multipole methods. *Journal of Computational Physics*, 217(1):100–122, 2006.

[79] Masanobu Shinozuka and George Deodatis. Simulation of stochastic processes by spectral representation. *Applied Mechanics Reviews*, 44:191, 1991.

[80] S. Singhal and L. Wu. Training multilayer perceptrons with the extended kalman algorithm. *Advances in neural information processing systems I*, 1:133, 1989.

[81] American Meteorological Society and G.W. Platzman. *The Dynamic Prediction of Wind Tides on Lake Erie*. Meteorological monographs. 1963.

[82] Hajoon Song, Ibrahim Hoteit, Bruce D Cornuelle, Xiaodong Luo, and Aneesh C Subramanian. An adjoint-based adaptive ensemble kalman filter. *Monthly Weather Review*, (2013), 2013.

[83] Hajoon Song, Ibrahim Hoteit, Bruce D Cornuelle, and Aneesh C Subramanian. An adaptive approach to mitigate background covariance limitations in the ensemble kalman filter. *Monthly Weather Review*, 138(7):2825–2845, 2010.

[84] Jacob Viborg Tornfeldt Sørensen and Henrik Madsen. Efficient kalman filter techniques for the assimilation of tide gauge data in three-dimensional modeling of the north sea and baltic sea system. *Journal of Geophysical Research: Oceans (1978–2012)*, 109(C3), 2004.

[85] Jacob Viborg Tornfeldt Sørensen and Henrik Madsen. Parameter sensitivity of three kalman filter schemes for assimilation of water levels in shelf sea models. *Ocean Modelling*, 11(3):441–463, 2006.

[86] M.L. Stein. *Interpolation of Spatial Data: Some Theory for Kriging*. Springer Series in Statistics. Springer New York, 1999.

[87] S Tanaka, Shintaro Bunya, Joannes J Westerink, Clint Dawson, and RA Luettich Jr. Scalability of an unstructured grid continuous galerkin

based hurricane storm surge model. *Journal of Scientific Computing*, 46(3):329–358, 2011.

[88] PGJ Ten Brummelhuis and AW Heemink. Parameter identification in tidal models with uncertain boundary conditions. *Stochastic Hydrology and Hydraulics*, 4(3):193–208, 1990.

[89] PGJ Ten Brummelhuis, AW Heemink, and HFP Van Den Boogaard. Identification of shallow sea models. *International journal for numerical methods in fluids*, 17(8):637–665, 1993.

[90] Michael K Tippett, Jeffrey L Anderson, Craig H Bishop, Thomas M Hamill, and Jeffrey S Whitaker. Ensemble square root filters*. *Monthly Weather Review*, 131(7):1485–1490, 2003.

[91] O-P Tossavainen, Julie Percelay, Andrew Tinka, Qingfang Wu, and Alexandre M Bayen. Ensemble kalman filter based state estimation in 2d shallow water equations using lagrangian sensing and state augmentation. In *Decision and Control, 2008. CDC 2008. 47th IEEE Conference on*, pages 1783–1790. IEEE, 2008.

[92] D. Tuan Pham, J. Verron, and M. Christine Roubaud. A singular evolutive extended kalman filter for data assimilation in oceanography. *Journal of Marine systems*, 16(3):323–340, 1998.

[93] H.L. Van Trees. *Detection, Estimation, and Modulation Theory*. Number pt. 1 in Detection, Estimation, and Modulation Theory. Wiley,

2004.

[94] M Verlaan and AW Heemink. Tidal flow forecasting using reduced rank square root filters. *Stochastic Hydrology and Hydraulics*, 11(5):349–368, 1997.

[95] C.B. Vreugdenhil. *Numerical methods for shallow-water flow*, volume 13. Springer, 1994.

[96] E.A. Wan, R. Van Der Merwe, and A.T. Nelson. Dual estimation and the unscented transformation. *Advances in Neural Information Processing Systems*, 12:666–672, 2000.

[97] Eric A Wan and Rudolph Van Der Merwe. The unscented kalman filter. *Kalman filtering and neural networks*, pages 221–280, 2001.

[98] AM Wasantha Lal. Calibration of riverbed roughness. *Journal of Hydraulic Engineering*, 121(9):664–671, 1995.

[99] Joannes J Westerink, Richard A Luettich, Jesse C Feyen, John H Atkinson, Clint Dawson, Hugh J Roberts, Mark D Powell, Jason P Dunion, Ethan J Kubatko, and Hasan Pourtaheri. A basin-to channel-scale unstructured grid hurricane storm surge model applied to southern louisiana. *Monthly Weather Review*, 136(3):833–864, 2008.

[100] Johannes J Westerink, Richard A Luettich, AM Baptists, NW Scheffner, and P Farrar. Tide and storm surge predictions using finite element model. *Journal of Hydraulic Engineering*, 118(10):1373–1390, 1992.

[101] J.S. Whitaker and T.M. Hamill. Ensemble data assimilation without perturbed observations. *Monthly Weather Review*, 130(7):1913–1924, 2002.

[102] T. Yanagi. *Coastal oceanography*, volume 1. Springer, 1999.

[103] Jun Zhang and Bruce Ellingwood. Orthogonal series expansions of random fields in reliability analysis. *Journal of Engineering Mechanics*, 120(12):2660–2677, 1994.

Vita

Talea Lashea Mayo was born in Colorado Springs, Colorado. She received the Bachelor of Science degree in Mathematics from Grambling State University in May, 2008, where she received the highest honors. Upon graduating, she began graduate studies in the Institute for Computational Engineering and Sciences at the University of Texas at Austin in August, 2008. She received the Master of Science degree in Computational and Applied Mathematics in May, 2010.

Email address: talea.mayo@gmail.com

This dissertation was typeset with LaTeX[†] by the author.

[†]LaTeX is a document preparation system developed by Leslie Lamport as a special version of Donald Knuth's TeX Program.